Contamination in Electromyography Signals and Noise Removal Techniques

Thandar Oo

A Thesis Submitted in Fulfillment of the Requirements for the Degree of

Doctor of Philosophy in Electrical Engineering

Prince of Songkla University

2019

Thesis Title	Contamination in Electromyography Signals and Noise Removal Techniques
Author	Miss Thandar Oo
Major Program	Electrical Engineering

Major Advisor

.....

(Assoc. Prof. Dr. Pornchai Phukpattaranont)

Examining Committee:

……..….Chairperson

(Asst. Prof. Dr.Suparerk Janjarasjitt)

……..…Committee

(Assoc. Prof. Dr.Pornchai Phukpattaranont)

……..….Committee

(Asst. Prof. Dr.Dujdow Buranapanichkit)

……..….Committee

(Dr.Chalakorn Karupongsiri)

……..….Committee

(Dr.Apidet Booranawong)

The Graduate School, Prince of Songkla University, has approved this thesis as fulfillment of the requirements for the Doctor of Philosophy Degree in Electrical Engineering.

……..…….……

(Prof. Dr.Damrongsak Faroongsarng)

Dean of Graduate School

This is to certify that the work here submitted is the result of the candidate's own investigations. Due acknowledgement has been made of any assistance received.

……Signature

(Assoc. Prof. Dr.Pornchai Phukpattaranont)

Major Advisor

……Signature

(Miss Thandar Oo)

Candidate

I hereby certify that this work has not been accepted in substance for any degree, and is not being currently submitted in candidature for any degree.

……..Signature

(Miss Thandar Oo)

Candidate

Thesis Title	Contamination in Electromyography Signals and Noise Removal Techniques
Author	Miss Thandar Oo
Major Program	Electrical Engineering
Academic Year	2018

ABSTRACT

The electromyography (EMG) signal can be contaminated with noise during data collection. For example, when the EMG signal is acquired from muscles in the torso, the electrocardiography (ECG) signal coming from heart activity can interfere. In this thesis, we proposed a novel method on noise removal and the signal-to-noise ratio (SNR) estimation algorithms. For the noise removal method, a technique based on discrete stationary wavelet transform (DSWT) is proposed to remove ECG interference from the EMG signal while taking into account the SNR. The contaminated EMG signal is decomposed using 5-level DSWT with the Symlet wavelet function. A clean EMG signal can then be obtained by inverse DSWT mapping of the new thresholded coefficients. The performance based on mean absolute error, correlation coefficient, and relative error shows that the DSWT method is better than a high-pass filter. For the SNR estimation method, we present a novel SNR estimation in the EMG signal contaminated with the ECG interference. We calculate the features from the EMG signals. Then, the features are used as an input of a neural network (NN). The NN output is an SNR estimate. The results showed that the waveform length was the best feature for estimating SNR. It gave the highest average correlation coefficient at 0.9663. These results suggested that the waveform length was able to be deployed not only in an EMG recognition system but also in an EMG signal quality measurement when the EMG signal was contaminated with the ECG interference.

ACKNOWLEDGEMENTS

The author would like to express her sincere gratitude to his valuable supervision, Assoc. Prof. Dr. Pornchai Phukpattaranont, Department of Electrical Engineering, Prince of Songkla University, who has consistently inspired her in this study and provided precious suggestions and advice. Without his attentive guidance, endless patience, and encouragement through the past year, this thesis would not have been possible to accomplish. Besides, the author has also acquired valuable insights through his instructions, not only in academic studies but also enthusiasm and vigour in life.

The author wishes to express her special thanks to the Graduate School, Prince of Songkla University through Thailand's Education Hub for ASEAN Countries (TEH-AC) scholarship.

Finally, the author is deeply appreciated her beloved family, who has always supported her everything through the difficult times. It is their love and support that always encourage her to stick on the difficult task of doing the thesis.

Thandar Oo

CONTENT

LIST OF TABLES

LISTS OF FIGURES

CHAPTER 1

INTRODUCTION

Electromyography (EMG) records electric currents produced in muscle contractions, acquired using electrodes. The electrode converts an ion current to an electron current so that it can be amplified and recorded by an electronic circuit. The EMG signal is generated from motor units, which are nerve-muscle functional units of the neuromuscular system [1,2]. The potential difference can be measured by either non-invasive electrodes for surface EMG signals or by invasive electrodes for needle EMG sampling intramuscular EMG signals [3].

There are a variety of applications for EMG signals. The EMG signal can be used not only as an electrodiagnostic medical technique but also as a neurophysiological technique for evaluating and recording the electrical activity produced by skeletal muscles [4,5]. Moreover, the EMG signal recorded from a muscle contraction has a variety of uses in clinical applications [6], evolvable hardware chip (EHC) development [7], robotic applications [8], modern human-computer interaction [9], and electrical wheelchair control [10].

An essential element for enabling the above-described applications is an EMG recognition system. The EMG recognition system consists of three cascaded modules, namely; data pre-processing, feature extraction, and classification [11,12]. The primary purpose of data pre-processing is to remove noise in the EMG signal, which is contaminated by the environment as it passes through or by various tissues [13]. In this thesis, we studied on noise detection and noise removal.

1.1. Literature review

1.1.1. Contamination in EMG

From literature reviews, there are four important types of noise contaminated in EMG signals, namely, (1) electrocardiography (ECG) interference [17-30], (2) power line interference [16,31-34], (3) motion artifact [14,35-37] and (4) baseline noise [14-15,38-39]. Details on each type of noise are as follows.

1.1.1.1. Electrocardiography (ECG) interference

ECG determines the electrical activity of the heart over a specified period of time. ECG is not only used for measurement and recording of electrical activity but also helps in measuring the rhythm and invariability of heart beat [40-43]. Fig. 1.1 shows the waveform of a normal ECG signal consisting of a P-wave, a QRS complex and a T-wave. The ECG waveform initiates with the P-wave. The QRS complex represents ventricular depolarization and is composed of three waves, which are the Q-wave, the R-wave and the S-wave. ECG interference has bandwidth in the range of 0.05 – 100 Hz [21-22]. The EMG signal can be contaminated by the ECG interference in some applications because of the proximity between the EMG measurement location such as trunk muscles and the heart. One of ECG interference removal algorithm applications is in EMG data acquisition for shoulder disarticulation prosthesis control where the electrodes are placed at the pectoralis muscle as shown in Fig. 1.2, which is very close to the heart [21]. As a result, contamination by ECG interference is unavoidable. Fig. 1.3 shows an example of the EMG signal contaminated with the ECG interference at a signal-to-noise ratio (SNR) level of 0 dB in time domain and power spectrum in frequency domain on the top and the bottom panels, respectively.

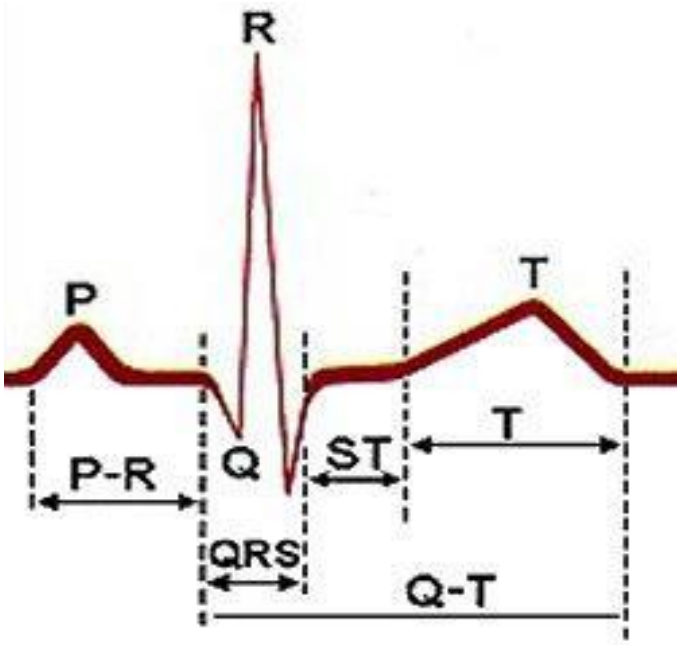

Fig. 1.1. ECG waveform consisting of a P-wave, a QRS complex, and a T-wave [28].

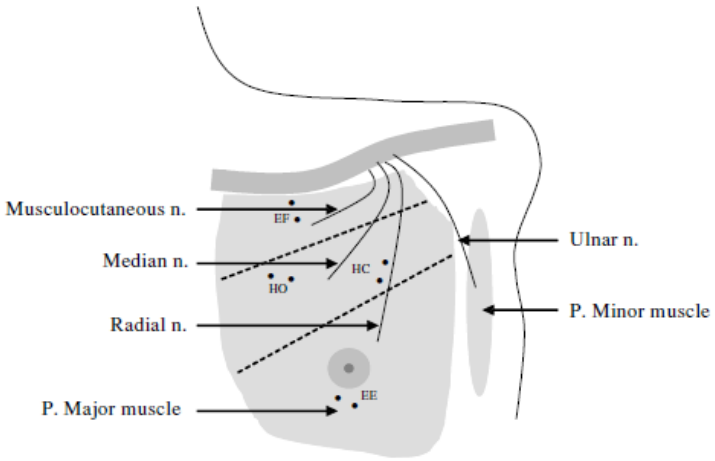

Fig. 1.2. Pectoralis muscle [21].

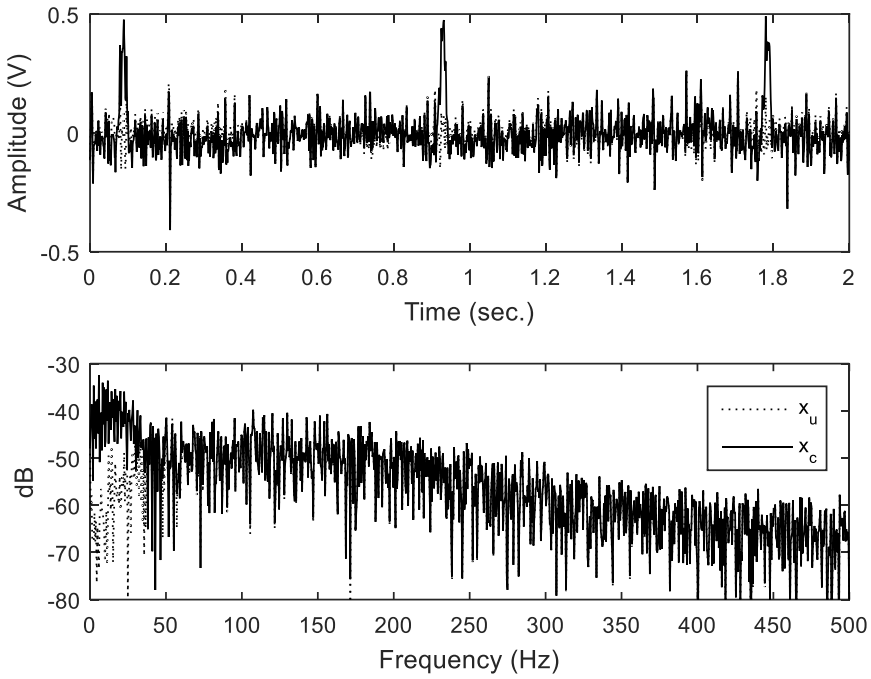

Fig. 1.3. The amplitude of EMG signals contaminated with ECG interference in the time domain at SNR 0 dB (Top panel) and its corresponding power spectrum in the frequency domain (Bottom panel). Dotted line: x_u is an uncontaminated EMG signal. Solid line: x_c is an EMG signal contaminated with ECG interference.

1.1.1.2. Power line interference

The power line interference is an essential source of noise. It is caused by either an induced current from the passing of a time-varying magnetic field on a closed loop formed by the electrode leads, the subject, and the signal amplifier or a displacement current induced from the capacitive coupling between the electrode leads and the subject body [25,31]. The most important source of such noise is power line interference at 50 Hz and its harmonics. The amplitude and frequency of the EMG signal can be changed by power line interference [32-33]. Moreover, it is possible that the amplitude of powerline noise is higher than the amplitude of the desirable EMG signal. Therefore, it causes serious reduction in SNR. To alleviate the mentioned problem, the use of a suitable electronic device, which has both high common mode rejection ratio (CMRR) and shielding cables, can reduce power line interference. Fig. 1.4 shows the amplitude of EMG signals contaminated with power line noise in time domain and its power spectrum in frequency domain at a SNR level of 0 dB. It can be clearly seen that the power line noise at 50 Hz occurs in the contaminated EMG signal.

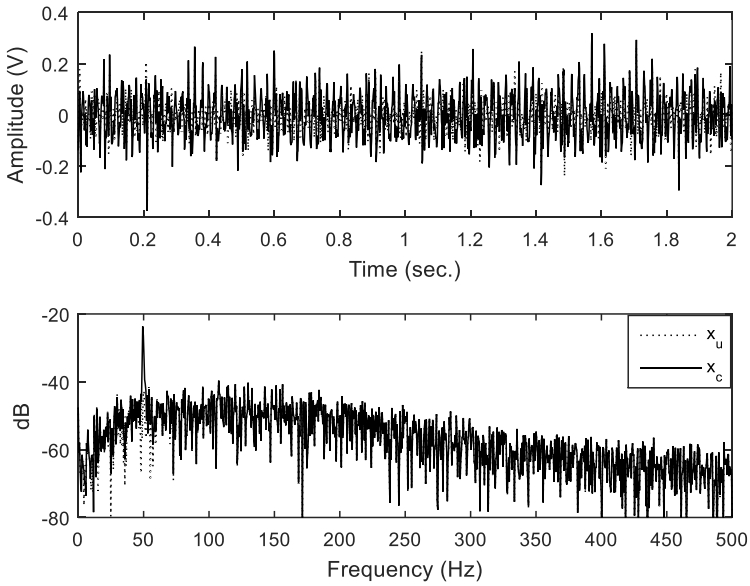

Fig. 1.4. The amplitude EMG signals contaminated with the power line noise in the time domain at SNR 0 dB (Top panel) and its corresponding power spectrum in the frequency domain (Bottom panel). Dotted line: x_u is an uncontaminated EMG signal. Solid line: x_c is an EMG signal contaminated with power line interference.

1.1.1.3. Motion artifact

Motion artefact can be divided into two categories, which are an electrode motion artefact and a cable motion artefact [37,44]. The electrode motion artefact consists of two sources. The first source is a relative movement at the contact area between the electrode and the skin. However, this type of artefact can be significantly reduced by using a built-in electrode consisting of a conductive gel or paste. As a result, this type of artefact is attenuated by the gel layer. The second source is the variations in potential difference and the skin potential due to the stretch or deformation of the skin. This type of artefact is can be decreased by reducing the skin impedance. The electrode motion artifact typically has a frequency range is less than 20 Hz [25,45-46].

The cables are connected between the electrodes and amplifier. They have a fundamental capacitance. In cable motion artifact, the voltage magnitude that forms in the cable is the multiplication of the current movement and the impedance electrode–skin added with the voltage caused by magnetic field. The amounts of the detected EMG are similar with that voltage. The frequency range of cable motion artifact has typically from 1 to 50 Hz [26,47-48]. There are two facts to reduce cable motion artifact: 1) reducing electrode-skin impedance and; 2) applying the shielded cables. Nevertheless, these shielded cables can be considered as a source of causing cable motion artifact. The resistance and distortion of the insulated cable generated with static charges can be caused by moving shielded cables and these cables disappear through the measurement system. Another obvious solution is to clear up the cable motion artifact is to use active electrodes based on an operational amplifier because of high input impedance and low output impedance which is built as a unity gain buffer [25]. Fig. 1.5 shows the amplitude of EMG signals contaminated with motion artifact in time domain and its power spectrum in frequency domain at a SNR level of 0 dB.

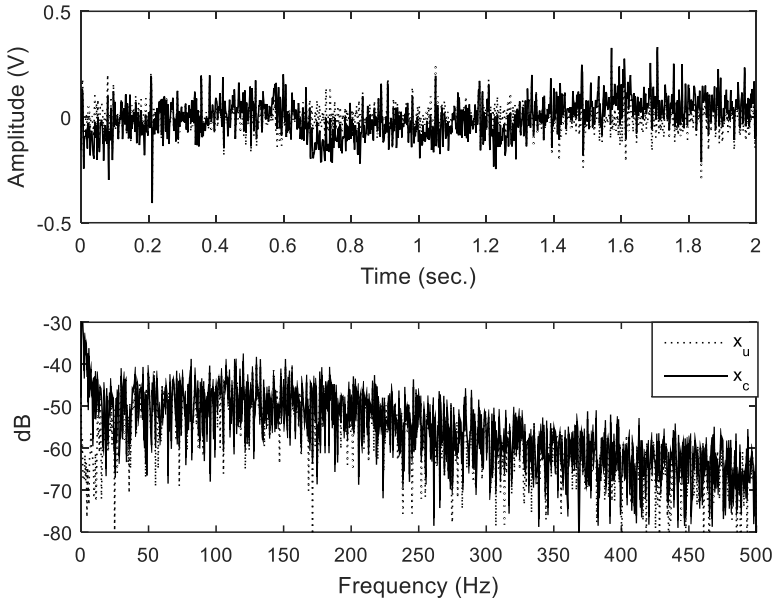

Fig. 1.5. The amplitude EMG signals contaminated with motion artefact in the time domain at SNR 0 dB (Top panel) and its corresponding power spectrum in the frequency domain (Bottom panel). Dotted line: x_u is an uncontaminated EMG signal. Solid line: x_c is an EMG signal contaminated with motion artifact.

1.1.1.4. Baseline noise

Baseline noise is a combination of two intrinsic sources, which are thermal noise and electrochemical noise [49-50]. It is generated not only from the amplification system of electronics, which is also called thermal noise, but also from the electro-chemical noise, which is located at the skin-electrode interface [51]. Fig. 1.6 shows an example of the baseline noise contaminated in the EMG signals at various levels on the top panel and its corresponding filtered the EMG signals at the bottom panel.

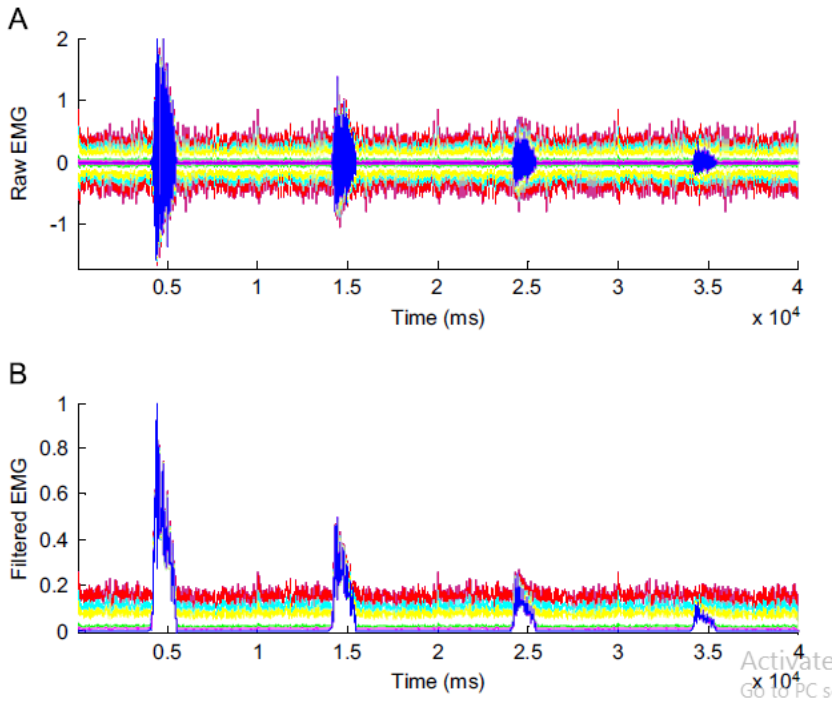

Fig. 1.6. An example of the baseline noise contaminated in EMG signals at various levels on the top panel and its corresponding filtered EMG signals at the bottom panel [15].

1.1.2. Noise removal techniques

There are several noise removal techniques in the literature review depending on the type of noise. This section will give the details of noise removal techniques describing by three types of noise including 1) ECG interference [52-62], 2) power line interference [49,62-63], and 3) motion artifact [44-47]. Details of each technique are as follws.

1.1.2.1. ECG interference

- **Digital filter**

High pass filtering is one of the most popular methods used for eliminating ECG interference from EMG signals [64-66]. Most of energy of ECG interference is in the range of 0 to 30 Hz. Therefore, high pass digital filtering with a 30 Hz cut-off frequency is used. There are two designs of high pass digital filtering used for ECG interference removal, i.e. a Butterworth filter [17], [21], [29], [30] and a

digital finite impulse response filter [20] as details shown in Table 1.1. High pass digital filtering is not only easily to implement but also performs satisfactory at rest and excellence at all levels of muscle voluntary contraction (MVC) evaluated. Hence, it provides the optimal balance between ease of implementation time investment and performance across all contractions and heart rate levels [17]. Moreover, another advantage is that the signal from additional channel does not require. However, some parts of EMG signals in the range of 0-30 Hz are also removed.

Table 1.1. High pass digital filtering used for removing ECG interference from the EMG signal.

Authors	Method
Janessa 2006 [17] and Vinzenz 2011 [29]	High pass digital filtering using a fourth-order Butterworth filter with cut-off frequency of 30 Hz.
Nienke 2012 [30]	High pass digital filtering using a second-order bi-directional Butterworth filter with cut-off frequency of 30 Hz
Sara 2016 [20]	High pass digital filtering using a digital finite impulse response filter with 100 coefficients based on a Hamming window design criteria at a cut-off frequency of 30 Hz
Zhou 2006 [21]	High pass digital filtering using a second-order Butterworth filter with cut-off frequency of 60 Hz, which provided the most suitable signals for myoelectric prosthesis control

- **Template subtraction**

Template subtraction is very useful for removing ECG interference from the contaminated EMG signals [67-68]. There are three main stages of template subtraction, namely, 1) creation of ECG template, 2) detection of ECG interference from the contaminated EMG signals, and 3) subtraction of ECG interference from the contaminated EMG signals [17], [20], [21], [23] as shown in Fig. 1.7. One advantage

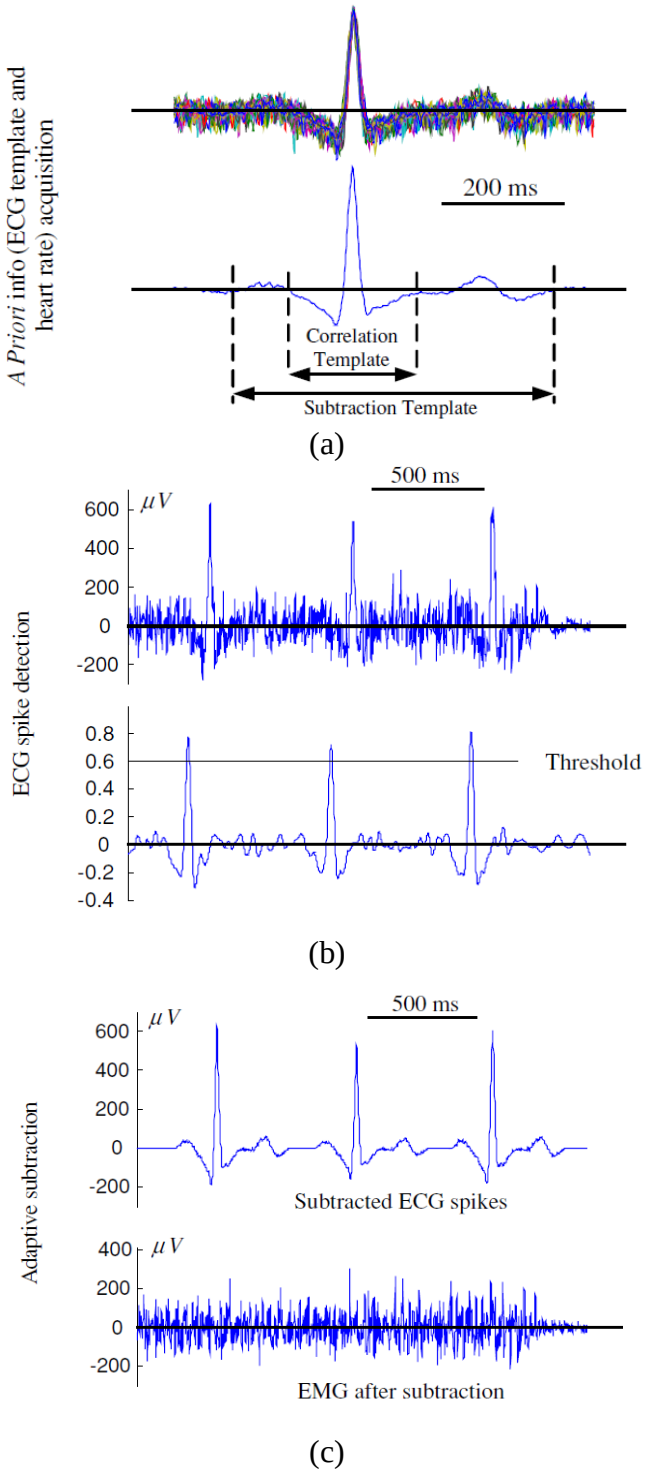

Fig. 1.7. Procedures of template subtraction (a) Create ECG template, (b) Detect ECG interference in the contaminated EMG signals, and (c) Subtract ECG template from the contaminated EMG signals [21].

of template subtraction method is its ability to remove the ECG interference without losing the EMG signals [21]. However, the template subtraction method may not be used for some clinical applications such as myoelectric prosthesis control because of its requirement on individual template creation for each participant and its heavy computation burdens of cross-correlation [17] [21]. Moreover, it requires additional ECG signal acquisition for accurate detection of QRS algorithms [21].

- **Adaptive filter**

Adaptive filter is a successful technique used for eliminating ECG interference from EMG signals because it is able to remove ECC signals from contaminated EMG signals when the spectra of EMG signals and ECG noise are overlapping [69-72]. Moreover, it can follow any change on the signal and noise by adaptively adjusting the filter coefficients, which are expected in some situations such as during a fatigue process [18,88,89]. Therefore, it can optimize the performance when it is applied to several types of muscles [19].

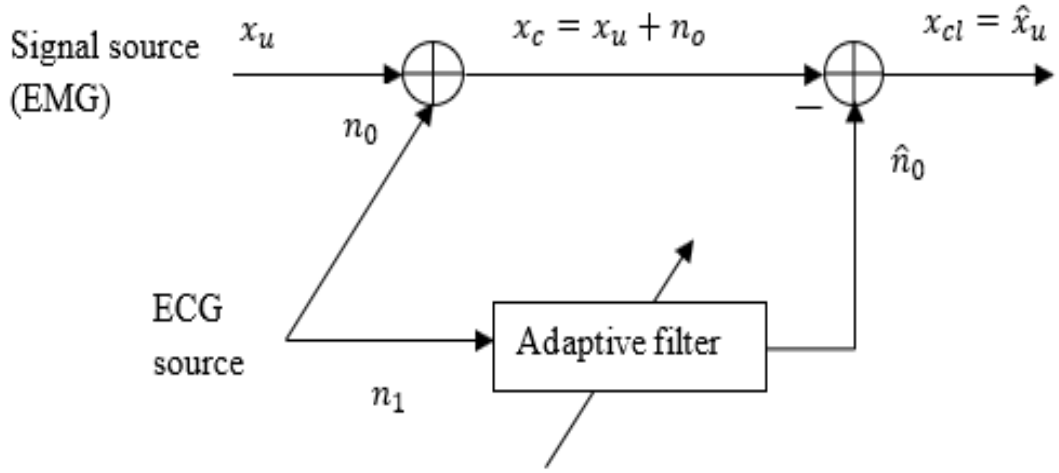

Fig. 1.8. Block diagram of an adaptive filter used for removing ECG interference

Fig. 1.8 shows the principle of the adaptive filter used for removing ECG interference from the contaminated EMG signals [18]. There are two input signals for the adaptive filter, x_c and n_1. While x_c is the contaminated EMG signal, which is the

combination between the uncontaminated EMG signal x_u and the ECG interference n_0, n_1 is the reference signal that is correlated with the ECG interference n_0. The adaptive filter is used to estimate the noise $\hat{n}_0$. Then, x_{cl}, an estimate for the uncontaminated EMG signal $\hat{x}_u$, can be determined by subtracting $\hat{n}_0$ from the contaminated EMG signal x_c.

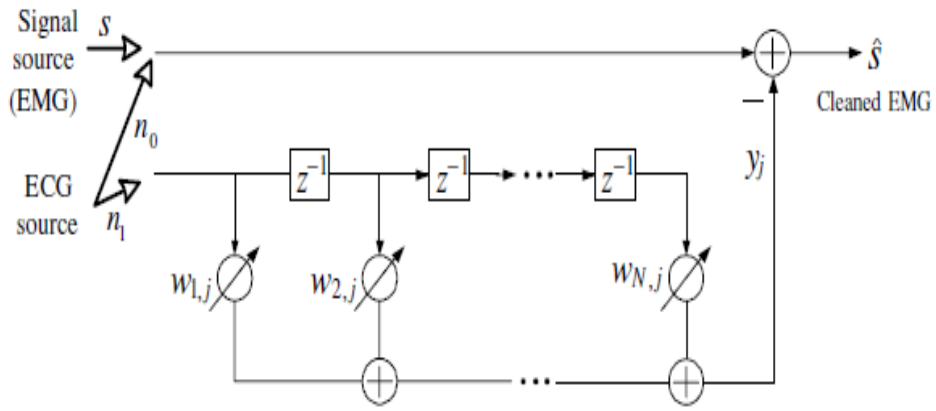

Fig. 1.9. The structure of the linear adaptive ECG noise canceller [21], [23].

There are 2 types of adaptive filter in the literature review, i.e., a linear adaptive filter and a nonlinear adaptive filter. Details of each type of the adaptive filter are given as follws.

- Linear techniques

Fig. 1.9 shows a structure of the linear adaptive ECG noise canceller, which is defined in the time domain by using a finite impulse response filter (FIR) with a length of N points [73-74]. The output of the linear adaptive ECG noise canceller can be expressed as [18],[20],[21]

$$y_j = \sum_{i=1}^{N} w_{i,j} n_{1,j-i+1} . \quad (1.1)$$

The algorithms used to optimize the coefficients $w_{i,j}$ include fast recursive least square algorithm (FRLS) [18], recursive least square algorithm (RLS) [19], [20], and least mean square algorithm (LMS) [21], [23]. Moreover, Table 1.2 shows the sources

of EMG signals and ECG reference signals as well as the parameters used in the linear adaptive filter from previous publications [18], [19], [20], [21], [23]. The adaptive filter or the adaptive noise canceller (ANC) is very suitable for adjusting the amplitude and phase of the reference signal to estimate the noise in the contaminated EMG signals. Then, the estimated noise is subtracted from the contaminated EMG signals so that the clean EMG signals can be obtained. However, it was reported in [20] that the noise was not well estimated and there is still noise in the estimate for the uncontaminated EMG signal. Moreover, some parts of uncontaminated EMG signals may be eliminated [20]. Another disadvantage of ANC was its heavy computational cost resulting in the difficulty for the implementation on clinical applications [20].

- Nonlinear techniques

Nonlinear adaptive filters used for ECG interference removal from previous publications include an artificial neural network (ANN) and an adaptive neuro-fuzzy inference system (ANFIS) [75-76]. Either ANN or ANFIS is applied for estimating ECG interference contaminated in the EMG signals similar to the linear adaptive noise canceller [77].

ANN is one of the successful nonlinear adaptive filters used for removing ECG interference [78]. In [22] and [24] the back propagation network (BPN) was used to estimate the ECG interference presenting in the EMG signals. Fig.1.10 shows a block diagram of a nonlinear adaptive filter based on BPN used for ECG interference removal [24]. The network architecture consists of two neurons in the input layer, 35 neurons in the one hidden layer and one neuron in the output layer.

Table 1.2. Algorithms, sources of EMG and ECG reference signals, and parameters used in the adaptive filter.

Authors	Algorithms	Sources of EMG and ECG reference signals	Parameters
Marque 2005 [18]	Fast recursive least square algorithm (FRLS)	• EMG from erector spinae muscles • ECG from left scapula	N/A
Guohua 2009 [19]	Recursive least square algorithm (RLS)	• EMG from the right trapezius muscles • ECG from the left trapezius muscles	Filter order 12 Forgetting factor 0.999 Regularization factor 0.1
Zhou 2005 [23], Zhou 2007 [21],	Least mean square algorithm (LMS)	• EMG from the reinnervated pectoralis muscles of the amputee • ECG from the pectoralis minor muscle	N/A
Sara 2016 [20]	Adaptive neuro-fuzzy inference system (ANFIS)	• EMG from biceps and deltoid muscles of the right side • ECG from the pectoralis muscle of the left side	N/A
Kezi 2009 [22]	Back propagation network (BPN)	• EMG from electrode site on the trunk and neck • ECG from the rectus abdominis, external oblique and erector spinae muscles	Epochs 1000, Goal = 0.65, Momentum =0.9, Show = 5, Learning rate = 0.5, Time infinity, 2 neurons in the input layer, 35 neurons in one hidden layer (TANSIG) and one neuron in the output layer (PURELIN).

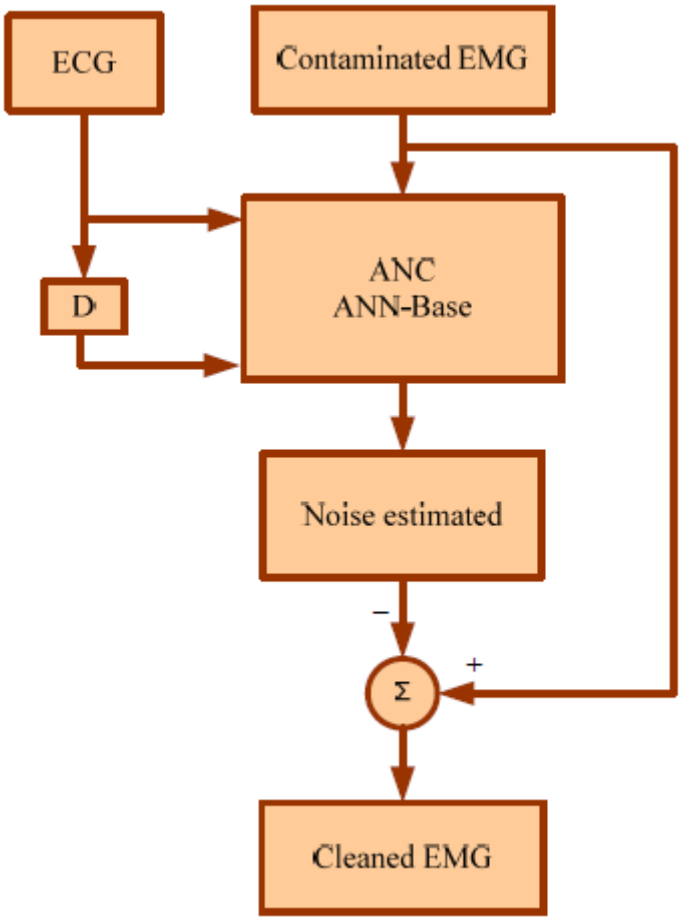

Fig. 1.10. Block diagram of a nonlinear adaptive filter based on BPN used for ECG interference removal [24].

The parameters used for training BPN to remove the ECG interference from EMG signals are as follows [22], [24]:epochs =1000, goal = 0.65, momentum =0.9, show = 5, learning rate = 0.5 and time = infinity. One of the disadvantages of BPN is that it requires multiple inputs and heavy computations because of its layers [20].

ANFIS combine network of the strengths of neutral network and fuzzy system. As a result, the calculation time for ANFIS technique is lower than that for ANN method [20]. Fig.1.11 shows the ANFIS structure used for ECG interference removal [20]. The ANFIS structure generally consists of two source inputs, five hidden layers, and one output. Details of the five hidden layers are as follows: the first layer is a

fuzzifier, the second layer is the fuzzy rules, the third layer is for normalization, the fourth layer is for identifying effective parameters and the fifth layer is the destination output. According to the Fig.1.11, the delayed ECG signal and the ECG interference contaminated with EMG signal were used for the ANFIS inputs. This delayed ECG signal was occurred when the ECG signal and ECG interference from different sources were collected. By using this delayed ECG signal, the noise estimation procedure is more efficient and effective.

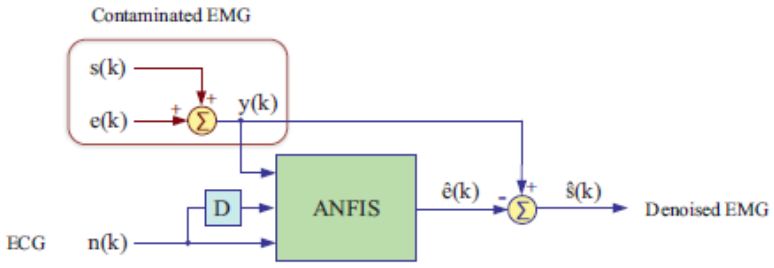

Fig. 1.11. Block diagram of a nonlinear adaptive filter based on ANFIS used for ECG interference removal [20].

- **Wavelet transform**

Wavelet transform is one of the ECG removal techniques in EMG signals. In contrast to an adaptive filter, one of its advantages is that it does not require a separately additional ECG reference channel [79-80]. Moreover, it is simple and fast [81]. However, some artifacts may remain in the contaminated EMG signal and part of the desired EMG signal may be removed [82]. Most energy of ECG interference is contributed to the wavelet coefficients located high-scale low-frequency components. Thus, with a proper threshold, we can remove most of ECG artifacts by truncating or shrinking the wavelet coefficients, which are the dominant part of the ECG interference.

Fig. 1.12 shows a schematic description of ECG interference removal using wavelet transform [23]. In the first stage, the EMG signal contaminated by the ECG interference x_c was decomposed by the wavelet transform into various subband signals.

Then, in the second stage, the subband signals are separated into two types of scales including low-scale high-frequency components and high-scale low-frequency components. Thirdly, the wavelet coefficients obtained from high-scale low-frequency components, which are contaminated by the ECG interference, are processed with a nonlinear thresholding procedure. In other words, the values of coefficient higher than the value of the threshold were set to zero. The values of threshold can be adjusted depending on the coefficients of background ECG interference, which are much greater than the neighbouring coefficients. Finally, the clean EMG signals x_{cl} is obtained from the new coefficients by using inverse wavelet transform.

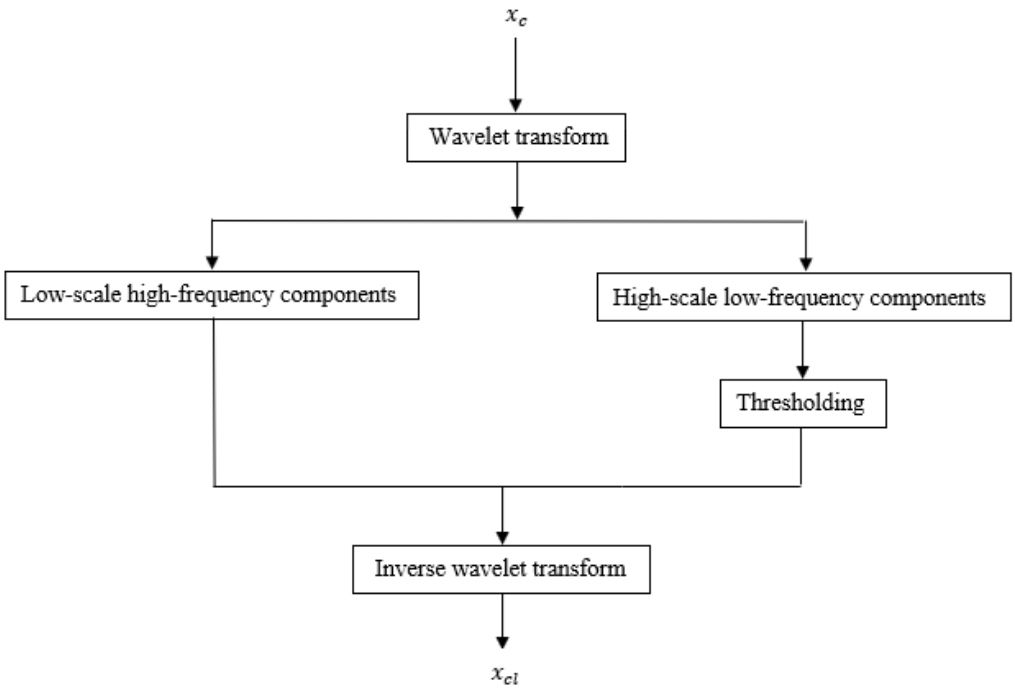

Fig. 1.12. Schematic description of ECG interference removal using wavelet transform

Fig. 1.13 shows an example of signal components from the ECG interference removal technique using wave transform. Fig. 1.13(a) shows the EMG signal contaminated by the ECG interference. After an seven-level wavelet decomposition with the forth-order Symlet wavelet as a wavelet function [21], the coefficients in high-scale low-frequency components at level cD5, cD6, and cD7 are shown in the left

panels of Fig.1.13 (b), (c), and (d), respectively. Then, they were processed with the nonlinear thresholding procedure. The coefficients after thresholding at level cD5, cD6, and cD7 are shown in the right panel of Fig.1.13 (b), (c), and (d), respectively. We can clearly see that the coefficients higher than the threshold were set to zero. Finally, Fig. 1.13(e) shows the clean EMG signal x_{cl}, which is obtained from the new coefficients by using inverse wavelet transform. Similarly, in [23], the forth-order Symlet wavelet was used as a wavelet function with eight-level wavelet decomposition. The nonlinear thresholding technique was applied with the coefficients of four-lowest frequency components, namely cD5, cD6, cD7, and cD8.

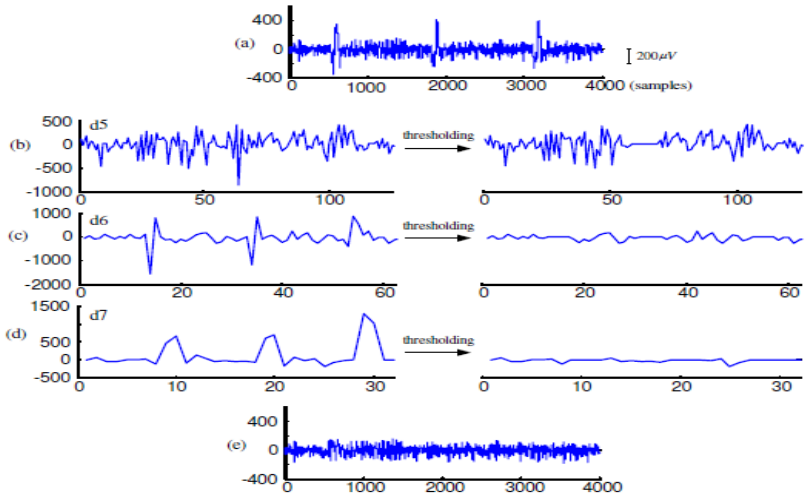

Fig.1.13. An example of signal components from the ECG interference removal technique using wavelet transform [21].

- **Combination techniques**

Combination techniques are generally composed of the combination of two or more methods to eliminate the ECG interference from the EMG signals. Details of the combination techniques are as follows.

- Template subtraction combined with a high pass filter

Combination method of a high pass filter with a template subtraction is used for removing the ECG interference contaminated in the EMG signals [17]. Five high pass filter with cut-off frequencies 20, 30, 40, 50, and 60 Hz were applied to the signals after performing with the template subtraction. However, the results show that there is no statistical improvement on the performance of the template subtraction combined with the high pass filter [17].

- Artificial neural network combined with wavelet transform

Artificial neutral network (ANN) and wavelet transform is combined and used for removing ECG interference from EMG signals [24]. Fig.1.14 shows a block diagram of the combination technique based on ANN and wavelet transform [24]. Firstly, the ECG interference is removed from the contaminated EMG signals by using a nonlinear adaptive filer based on the neural network. Therefore, a large amount of ECG noises are removed during this process. However, low-frequency noise components remain in the signals, which can be further removed by using wavelet transform with a nonlinear thresholding technique in the second stage.

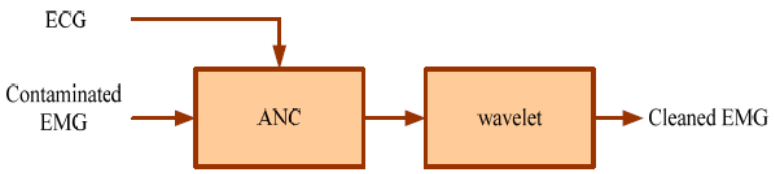

Fig.1.14. A combination of ANN and wavelet transform technique [24].

- ANFIS combined with wavelet transform

Combination of an adaptive neuro-fuzzy inference system (ANFIS) and a wavelet transfrom is a successful ECG removal technique in the contaminated EMG signals [20,83]. Fig.1.15 shows a block diagram of the combination technique based on ANFIS and wavelet transform [19]. ANFIS, which can be considered as a nonlinear adaptive noise filtering, was used for removing ECG interference in the first step [84].

Then, the wavelet transfrom with nonlinear thresholding process, was used in the second step for removing the residual ECG interference between 0 and 15 Hz. In other words, the output signals from ANFIS was decomposed by the fourth order Symlet wavelet. Then, the wavelet coefficients in the low frequency scales were processed with a nonlinear thresholding tecnique, where the absolute value of the coefficients greater than a predefined threshold was set to zero [20].

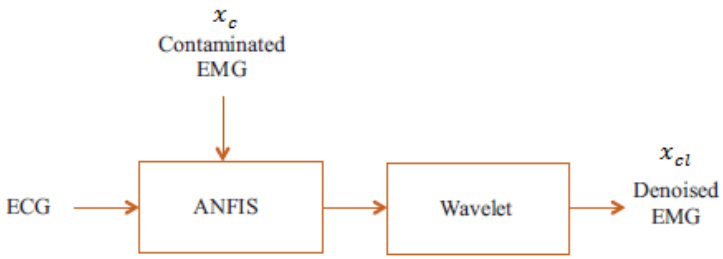

Fig. 1.15. A combination of ANFIS and wavelet transform [20].

- Performance evaluations

Table 1.3 shows the comparisons of mean and standard deviation from various techniques discussed in Section 1.1.2.1 for removal of ECG interference from the contaminated EMG signal. Results showed that the performance based on SNR, RE, R, and MFRE, from the combination technique are better than other removal techniques, i.e. ANFIS, ANN, template subtraction, adaptive filtering, wavelet transform, and high pass filtering. ANFIS combined with wavelet transform is faster than a combination method of ANN and wavelet transform. As a result, although the similar performance between ANFIS+wavelet and ANN+wavelet is obtained, ANFIS combined with wavelet uses less computation time than a combination of ANN and wavelet transform.

Table.1.3. Comparisons of mean and standard deviation from various techniques for removal of ECG interference from the contaminated EMG signal.

Methods	SNR (dB)	RE	R	MFRE	ET (s)
ANFIS-wavelet [20]	14.97±1.34	0.02±0.02	0.99±0.02	0.12±0.01	0.27
ANN-wavelet [24]	15.41±1.57	0.01±0.00	0.98±0.00		
ANFIS [20]	12.27±1.06	0.04±0.01	0.97±0.01	0.21±0.05	0.12
ANN [20]	11.85±1.16	0.05±0.02	0.96±0.01	0.23±0.03	0.31
ANN [24]	11.90±1.53	0.05±0.02	0.96±0.01		
Subtraction [20]	11.41±0.91	0.05±0.02	0.96±0.01	0.26±0.07	0.42
Subtraction [24]	11.47±1.33	0.05±0.02	0.96±0.00		
RLS [20]	7.89±1.33	0.12±0.03	0.92±0.02	0.65±0.11	69
RLS [24]	8.09±1.29	0.12±0.04	0.92±0.02		
Wavelet [20]	5.26±0.69	0.14±0.12	0.86±0.03	0.71±0.13	0.15
Wavelet [24]	5.36±0.81	0.15±0.03	0.86±0.03		
HPF [20]	7.75±0.79	0.12±0.05	0.89±0.01	0.82±0.12	0.03
HPF [24]	7.63±0.49	0.11±0.04	0.02±0.01		

ET: Estimated calculation time

1.1.2.2. Power line interference

- **Digital filter**

Digital filter is used for removing power line interference from contaminated EMG signals [85-87]. The digital Butterworth filter proposed by Mello [26] was designed based on the frequencies characteristics of the power line signal. Thus, it was implemented as the convolution of six stop-band second-order Butterworth digital filters with rejection bands of 59–61, 119–121, 179–181, 239–241, 299-301, and 359-361 Hz. Moreover, a high-pass second-order Butterworth digital filter with cut-off frequency of 10 Hz and a low-pass eight-order Butterworth digital filter with cut-off frequency of 400 Hz were used for removing low and high frequency noise. The zero-phase filters were implemented on both the forward and reverse directions to obtain zero phase distortion. Note that, the stop-band filter was used instead of a notch filter

because it gave a better efficiency when the power line noise became a broadband noise with increased energy in higher harmonics due to saturation by the amplification.

Later, Butterworth, Chebyshev, and Elliptic digital comb filters were used for removing power line interference from the contaminated EMG signals in [16]. They were implemented as a cascade of four stop-band second-order filters with rejection bands of 49–51, 99–101, 149–151 and 199–201 Hz. Moreover, zero-phase digital filtering was performed to avoid any phase shift [16].

- **Adaptive filter**

Fig. 1.16 shows a basic structure of the adaptive Laguerre filter, which can be considered as a generalization of transversal filter. While $L_0(z)$ is a single pole low-pass filter, $L(z)$ is a first order all-pass filter. The poles of all-pass filters are the same as the poles of low pass filter. The transfer function of $L_0(z)$ and $L(z)$ are given by [27]

$$L_o(z) = \frac{\sqrt{1-a^2}}{1-az^{-1}} \tag{1.2}$$

$$L(z) = \frac{z^{-1}-a}{1-az^{-1}}, |a| < 1. \tag{1.3}$$

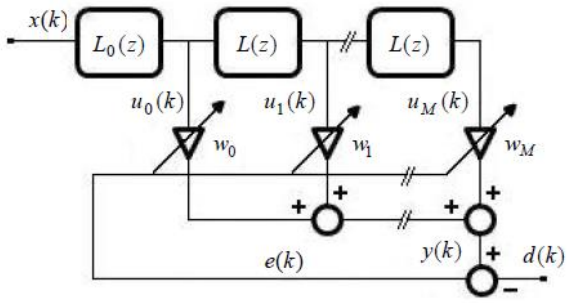

Fig. 1.16. The adaptive Laguerre filter [27].

The weight of the adaptive Laguerre filter was optimized using an LMS algorithm as given by

$$W(k+1) = W(k) + \mu U(k)e(k). \quad (1.4)$$

Fig. 1.17 shows a block diagram of the adaptive power line noise canceller based on the adaptive Laguerre filter proposed in [27]. The reference signal that is correlated with the ECG interference is mathematically constructed by [27]

$$PLI_{ref} = \cos(2\pi 50t)+\cos(2\pi 100t)+\cos(2\pi 200t)+\cos(2\pi 300t)+\cos(2\pi 400t). \quad (1.5)$$

The LMS algorithm was used for adjusting the locations of the poles and zeros. As a result, the optimum weights of the Laguerre filter can be obtained. Finally, the power line interference $y(k)$ was estimated by the weighted linear combination of the filter outputs in the adaptive Laguerre filter.

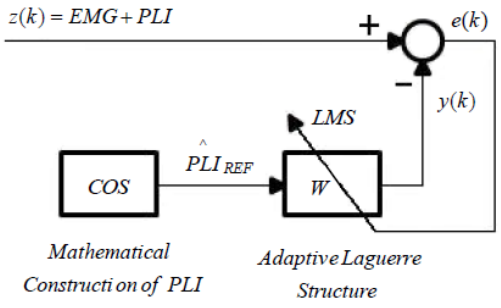

Fig. 1.17. Block diagram of the adaptive power line noise canceller based on an adaptive Laguerre filter proposed in [27].

In [16], the adaptive Laguerre filter was applied to remove power interference at frequency 50, 100, 150, and 200 Hz for comparisons with other techniques. As a result, the complex poles of the adaptive Laguerre filter was set at the frequencies of 75, 125 and 175 Hz, respectively as suggested in the design by [27].

- **Wavelet transform**

Discrete stationary wavelet packet transform (DSWPT) is used to remove power line interference from the contaminated EMG signals [16,90-92]. DSWPT is a shift-invariant transformation [93]. Fig. 1.18 shows the diagram of decomposition step in DSWPT. While the signal cA_j at level j is decomposed by a low pass filter F_j resulting in the low frequency signal cA_{j+1} at level j +1, the signal cA_j at level j is decomposed

by a high pass filter G_j resulting in the high frequency signal cD_{j+1} at level j +1. The fourth-order Meyer wavelet was used as a wavelet function with three-level wavelet decomposition.

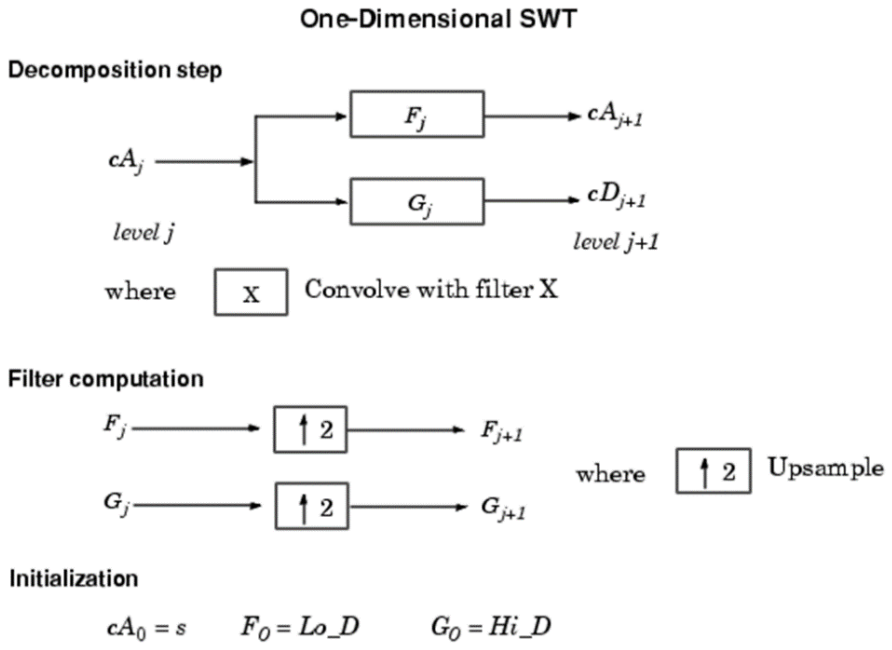

Fig. 1.18. The block diagram of decomposition step in DSWPT.

Fig. 1.19 shows the flowchart used for removing power line interference at frequency 50, 100, 150, and 200 Hz based on DSWPT [16]. It consisted of 5 steps: (1) Detrend and resample signal to obtain a sampling frequency of 1000 Hz, (2) Perform DSWPT decomposition, (3) Estimate rough amplitude and phase of the noise signals, (4) Estimate fine amplitude and phase of the noise signals, and (5) Estimate the EMG signal by subtracting the fine estimation of power line interference from Step (4) from the contaminated EMG signal.

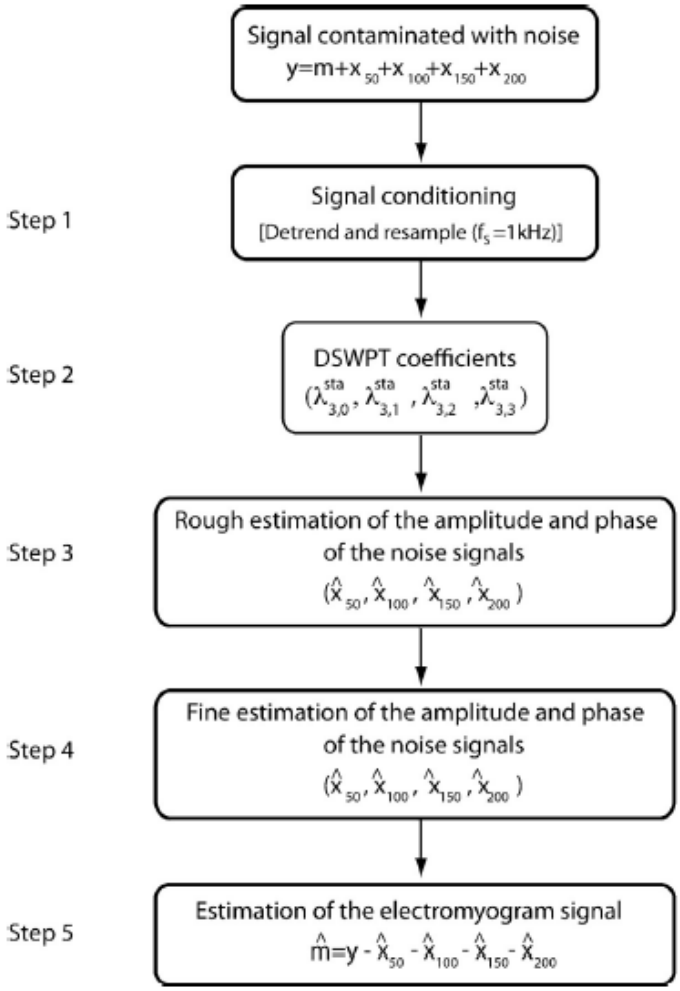

Fig. 1.19. The flowchart used for removing power line interference based on DSWPT [16].

- **Performance evaluations**

Table 1.4 shows the comparisons of mean and standard deviation from various techniques discussed in Section 1.1.2.2 for removal of power line interference from the contaminated EMG signal using R. The DSWPT technique can present the best performance for simulation data and real data compared with the other filters, i.e., the digital Butterworth filter Type 1 and 2 [26], the adaptive Laguerre filter [28], Chebyshev filter [26], and Elliptic filter [26]. Moreover, it is important to note that the obtained correlation coefficient results remain almost constant for all the analyzed

cases, independently of the SNR values of the noisy signal. The correlation coefficient is 0.98–0.99.

Table 1.4. Comparisons of mean and standard deviation from various techniques for removal of power line interference from the contaminated EMG signal using R [16].

SNR	-20 dB	-10 dB	0 dB	10 dB	20 dB
Without filtering	0.1±0.08	0.3±0.07	0.71±0.03	0.95±0.00	1
DSWPT [16]	0.98±0.04	0.99±0.01	0.99±0.01	0.99±0.01	0.99±0.01
Adaptive filter [16]	0.1±0.08	0.3±0.08	0.68±0.09	0.91±0.01	0.94±0.02
Butterworth (Type 1) [16]	0.39±0.20	0.78±0.09	0.95±0.02	0.98±0.01	0.98±0.01
Butterworth (Type 2) [16]	0.49±0.09	0.86±0.04	0.96±0.02	0.98±0.01	0.98±0.01
Cheyshev (Type2) [16]	0.33±0.08	0.74±0.05	0.96±0.02	0.99±0.01	0.99±0.01
Elliptic (Type 2) [16]	0.33±0.08	0.74±0.05	0.96±0.02	0.99±0.01	0.99±0.01

1.1.2.3. Motion artifact

- **Digital filter**

There are a variety of digital filtering techniques for removing motion artifacts from previous publications. A high-pass eighth-order Chebyshev filter with cut-off frequency of 20 Hz is used for removing the motion artifacts from contaminated EMG signals in [30]. Fig. 1.20 (a)-(c) show the synthetic signal simulating two bursts of muscular contraction with a SNR 15 dB, the same signal corrupted by a real motion artifact and noise removal by the Chebyshev filter. We can see that the Chebyshev filter is not suitable for extracting bursts in the case of high motion artifacts superposed to the trace. In addition, a high-pass second-order Butterworth filter at a corner frequency of 20 Hz and a slope of 12 dB per octave is used for removing the motion artifacts from contaminated EMG signals in [14].

A moving average filter is also used for removing motion artifacts from EMG signals [30]. It was implemented by using a window consisting of 49 samples and shifting on the signal by one sample step at sampling frequency 1000 Hz. The average

data sample was estimated in each step. As a result, the value obtained from these steps was assigned to the central window sample. Then, the motion artifact was removed by subtracting the average data sample from the contaminated EMG signal. Moreover, a moving median filter was used to estimate the motion artifact and was subtracted from the contaminated EMG signal [30].

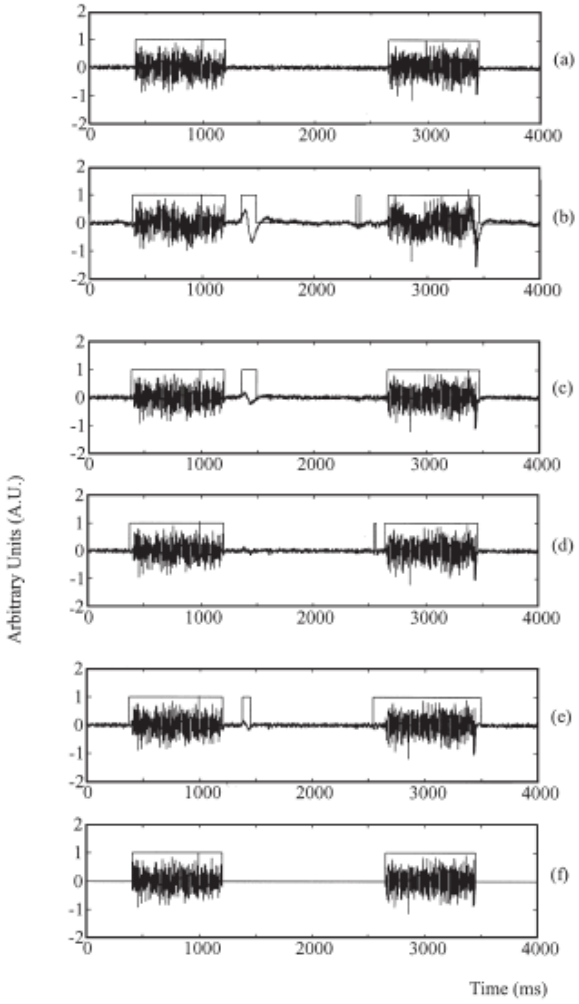

Fig. 1.20. (a) The synthetic signal generated by amplitude modulating a white noise sequence in order to obtain a signal simulating two bursts of muscular contraction with a SNR 15 dB. (b) The same signal corrupted by a real motion artifact. (c) Noise removal by the high pass filter. (d) Noise removal by moving average filter. (e) Noise removal by moving median filter. (f) Noise removal by wavelet procedures [30].

- **Wavelet transform**

Adaptive thresholding in wavelet transform was used for removing motion artifacts from contaminated EMG signals [30]. The wavelet function used was an orthogonal Meyer wavelet. After the contaminated signal was decomposed using discrete wavelet transform, the wavelet coefficients were categorized into 2 classes, namely, a burst zone comprising the mixture of artifacts and EMG signals and an inter-burst zone consisting of only the artifacts. Then, the adaptive threshold was computed to suppress the wavelet coefficients from the artifacts. Finally, an inverse discrete wavelet transform was used to produce the cleaned EMG signal. Fig. 1.20 (d)-(f) shows the performance results of noise removal by moving average filter, moving median filter, and wavelet procedures in [30]. Results show that the wavelet transform technique gives the best performance.

Table 1.5. Comparisons of mean and variance of the MSE values from 4 techniques for removal of motion artifacts in [30].

MSE	High-pass	Moving median	Moving average	Wavelet
Mean value	$2.41.10^{-3}$	$1.78.10^{-3}$	$1.5.10^{-3}$	$1.3.10^{-3}$
Variance	$2.6.10^{-6}$	$7.1.10^{-7}$	$6.7.10^{-7}$	$4.4.10^{-7}$

Table 1.5 shows the comparisons of mean and variance of the MSE values from 4 techniques for removal of motion artifacts from the contaminated EMG signal discussed in Section 1.1.2.1. Results show that the wavelet transform technique gives the best performance, which agrees well with the signal plots shown in Fig. 1.20.

1.2. Research objective

- To develop a novel algorithm for estimating SNR and removing the noise contaminated in the EMG signal in order to obtain the high quality EMG signal.

1.3. Research scope

- In this thesis, only three types of noise contaminated in the EMG signal, namely, ECG interference, power line interference, and motion artifact, will be focused.

1.4. Contribution to this thesis

This thesis studied the contaminations in the EMG signal and corresponding noise removal techniques. We have developed a novel SNR estimating algorithm and a novel noise removal algorithm for three types of noise contaminated in the EMG signal, i.e. ECG interference, power line interference, and motion artifact. On the one hand, for the SNR estimating algorithm, we calculate the feature that is popularly used in recognizing EMG signals. Then, the feature is used as an input of a neural network (NN). The NN output is an SNR estimate. The results showed that the high average correlation coefficient was obtained. On the other hand, for the noise removal algorithm, we proposed to remove noise from the EMG signal while taking into account the SNR. The contaminated EMG signal is decomposed using DSWT. The coefficients for the levels that are contaminated by noise are set to zero when their absolute values are less than or equal to a threshold determined for each SNR level. A clean EMG signal can then be obtained by inverse DSWT mapping of the new thresholded coefficients. The performance based on mean absolute error, correlation coefficient, and relative error shows that the DSWT method is better than a high-pass filter.

1.5. Thesis structure

This thesis is partitioned into five chapters including Chapter 1 Introduction, Chapter 2 Background Chapter 3 Materials and Methods, Chapter 4 Results and Discussion, and Chapter 5 Conclusions. The details of each chapter are described as follows.

Chapter 1 represents the introduction to EMG signal, applications of EMG signal, and an EMG recognition system. The literature review based on types of noise contaminated in EMG signals is presented to point out the study direction.

Chapter 2 describes the background theories of methods used in this research consisting of discrete stationary wavelet transform (DSWT), feature calculation and neural network.

Chapter 3 presents the data generation and methods used in this thesis. The methods can be divided into five main sections: ECG interference removal algorithm based on DSWT, SNR estimation in EMG signals contaminated with ECG interference, threshold estimation EMG signals contaminated with ECG interference, SNR estimation in EMG signals contaminated with powerline interference, SNR estimation in EMG signals contaminated with motion artifact.

Chapter 4 shows and discusses the results from the EMG signal analysis described in Chapter 3. The results are divided into five main sections according to the methods in Chapter 3: removal of ECG interference based on DSWT, threshold estimation EMG signals contaminated with ECG interference, SNR estimation in EMG signals contaminated with ECG interference, SNR estimation in EMG signals contaminated with power line interference, and SNR estimation in EMG signals contaminated with motion artifact.

Chapter 5 presents the conclusions of the noise removal algorithm in the EMG signals contaminated, SNR estimation in EMG signals contaminated with noise, and threshold estimation in EMG signals contaminated with noise described in Chapter 3, the summary of this thesis, and future work.

CHAPTER 2

BACKGROUND

In this chapter, the background theories of methods used in this research are mentioned. The details of discrete stationary wavelet transform (DSWT) are presented in Section 2.1. The description of feature calculation and neural network are described in Section 2.2 and Section 2.3, respectively.

2.1 DSWT

DWT may be replaced with DSWT in some applications where time-invariance is required. DSWT can be implemented by removing the down-samplers and up-samplers in DWT, and by modifying the filters by upsampling the coefficients from the previous decomposition level. However, DSWT is a redundant transform, which contains the same number of samples between the input and the output at each decomposition level [94].

Let $x[n]$ be a signal to be decomposed using L- level DSWT. Two outputs from first level decomposition consist of the approximation coefficients, cA1, from the convolution between a low-pass filter $h_1[n]$ and the input signal $x[n]$ and the detail coefficients, cD1, from the convolution between a high-pass filter $g_1[n]$ and the input signal $x[n]$. Note that the lengths of $x[n]$, cA1, and cD1 are the same. In the next level decomposition, the approximation coefficients, cA1, will be used as input. The filters $h_1[n]$ and $g_1[n]$ are modified by upsampling to $h_2[n]$ and $g_2[n]$. The outputs from second level decomposition can be obtained by convolving cA1 with $h_2[n]$ and $g_2[n]$ resulting in the approximation coefficients cA2 and the detail coefficients cD2, respectively. We can keep repeating these operations until the decomposition level L is reached. Fig.2.1 (a) and (b) shows an example of 5-level DSWT decomposition and the upsampling operation for the filters at each decomposition level, respectively. Fig. 2.2 shows an example of 5-level DSWT reconstruction, where $h_j'[n]$ and $g_j'[n]$ are reconstruction low-pass and high-pass filters at level j, respectively.

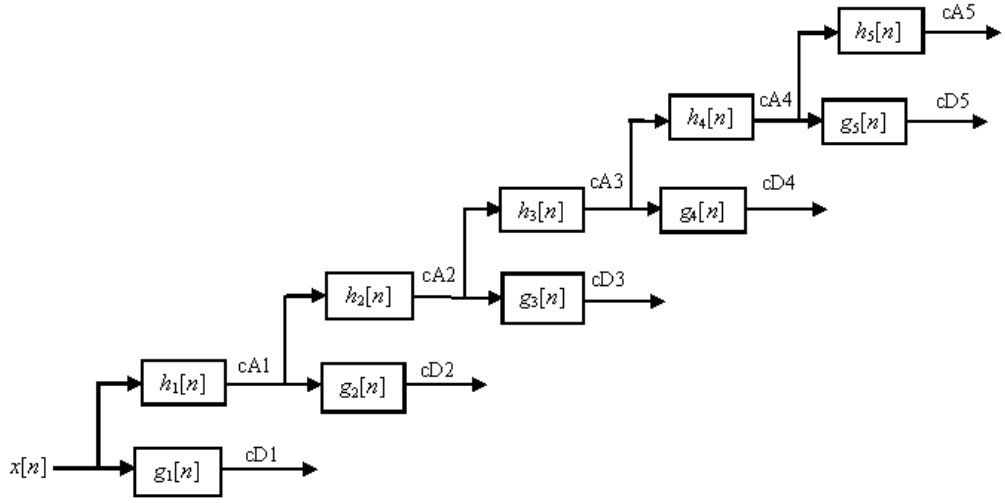

(a)

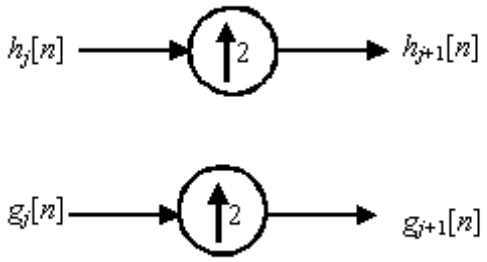

(b)

Fig. 2.1. (a) Example of 5-level DSWT decomposition. (b) Upsampling operation for the filters in each decomposition level [95].

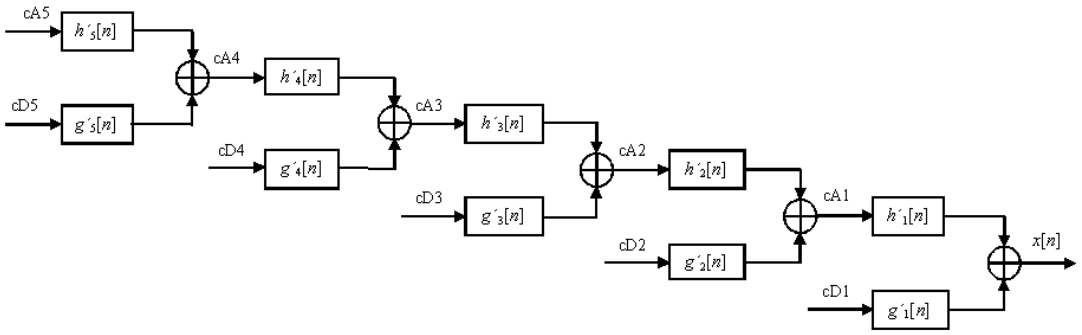

Fig. 2.2. Example of 5-level DSWT reconstruction [95].

2.2 Feature calculation

Feature calculation plays a vital role in improving the performance of the EMG signal recognition system. It is not only a process for reducing the dimensionality of the EMG signals but also useful in extracting significant information. Based on the literature review, the features used with the EMG signal can be categorized into 3 groups, namely, amplitude based features, frequency based features, and statistics based features. We selected two popular features from each group as a representation. We do not randomly select any features into our algorithm development to increase relevance and avoid redundancy. In this thesis, six popular features for the EMG signal recognition are used in estimating SNR including skewness (SKEW), kurtosis (KURT), mean absolute value (MAV), wavelength (WL), zero crossing (ZC), and mean frequency (MNF). While KURT and SKEW are statistics based features, MAV and WL represent the category of amplitude based features. Besides, ZC and MNF are from the category of frequency based features. Brief details of each feature calculation are as follows.

- SKEW is a measure of asymmetry in probability distribution from EMG amplitudes. It is given by [96,97]

$$\text{SKEW} = \frac{\frac{1}{N}\sum_{i=1}^{N}(x_i-\mu)^3}{\left(\sqrt{\frac{1}{N}\sum_{i=1}^{N}(x_i-\mu)^2}\right)^3}, \tag{2.1}$$

  where μ is an average value, xi is the normalized EMG amplitude, and N is the total number of EMG samples under calculation.

- KURT is used to measure the tail characteristic of the probability distribution from the EMG amplitudes. It can be expressed as [97-99]

$$\text{KURT} = \left[\frac{\frac{1}{N}\sum_{i=1}^{N}x_i^4}{\left(\frac{1}{N}\sum_{i=1}^{N}x_i^2\right)^2}\right]\text{-3.} \tag{2.2}$$

- MAV is defined as one of the most popular features and widely used in the analysis of the EMG signal. MAV can be calculated by an average of the absolute values of the EMG amplitudes in a sampled segment. It can be given by [11,100]

$$\text{MAV}=\frac{1}{N}\sum_{i=1}^{N}|x_i| \tag{2.3}$$

- WL is used for measuring the complication of the EMG signal and the increase in the length of EMG waveform over a time segment, which can be expressed as [11]

$$\text{WL}=\sum_{i=1}^{N\text{-}1}|x_{i+1}\text{-}x_i| \tag{2.4}$$

- ZC is determined to quantify the frequency information of the EMG signal. It is defined as the number of times that the EMG amplitudes pass the zero level. We can add the threshold to prevent low voltage fluctuations or background noise. ZC is described by [11,101]

$$\text{ZC}=\sum_{i=1}^{N\text{-}1}[f(x_i\times x_{i+1})\text{and}|x_i\text{-}x_{i+1}|\geq 10] \tag{2.5}$$

where $$f(x)=\begin{cases}1, \text{if } x<0\\ 0, \text{otherwise}\end{cases}$$

- MNF is the sum of the product of the EMG power spectrum and the frequency divided by the total sum of the spectrum intensity. It is also known as not only the average frequency but also the center frequency or the spectral center of gravity [11,102]. It can be given by [11,103]

$$\text{MNF}=\sum_{j=1}^{M}f_jP_j/\sum_{j=1}^{M}P_j \tag{2.6}$$

where f_j is the frequency of the spectrum at frequency bin j, $P_j$is the EMG power spectrum at frequency bin j, and M is the number of the frequency bins.

2.3 Neural network

Neural network (NN) has been successfully applied to a variety of applications, such as speech recognition [104], image analysis [105] and adaptive control [106]. In this paper, NN was used to estimate the SNR when the features described in Section 2.1 were the input. We used a two-layer feedforward network with a sigmoid transfer function in the hidden layer and a linear transfer function in the output layer. Levenberg-Marquardt optimization was performed as a network training function in updating weight and bias values [107]. We evaluated performance between the SNR target and the estimated SNR from NN using a correlation coefficient (CC), which can be expressed as [17,20,108]

$$\mathrm{CC} = \frac{\sum_{i=1}^{N}(s_t(i)-\bar{s}_t)(s_e(i)-\bar{s}_e)}{\sqrt{\sum_{i=1}^{N}(s_t(i)-\bar{s}_t)^2}\sqrt{\sum_{i=1}^{N}(s_e(i)-\bar{s}_e)^2}}, \tag{2.7}$$

where s_t is the true SNR and s_e is the estimated SNR. CC values measure the correlation between outputs and targets. While a CC value of 1 means a close relationship, a CC value of 0 is a random relationship.

CHAPTER 3

METHODS

In this chapter, the data generation and methods used in this research are described. The details of data are described in Section 3.1. The materials and methods of ECG interference removal algorithm based on DSWT and SNR estimation in EMG signals contaminated with ECG interference are described in Section 3.2 and Section 3.3. The materials and methods for threshold estimation in EMG signals contaminated with ECG interference, SNR estimation in EMG signals contaminated with power line interference, and SNR estimation in EMG signals contaminated with motion artifact are mentioned in Section 3.4, Section 3.5, and Section 3.6, respectively.

3.1. Data generation

3.1.1. Simulated EMG

Simulated EMG signals were used in this thesis because we would like to make sure that there was no noise contaminated in the EMG signal. The simulated EMG is generated by filtering white Gaussian noise with a band-pass filter, whose transfer function is given by [108]

$$H(f) = \frac{jf_U^2 f}{(f_L+jf)(f_U+jf)^2} \tag{3.1}$$

where f_L is the lower frequency parameter, which is random from 30-60 Hz and f_U is the upper-frequency parameter, which is random from 30-100 Hz plus f_L. The band-pass filter $H(f)$ was implemented based on Least P-norm optimal IIR filter design. The length of each signal was 2000 samples, which is equivalent to 2 s at a sampling rate of 1000 Hz. Fig. 3.1 shows the waveform of simulated EMG generated with f_L = 45 Hz and f_U = 110 Hz in the time domain (Top panel) and corresponding power spectra in the frequency domain (Bottom panel). We can see that the power spectrum from simulated EMG signal (solid line) agrees well with that from the bandpass filter $H(f)$ (dotted line).

3.1.2. Simulated ECG

We generate simulated ECG signals using a dynamical model based on three coupled ordinary differential equations, which can be expressed as [109]

$$\dot{x} = \alpha x - \omega y \tag{3.2}$$

$$\dot{y} = \alpha y + \omega x \tag{3.3}$$

$$z = -\sum_{i \in \{P,Q,R,S,T\}} a_i \dot{\Delta\theta}_i \exp\left(-\frac{\Delta\theta_i^2}{2b_i^2}\right) - (z - z_0) \tag{3.4}$$

where, $\alpha = 1 - \sqrt{x^2 + y^2}$, $\Delta\theta_i = (\theta - \theta_i) \bmod 2\pi$, $\theta = \text{atan2}(y,x)$ (the four quadrant arctangent of the real parts of the elements of x and y, with $-\pi \leq \text{atan2}(y,x) \leq \pi$) and ω is the angular velocity of the trajectory as it moves around the limit cycle. The parameters θ_i, a_i, and b_i for the PQRST points were suggested by visualization of ECG from a healthy subject. In this paper, the values used for all three parameters in the simulation are given in Table 3.1. The simulated ECG signal was generated with a sampling frequency of 256 Hz. Mean heart rate was randomly selected from 60-100 beats per minute. We chose the length of the analyzed signals to be 2 s. The heart rate was randomly selected between 60-100 beats per minute. As a result, two to three normal beats of ECG interferences were seen in the contaminated EMG signals as shown in Fig. 4.1. If the length was too short, we might not see the ECG interference and could not compute the optimum threshold. We required additional calculations to set the heart rate, which were not included in Equation (3.2)-(3.4). Fig. 3.2 shows an example of simulated ECG signals from 2 mean heart rates in the time domain (Top panel) and their power spectra in the frequency domain (Bottom panel).

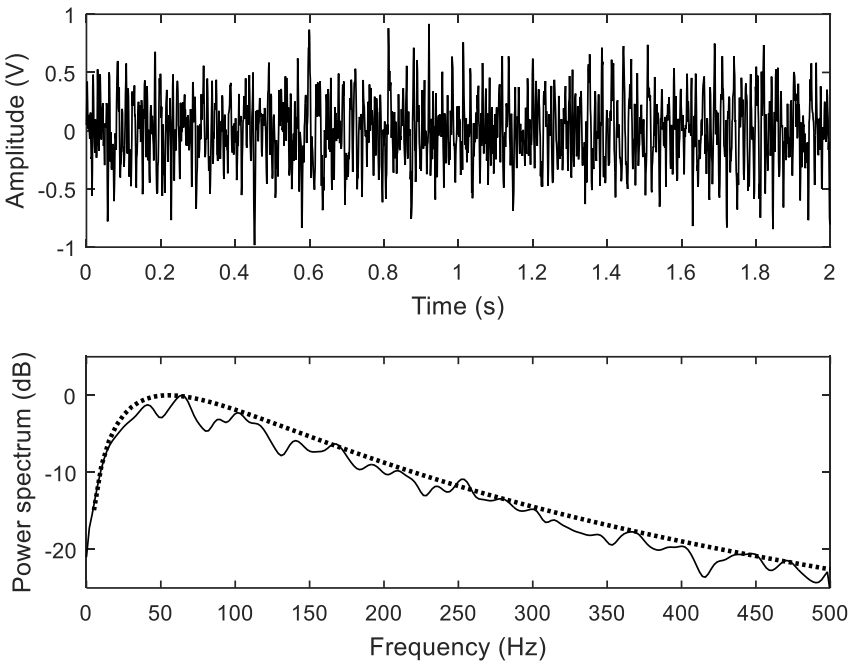

Fig. 3.1. Simulated EMG in the time domain (Top panel) and its power spectrum in the frequency domain (Bottom panel). Solid line: Power spectrum from the simulated EMG signal. Dotted line: Frequency response of the bandpass filter *H(f)*.

Table 3.1. Specific parameters used for generating simulated ECG.

Parameter	Description	P	Q	R	S	T
θ_i (degrees)	Angles of extrema	-70	-15	0	15	100
a_i	z-position of extrema	1.2	-5.0	30.0	-7.5	0.75
b_i	Gaussian width of peaks	0.25	0.1	0.1	0.1	0.4

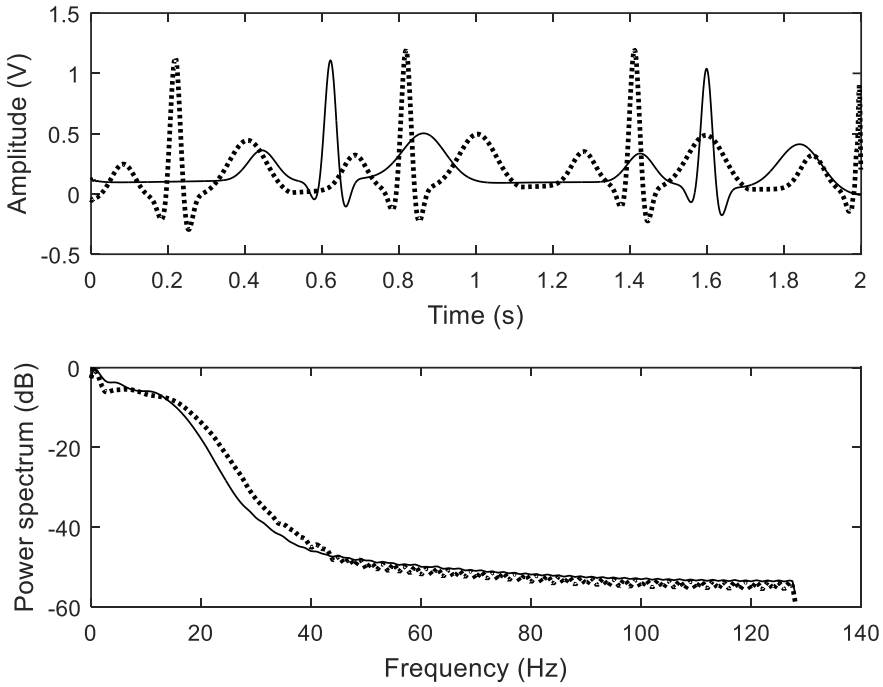

Fig. 3.2. Examples of simulated ECG signals in the time domain (Top panel) and their power spectra in the frequency domain (Bottom panel) when the mean heart rates are 60 (solid line) and 100 (dotted line) beats per minute.

3.1.3. Real ECG

The real ECG signal was obtained from the MIT-BIH arrhythmia database. We acquire a normal ECG beat from 40 records with 20 s for each record. Subsequently, each record was resampled from 360 Hz to 1000 Hz to match with the sampling rate of the EMG signal. Finally, each 20-s data were segmented into 2 s data.

3.1.4. Simulated power line interference

Simulated power line interference is generated by adding a sine wave with a random phase (without harmonics) to the required SNR level. The simulated power line interference signal was generated with a sampling frequency of 1000 Hz.

Phase is random between [0 2π] and frequency is random between 49.5 and 50.5 Hz [110].

3.1.5. Simulated motion artifact

Simulated motion artifact was generated by filtering white Gaussian noise with the fourth-order Butterworth low-pass filter at a cut-off frequency 20 Hz. A sampling frequency of 1000 Hz was used [14,111].

3.1.6. EMG contamination

We generated 9 types of EMG signals contaminated with ECG interference, namely with SNR levels from, -20 dB to 20 dB at 5 dB increments. The SNR was calculated using the equation given by

$$\mathrm{SNR} = 10\log_{10}\left(\frac{\mathrm{P}_x}{\mathrm{P}_n}\right), \tag{3.5}$$

where P_x was an average power of the EMG signal and P_n was an average power of the ECG interference. Two datasets were generated. While the first dataset consisted of the simulated EMG signal contaminated with the simulated ECG interference, the second dataset comprised the simulated EMG signal contaminated with real ECG interference. Details of generating each dataset are as follows.

- Simulated EMG contaminated with simulated ECG (SMSC): Fifty simulated ECG signals and 50 simulated EMG signals were randomly chosen and mixed with amplitude scaling to produce the EMG signals contaminated with ECG at each desired level of SNR.
- Simulated EMG contaminated with real ECG (SMRC): The procedure was similar as for the first dataset, except that the simulated ECG signals were replaced with real ECG signals. As a result, fifty simulated EMG signals contaminated with real ECG interference were obtained at each SNR level.

3.2. Removal of ECG interference based on DSWT

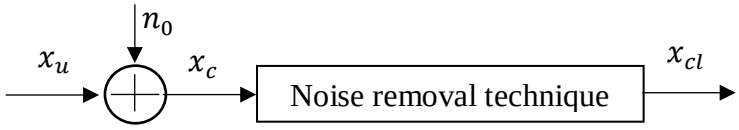

Fig. 3.3. General block diagram of noise removal in the contaminated EMG signal.

We describe a noise removal model in this section. Fig. 3.3 shows a general block diagram of noise removal in the contaminated EMG signal where x_u is an uncontaminated EMG signal, n_0 is ECG interference, x_c is a contaminated EMG signal, and x_{cl} is a contaminated EMG signal that is cleaned by noise removal. After noise removal, the performance of the technique can be measured using criteria based on the mean absolute error (MAE), correlation coefficient (CC), and relative error (RE). We determined three performance measurement methods in this thesis, i.e., the mean absolute error (MAE), correlation coefficient (CC), and relative error (RE). While MAE measures the difference of the clean EMG signal from the uncontaminated EMG signal in the time domain, RE measures the difference in the frequency domain. On the other hand, CC indicates the similarity between the clean and uncontaminated EMG signals. We determined all three measure methods to demonstrate the consistent performance of the proposed algorithm. The MAE can be expressed as [16]

$$\text{MAE} = \frac{1}{N}\sum|x_u - x_{cl}|. \tag{3.6}$$

The closer MAE is to 0, the better is the noise removal. The CC is given by [16,17],

$$\text{CC} = \frac{\sum_{i=1}^{N}(x_u(i)-\bar{x}_u)(x_{cl}(i)-\bar{x}_{cl})}{\sqrt{\sum_{i=1}^{N}(x_u(i)-\bar{x}_u)^2}\sqrt{\sum_{i=1}^{N}(x_{cl}(i)-\bar{x}_{cl})^2}}, \tag{3.7}$$

where x_u is the mean value of uncontaminated EMG signal and x_{cl} is the mean value of the cleaned EMG signal. The closer CC is to 1, the better is the noise removal. The RE can be expressed as [20, 24]

$$\text{RE}= \frac{\sum\{P_{x_u}(f)\text{-}P_{x_{cl}}(f)\}^2}{\sum P_{x_u}(f)^2}, \tag{3.8}$$

where $P_{x_u}(f)$ is the power spectrum of uncontaminated EMG signal and $P_{x_{cl}}(f)$ the power spectrum of the cleaned EMG signal. The closer RE is to 0, the better is the noise removal.

The proposed method for removing the ECG interference from the EMG signal based on DSWT consists of 3 main stages, namely, DSWT decomposition, thresholding, and DSWT reconstruction. Details on each stage are as follows.

Stage (1) Decompose the contaminated EMG signal using 5-level DSWT with the Symlet wavelet function. The Symlet wavelet function was chosen in this paper from the guideline on its successful removal of ECG interference from EMG signal in previous publications [21, 24]. Table 3.2 shows the frequency bands for the wavelet coefficients in the decomposition. We can see that the cutoff frequency of HPF used for removing ECG interference, which is 30 Hz [17, 21, 29, 30], agrees well the combined frequency range of cA5 and cD5.

Table 3.2. Frequency bands in the 5-level DSWT decomposition.

Level (*k*)	cA*k* (Hz)	cD*k* (Hz)
1	0-250	250-500
2	0-125	125-250
3	0-62.5	62.5-125
4	0-31.25	31.25-62.5
5	0-15.625	15.625-31.25

Stage (2) Process the coefficients at cD4 and cD5, which are contaminated by the ECG interference, with a nonlinear thresholding procedure. In other words, the coefficients for cD4 and cD5, whose absolute values are less than or equal to the threshold value, are set to zero. The threshold values are varied from 0 to 10 with increments of 1. As a result, 11×11 = 121 combinations of threshold

levels for cD4 and cD5 are tested. The thresholds that give the best performance based on MAE are selected as optimal. Note that the coefficients in cA5 are set to zero because there are no EMG components in this frequency band.

Stage (3) Obtain the clean EMG signal by applying inverse DSWT to the new coefficients after thresholding from Stage (2).

The performance of the DSWT method was compared with the linear filter technique based on Butterworth HPF [17]. The Butterworth filter was designed using a fourth-order HPF with cutoff frequency 30 Hz and was implemented in both forward and reverse directions to avoid phase distortions. The performance of the DSWT method was evaluated and compared based on MAE, CC, and RE using mean and standard deviation from 50 signal implementations at each SNR.

3.3. SNR estimation in EMG signals contaminated with ECG interference

3.3.1. Feature evaluation in EMG signals contaminated with ECG interference

We describe the method used for evaluating features in this section. Firstly, we generated the EMG signals contaminated with the ECG interferences at 5 SNR levels from -20 dB to 0 dB with a step size of 5. The SNR [-20, 0] dB was of interest because we obtained an excellent detection on the type of noise when the SNR is lower than 0 dB [37]. After the type of noise was known, SNR was estimated with the algorithm that was appropriate to the detected type of noise. The dataset contained the contamination of the simulated EMG signal with the real ECG interference. Fifty real ECG signals were randomly chosen and were amplitude scaling with fifty simulated EMG signals at each SNR level. The SNR was calculated using the Equation (3.5).

Secondly, after the contaminated EMG signal was generated, it was normalized to have unit energy. Normalization was described by

$$x_i = \frac{x_j}{\sqrt{\sum_{i=1}^{N} x_j^2}} \tag{3.9}$$

where x_i is the normalized EMG amplitude, x_j is the EMG amplitude, and N is the length of the signal. Subsequently, the cD4 and cD5 coefficients were determined from the normalized EMG signals. The cD4 and cD5 coefficients were of interest in this study because their frequency bands, namely 31.25-62.5 Hz and 15.625-31.25 Hz, correspond to the frequency component of the ECG interference. Moreover, the Symlet wavelet function was used as suggested from [21].

Finally, we generated six features, namely, SKEW, KURT, MAV, WL, ZC, and MNF, from 50 normalized contaminated EMG signals, cD4, and cD5 coefficients for each SNR level. The boxplots of each feature as a function of 5 SNR levels were used in the evaluation.

3.3.2. Training and testing data preparation for SNR estimation

The EMG signals contaminated with the ECG interference were generated using uniformly random SNR in the range of [-20, 0] dB. Subsequently, we generated two datasets. The first dataset comprised the contamination of simulated EMG signal with the simulated ECG interference. The second dataset contained the contamination of the simulated EMG signal with the real ECG interference. Details of each dataset generation are as follows.

- Contamination of simulated EMG with simulated ECG (SMSC): Three hundred pairs of simulated ECG and EMG signals were randomly selected and combined with amplitude scaling to obtain the EMG signals contaminated with the ECG interference in the range of SNR levels from -20 to 0 at a uniform random distribution. This dataset was used in the training step.
- Contamination of simulated EMG with real ECG (SMRC): This dataset has the same generation process as the SMSC dataset except substituting the simulated ECG signals with the real ECG signals. One hundred simulated EMG signals and 100 real ECG signals were randomly chosen. Subsequently, they were combined to achieve SNR in the range of [-20 0]

dB with a uniform random distribution. This dataset was used in the testing step.

After EMG contamination, we normalize signals and calculate features from both SMSC and SMRC dataset using the method described in Section 3.2.

3.3.3. SNR estimation algorithm

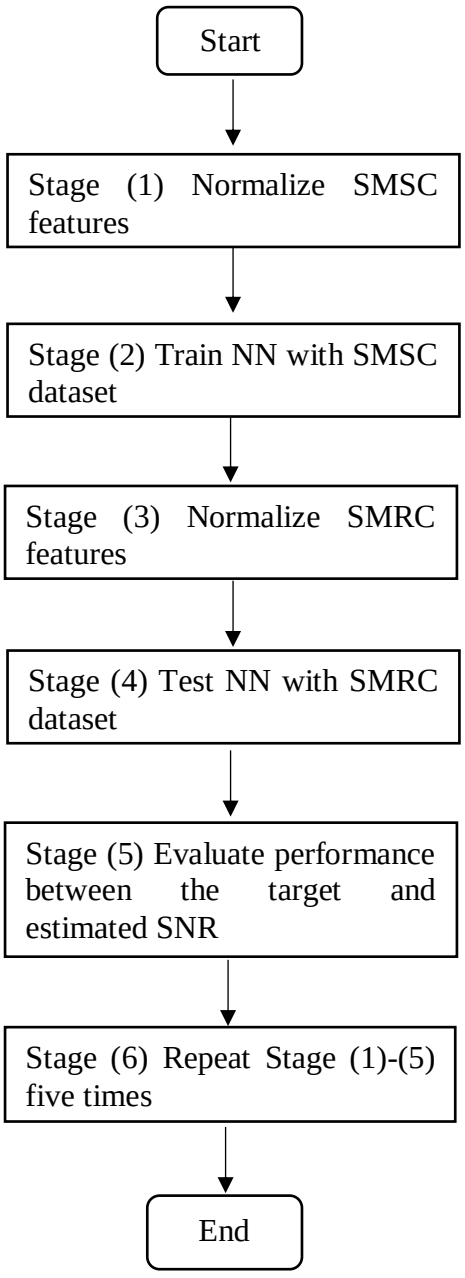

Fig. 3.4. Flowchart of SNR estimation algorithm.

The proposed method for estimating SNR consists of 6 main stages shown in the flowchart of Fig. 3.4. Details on each stage in the flowchart are as follows.

- Stage (1) Normalize each feature from the SMSC dataset by

$$z = \frac{f - \mu}{\sigma} \tag{3.10}$$

  where f is a feature, μ and σ are the mean and standard deviation of each feature, respectively.
- Stage (2) Train NN with the normalized features from Stage (1). The input vectors and targets vectors will be randomly divided into three sets as follows: 70% will be used for training, 15% will be used to validate that the network is generalizing and to stop training before overfitting. The last 15% will be used as a completely independent test of generalization. The number of hidden neurons is 20.
- Stage (3) Normalize each feature from the SMRC dataset using Equation (3.10) and use them as the testing data.
- Stage (4) Apply the trained NN from Stage (2) to the testing data from Stage (3).
- Stage (5) Evaluate performance between the SNR target and the estimated SNR from NN using CC.
- Stage (6) Repeat Stage (1)-(5) for five times using new generated SMSC and SMRC data. Evaluate the performance of the proposed algorithm using the mean and standard deviation from 5 CC values.

3.4. Threshold estimation in EMG signals contaminated with ECG interference

3.4.1. Training and testing data preparation

The EMG signals contaminated with the ECG interference were generated using uniformly random SNR in the range of [-20, 0] dB. Subsequently, we

generated two datasets. The first dataset comprised the contamination of simulated EMG signal with the simulated ECG interference. The second dataset contained the contamination of the simulated EMG signal with the real ECG interference. Details of each dataset generation are as follows.

- Contamination of simulated EMG with simulated ECG (SMSC): Three hundred pairs of simulated ECG and EMG signals were randomly selected and combined with amplitude scaling to obtain the EMG signals contaminated with the ECG interference in the range of SNR levels from -20 to 0 at a uniform random distribution. Subsequently, the two optimal thresholds, i.e. Th1 for cD4 and Th2 for cD5, were determined using the method described in Section 3.2. This dataset was used in the training step.
- Contamination of simulated EMG with real ECG (SMRC): This dataset has the same generation process as the SMSC dataset except substituting the simulated ECG signals with the real ECG signals. One hundred simulated EMG signals and 100 real ECG signals were randomly chosen. Subsequently, they were combined to achieve SNR in the range of [-20 0] dB with a uniform random distribution. This dataset was used in the testing step to estimate the threshold values $Th1_{est}$ and $Th2_{est}$.

After EMG contamination, we normalize signals and calculate features from both SMSC and SMRC dataset using the method described in Section 3.2.

3.4.2. Threshold estimation algorithm

The proposed method for estimating the threshold value for ECG interference removal based on DSWT has the same generation process as the SNR estimation algorithm as shown in the flowchart of Fig. 3.4 except substituting the threshold input with the SNR input.

3.5. SNR estimation in EMG signals contaminated with power line interference

3.5.1. Feature evaluation in EMG signals contaminated with power line interference

We describe the method used for evaluating features in this section. Firstly, we generated the EMG signals contaminated with the power line interference at 5 SNR levels from -20 dB to 0 dB with a step size of 5. The SNR [-20, 0] dB was of interest because we obtained an excellent detection on the type of noise when the SNR is lower than 0 dB [37]. After the type of noise was known, SNR was estimated with the algorithm that was appropriate to the detected type of noise. The dataset contained the contamination of the simulated EMG signal with the simulated power line interference. Fifty simulated power line interference signals were randomly chosen and were amplitude scaling with fifty simulated EMG signals at each SNR level. The SNR was calculated using the Equation (3.5).

Secondly, after the contaminated EMG signal was generated, it was normalized to have unit energy. Normalization was described by Equation (3.9).

Finally, we generated six features, namely, SKEW, KURT, MAV, WL, ZC, and MNF, from 50 normalized contaminated EMG signals, cD4, and cD5 coefficients for each SNR level. The boxplots of each feature as a function of 5 SNR levels were used in the evaluation.

3.5.2. Training and testing data preparation for SNR estimation

The EMG signals contaminated with the power line interference were generated using uniformly random SNR in the range of [-20, 0] dB. Subsequently, we generated two datasets. The first dataset comprised the contamination of simulated EMG signal with the simulated power line interference. Details of each dataset generation are as follows.

- Contamination of simulated EMG with simulated power line interference (SMSC): Three hundred pairs of simulated power line interference and EMG signals were randomly selected and combined with amplitude scaling

to obtain the EMG signals contaminated with the power line interference in the range of SNR levels from -20 to 0 at a uniform random distribution. This dataset was used in the training step. One hundred simulated EMG signals and 100 simulated power line interference signals were randomly chosen. Subsequently, they were combined to achieve SNR in the range of [-20 0] dB with a uniform random distribution. This dataset was used in the testing step.

After EMG contamination, we normalize signals and calculate features from SMSC dataset using the method described in Section 3.2.

3.5.3. SNR estimation algorithm

The proposed method for estimating SNR has the same generation process as the SNR estimation algorithm as shown in the flowchart of Fig. 3.4 except substituting the powerline interference input with the ECG interference input.

3.6. SNR estimation in EMG signals contaminated with motion artifact

3.6.1. Feature evaluation in EMG signals contaminated with motion artifact

We describe the method used for evaluating features in this section. Firstly, we generated the EMG signals contaminated with the motion artifact at 5 SNR levels from -20 dB to 0 dB with a step size of 5. The SNR [-20, 0] dB was of interest because we obtained an excellent detection on the type of noise when the SNR is lower than 0 dB [37]. After the type of noise was known, SNR was estimated with the algorithm that was appropriate to the detected type of noise. The dataset contained the contamination of the simulated EMG signal with the simulated motion artifact. Fifty simulated motion artifact signals were randomly chosen and were amplitude scaling with fifty simulated EMG signals at each SNR level. The SNR was calculated using the Equation (3.5).

Secondly, after the contaminated EMG signal was generated, it was normalized to have unit energy. Normalization was described by Equation (3.9).

Finally, we generated six features, namely, SKEW, KURT, MAV, WL, ZC, and MNF, from 50 normalized contaminated EMG signals, cD4, and cD5 coefficients for each SNR level. The boxplots of each feature as a function of 5 SNR levels were used in the evaluation.

3.6.2. Training and testing data preparation for SNR estimation

The EMG signals contaminated with the motion artifact were generated using uniformly random SNR in the range of [-20, 0] dB. Subsequently, we generated two datasets. The first dataset comprised the contamination of simulated EMG signal with the simulated motion artifact. Details of each dataset generation are as follows.

- Contamination of simulated EMG with simulated motion artifact (SMSC): Three hundred pairs of simulated motion artifact and EMG signals were randomly selected and combined with amplitude scaling to obtain the EMG signals contaminated with the motion artifact in the range of SNR levels from -20 to 0 at a uniform random distribution. This dataset was used in the training step. One hundred simulated EMG signals and 100 simulated motion artifact signals were randomly chosen. Subsequently, they were combined to achieve SNR in the range of [-20 0] dB with a uniform random distribution. This dataset was used in the testing step.

After EMG contamination, we normalize signals and calculate features from SMSC dataset using the method described in Section 3.2.

3.6.3. SNR estimation algorithm

The proposed method for estimating SNR has the same generation process as the SNR estimation algorithm as shown in the flowchart of Fig. 3.4 except substituting the motion artifact input with the ECG interference input.

CHAPTER 4

RESULTS AND DISCUSSION

In this chapter, the results of the ECG interference removal algorithm based on DSWT as described in Chapter 3 are shown and discussed. The results of performance evaluation for the ECG interference removal algorithm based on DSWT using MAE, CC, and RE, respectively, compared to HPF as mentioned in Section 4.1. The results of feature evaluation and SNR estimation for ECG interference contaminated in the EMG signal as given in Section 4.2. The results of threshold estimation in EMG signals contaminated with ECG interference Section 4.3. The results of feature evaluation and SNR estimation for power line interference as discussed in Section 4.4 and motion artifact as described in Section 4.5.

4.1. Removal of ECG interference based on DSWT

4.1.1. Results

We implemented the ECG interference removal algorithm based on DSWT as described in Section 3.2. In this section, we demonstrate the results of its performance using MAE, CC, and RE in Table 4.1, 4.2, and 4.3, respectively.

Table 4.1 shows a comparison of MAE for DSWT and HPF noise removal techniques using SMSC and SMRC datasets indicating that DSWT outperforms HPF. Across the SMSC cases, MAE from DSWT decreased approximately from 0.15 to 0.08 when SNR increased from -20 to 20 dB. However, MAE for HPF was quite comparable at every SNR, at approximately 0.20. Across SMRC cases, we can see a similar trend as with SMSC for SNR from 0 to 20 dB. However, with SNR from -20 to -5 dB, MAE across SMRC was higher than across SMSC when compared by SNR.

A comparison of CC for DSWT and HPF noise removal techniques across SMSC and SMRC datasets is shown in Table 4.2. The results show that CC for DSWT was better than for HPF. When the SNR increased from -20 to 20 dB, the CC

for DSWT increased from 0.96 to 0.99 across SMSC cases. However, CC for HPF was entirely consistent at approximately 0.96, independent of the SNR. With SMRC data, at SNR from 0 to 20 dB, we can see a similar trend as with SMSC.

Table 4.1. Comparison of MAE for DSWT and HPF noise removal techniques.

SNR(dB)	SMSC		SMRC	
	DSWT	HPF	DSWT	HPF
-20	0.1598±0.0301	0.2296±0.0359	0.4146±0.1034	0.7396±0.2293
-15	0.1468±0.0305	0.2071±0.0465	0.2968±0.0717	0.4181±0.1266
-10	0.1286±0.0252	0.2122±0.0520	0.1930±0.0401	0.2894±0.0567
-5	0.1180±0.0289	0.2021±0.0393	0.1600±0.0306	0.2477±0.0493
0	0.1168±0.0295	0.2097±0.0441	0.1311±0.0288	0.2167±0.0430
5	0.1070±0.0226	0.2057±0.0501	0.1070±0.0248	0.2129±0.0488
10	0.0986±0.0223	0.2189±0.0460	0.0987±0.0212	0.2021±0.0421
15	0.0871±0.0195	0.2060±0.0409	0.0942±0.0225	0.2137±0.0440
20	0.0829±0.0187	0.2129±0.0464	0.0832±0.0180	0.2065±0.2078

Table 4.2. Comparison of CC for DSWT and HPF noise removal techniques.

SNR(dB)	SMSC		SMRC	
	DSWT	HPF	DSWT	HPF
-20	0.9564±0.0156	0.9529±0.0143	0.8373±0.0808	0.5813±0.1577
-15	0.9717±0.0105	0.9634±0.0169	0.9161±0.0356	0.7948±0.1021
-10	0.9815±0.0066	0.9615±0.0197	0.9611±0.0171	0.9019±0.0512
-5	0.9856±0.0067	0.9663±0.0125	0.9738±0.0097	0.9418±0.0268
0	0.9863±0.0075	0.9634±0.0162	0.9813±0.0084	0.9582±0.0175
5	0.9889±0.0047	0.9645±0.0186	0.9876±0.0069	0.9609±0.0184
10	0.9915±0.0038	0.9601±0.0180	0.9903±0.0043	0.9655±0.0151
15	0.9937±0.0028	0.9652±0.0137	0.9919±0.0038	0.9624±0.0154
20	0.9944±0.0028	0.9618±0.0171	0.9943±0.0023	0.9644±0.0155

Table 4.3. Comparison of RE for DSWT and HPF noise removal techniques.

SNR(dB)	SMSC		SMRC	
	DSWT	HPF	DSWT	HPF
-20	0.0153±0.0199	0.0514±0.0420	0.2045±0.2263	45.38±67.2631
-15	0.0142±0.0152	0.0607±0.0546	0.1054±0.2155	2.0230±3.7012
-10	0.0120±0.0136	0.0774±0.0634	0.0164±0.0170	0.2648±0.4327
-5	0.0124±0.0210	0.0647±0.0399	0.0586±0.0624	0.0724±0.0866
0	0.0258±0.0340	0.0798±0.0550	0.0346±0.0389	0.0666±0.0560
5	0.0380±0.0435	0.0791±0.0617	0.0102±0.0129	0.0723±0.0616
10	0.0074±0.0094	0.0892±0.0582	0.0047±0.0069	0.0651±0.0496
15	0.0137±0.0172	0.0727±0.0464	0.0051±0.0057	0.0825±0.0494
20	0.0066±0.0117	0.0770±0.0521	0.0046±0.0048	0.0748±0.0547

However, for SNR from -20 to -5 dB, CC across SMRC was lower than across SMSC when compared at similar SNR.

Table 4.4. Comparison of optimal threshold levels based on MAE.

SNR(dB)	SMSC		SMRC	
	cD4	cD5	cD4	cD5
-20	7.98±1.86	5.76±1.29	4.70±2.44	3.74±2.51
-15	9.42±0.84	5.30±1.09	6.02±1.60	4.70±2.53
-10	8.00±0.90	4.92±1.29	7.36±1.75	5.02±1.86
-5	7.42±0.99	4.90±1.11	7.26±1.12	5.78±1.63
0	7.42±0.97	4.76±0.92	7.26±1.10	5.14±1.26
5	7.12±1.02	5.04±1.34	7.12±0.92	4.70±1.04
10	7.16±1.09	5.34±1.26	7.22±0.79	4.90±1.31
15	7.00±0.99	5.62±1.24	7.48±1.18	5.30±1.30
20	7.16±1.15	5.38±1.14	7.40±1.23	5.22±1.07

A comparison of RE for DSWT and HPF noise removal techniques is shown in Table 4.3. Across SMSC, RE for DSWT was better than for HPF. Across SMRC, we can see that DSWT (0.2) provided a significantly better average RE than HPF (45.4) at SNR -20 dB. Also, a similar pattern is seen for SNR -15 and -10 dB.

The SNR of the contaminated EMG signal affected the optimal threshold level. Table 4.4 shows the optimal threshold levels based on MAE in DSWT noise removal. For DSWT, significant differences in the threshold levels between the two datasets are observed at SNR -20 and -15 dB for both cD4 and cD5. The threshold levels with SMRC are smaller than those with SMSC, which may be caused by an attempt to remove other types of artifacts, such as power line interference, contaminating the EMG signals.

4.1.2. Discussion

In this section, we explored more insights of the results from Section 4.1.1. Fig. 4.1 shows an example of signals from DSWT thresholding. Fig. 4.1(a) shows the EMG signal contaminated with simulated ECG at SNR of -20 dB. Fig. 4.1(b) depicts the signals from DSWT at cD4 decomposition level before thresholding with a dotted line and after thresholding with a solid line. The optimal threshold is 8. Therefore, the coefficients from cD4 decomposition level before thresholding, whose absolute values are greater than 8, are truncated to 0. Fig.4.1(c) shows similar processing for coefficients in cD5 decomposition level with the optimal threshold 6. Fig. 4.1(d)-(f) show the results from the EMG signal

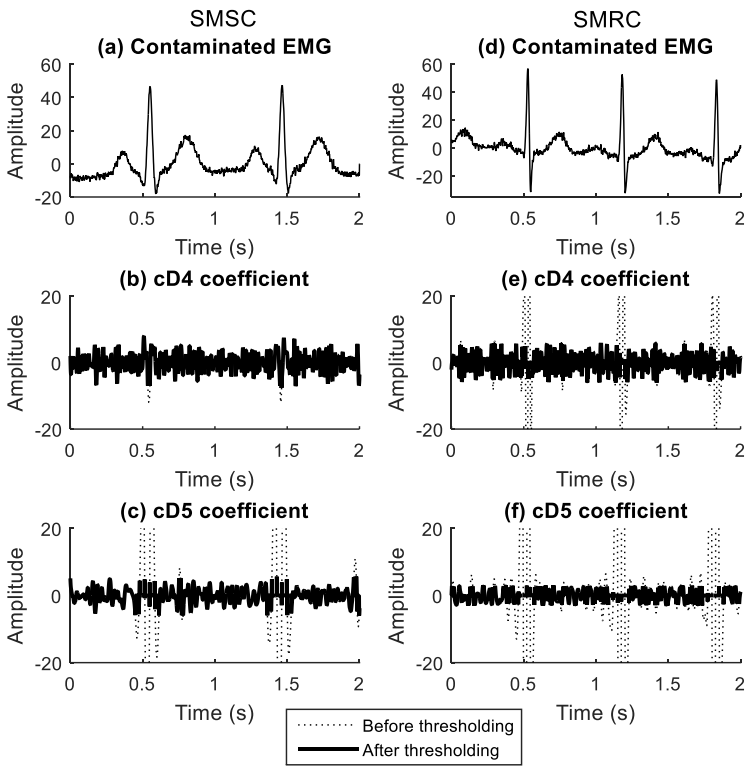

Fig. 4.1. While the left column shows an example of results with SMSC, the right column shows an example of results with SMRC data. The top, middle, and bottom rows show EMG signal contaminated with ECG at SNR -20 dB, signals from DSWT at cD4 decomposition level, and signals from DSWT at cD5 decomposition level, respectively. Dotted line: Detail coefficients before thresholding. Thick line: Detail coefficients after thresholding.

contaminated with real ECG at SNR of -20 dB. The optimal thresholds for the coefficients in cD4 and cD5 decomposition levels are 6 and 3, respectively. We can see the ECG signal component in cD4 of SMRC, but it is invisible in SMSC. These results indicate that the real ECG signal has the frequency range 32.5-62.5 Hz, which cannot be removed using the Butterworth HPF with cutoff frequency 30 Hz as proposed in [10].

After thresholding, the cleaned EMG signal was reconstructed. Fig. 4.2(a) shows the cleaned EMG signal from DSWT obtained by inverse DSWT of thresholded coefficients, from Fig. 4.1(b)-(c), compared with the cleaned EMG signal from HPF (Fig. 4.2(b)) and the uncontaminated EMG signal (Fig. 4.2(c)). We can see

that both DSWT and HPF give similar waveforms compared to the uncontaminated EMG signal. Fig. 4.3(a) shows the absolute errors of cleaned EMG signal from DSWT and uncontaminated EMG signal (solid line) compared to those of the cleaned EMG signal from HPF and uncontaminated EMG signal (dotted line). We can see that the results from DSWT are better than from HPF, which matches the MAE for DSWT (0.1771) being better than that for HPF (0.2563). Fig. 4.3(b) shows the power spectrum for DSWT (thick line) compared with those for HPF (thin line) and uncontaminated EMG (dotted line). The power spectrum for DSWT is closer to that from uncontaminated EMG compared to that from HPF. These results are in agreement with RE. In other words, RE for DSWT is 0.0131 compared to 0.0460 for HPF.

Fig. 4.2. Example of cleaned signals and the uncontaminated EMG signal from SMSC.

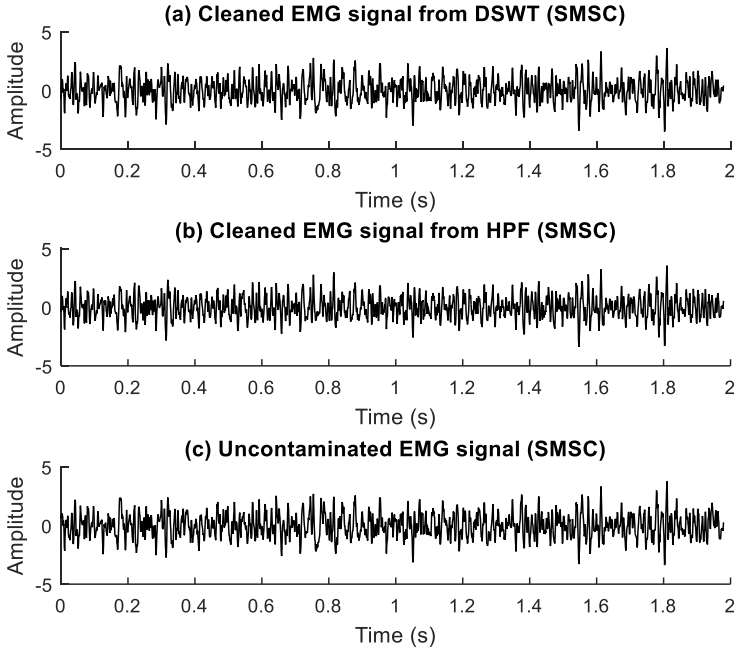

(a) Cleaned EMG signal obtained by inverse DSWT of thresholded decomposition, from Fig. 7(b)-(c) . (b) Cleaned EMG signal from HPF. (c) Uncontaminated EMG signal.

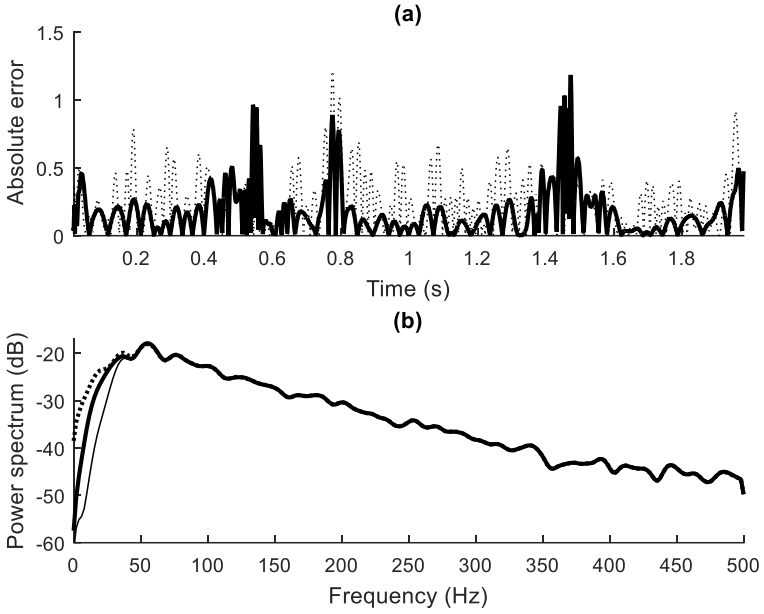

Fig. 4.3. Comparison of cleaned EMG signals and uncontaminated EMG signal in SMSC data. (a) Absolute errors of cleaned EMG signal from DSWT and uncontaminated EMG signal (solid line) compared to those of cleaned EMG signal from HPF and uncontaminated EMG signal (dotted line). (b) The power spectrum of cleaned EMG signal from DSWT (thick line) compared to that of uncontaminated EMG signal (dotted line) and cleaned EMG signal from HPF (thin line).

Similar results were obtained from SMRC data. Fig. 4.4 shows cleaned signals and their corresponding uncontaminated EMG signal in SMRC data. In Fig. 4.4 (b), we can see that HPF cannot completely remove ECG interference at a time around 0.4-0.6s, 1.2s, and 1.8-2s. These may be caused by other types of noise, such as power line interference in the EMG signals. However, the cleaned EMG signal from DSWT shown in Fig. 4.4(a) not only provides a significantly better result than HPF but also has an excellent agreement with the uncontaminated EMG signal shown in Fig. 4.4 (c).

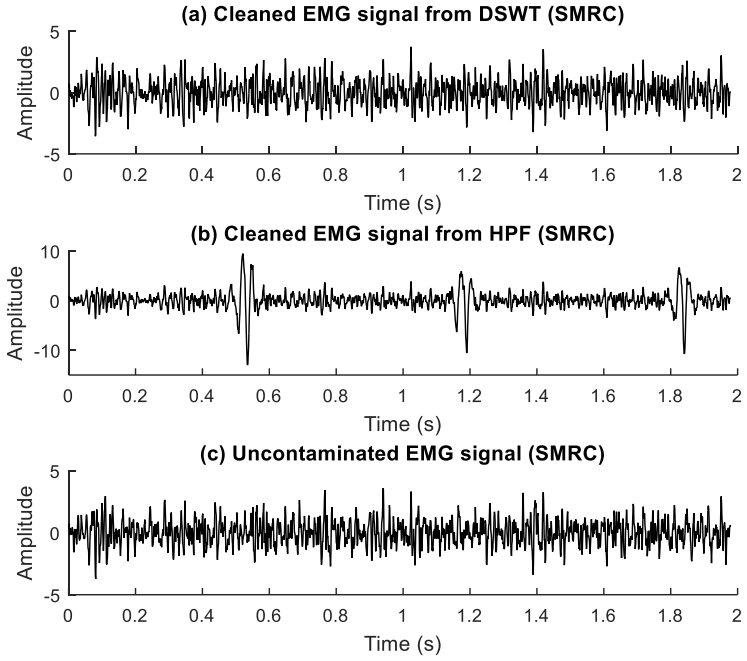

Fig. 4.4. Example of cleaned signals and the uncontaminated EMG signal from SMRC. (a) Cleaned EMG signal from DSWT based algorithm as in Fig. 7(e)-(f). (b) Cleaned EMG signal from HPF. (c) Uncontaminated EMG signal.

The absolute errors of cleaned EMG signal from DSWT and uncontaminated EMG signal (solid line) compared to those of cleaned EMG signal from HPF and uncontaminated EMG signal (dotted line) are shown in Fig. 4.5(a). We can see that DSWT gives better results than HPF does. As a result, MAE and CC for DSWT are noticeably better than those for HPF. In other words, while MAE and CC for DSWT are 0.4490 and 0.8353, MAE and CC for HPF are 0.8298 and 0.4831. Fig. 4.5(b) shows the power spectra for DSWT (thick line), HPF (thin line), and uncontaminated EMG (dotted line). We can see that the power spectrum for DSWT is comparable with that for uncontaminated EMG. However, the power spectrum for HPF is significantly different from that of uncontaminated EMG. These results agree with RE for DSWT (0.1947) compared with that for HPF (43.6027).

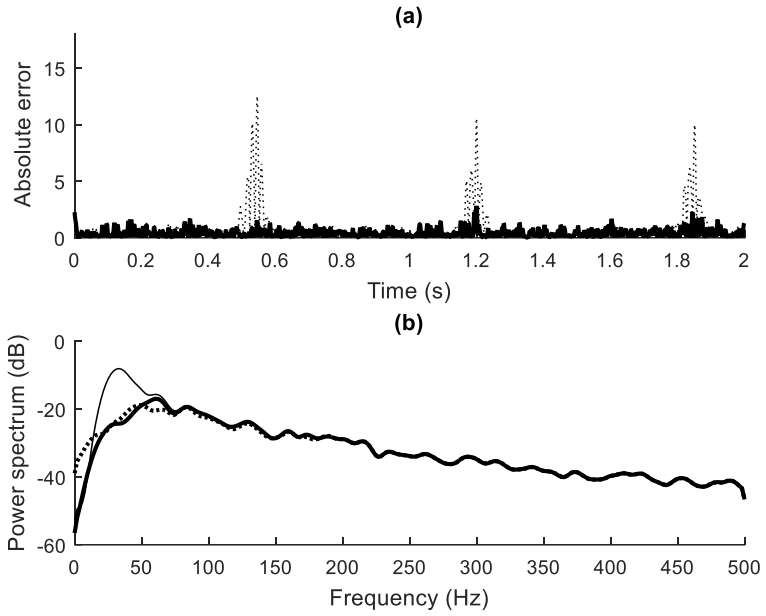

Fig. 4.5. Comparison of cleaned EMG signals and uncontaminated EMG signal from SMRC. (a) Absolute errors of cleaned EMG signal from DSWT and uncontaminated EMG signal (solid line) compared to those of cleaned EMG signal from HPF and uncontaminated EMG signal (dotted line). (b) The power spectrum of cleaned EMG signal from DSWT (thick line) compared to that of uncontaminated EMG signal (dotted line) and cleaned EMG signal from HPF (thin line).

When there are variations in the EMG recording, the power spectra of the EMG signal change. For example, the dominant frequency of the EMG recording decreases as a result of muscle fatigue, which can be measured using the median frequency [23]. The performances that we reported were based on the average and standard deviation of MAE, CC, and RE from the simulated EMG signals generated by the band-pass filter with variation in bandwidths. Therefore, the proposed approach would be applicable from the perspective of variations in the EMG recording.

4.2. SNR estimation in EMG signals contaminated with ECG interference

4.2.1. Results

4.2.1.1. Feature evaluation

We determined six features with the contaminated EMG signals at five SNR levels generated using the method given in Section 3.3.1. Fig. 4.6 shows the boxplots from six features determined using SMRC data as a function of SNR. Fig. 4.6(a) shows the boxplots of SKEW from raw, cD4, and cD5 data in the top, middle, and bottom panels, respectively. Fig. 4.6(b)-(f) show similar boxplots from other five features, namely, KURT, MAV, WL, ZC, and MNF. The WL feature from the raw EMG data gives the best separation of boxplot as shown in the top panel of Fig. 4.6(d). However, the SKEW features from cD4 and cD5 decomposition levels do not give good separation of boxplot as shown in Fig 4.6(a).

4.2.1.2. SNR estimation

We implemented the SNR estimation algorithm as described in Section 3.3.2 and demonstrated the performance of SNR estimation for a single feature and paired features using CC in Table 4.5 and 4.6, respectively. Table 4.5 shows the mean and standard deviation for CC from different single features obtained with the SMRC data when these six features are calculated using raw, cD4, and cD5 EMG data. We can see that the WL feature from the raw EMG data gives the best average CC at 0.9663. The best average CCs from cD4 and cD5 are 0.7738 and 0.8359, respectively. These results show that the SNR estimation of the EMG signal contaminated with the ECG interference using the raw EMG data is better than that from the DSWT data. Table 4.6 shows the mean and standard deviation for CC from different pairs of features obtained with the SMRC data. We can see that the combination of WL and MNF (WL+MNF) from the raw EMG data gives the best average CC at 0.9566. Fig 4.7 shows an example of the correlation plot for the SNR estimation from NN with the WL feature from the

raw EMG data. The cc value of 0.9784 agrees well with the results from the WL feature using the raw data (0.9663 ± 0.0085) shown in Table 4.5.

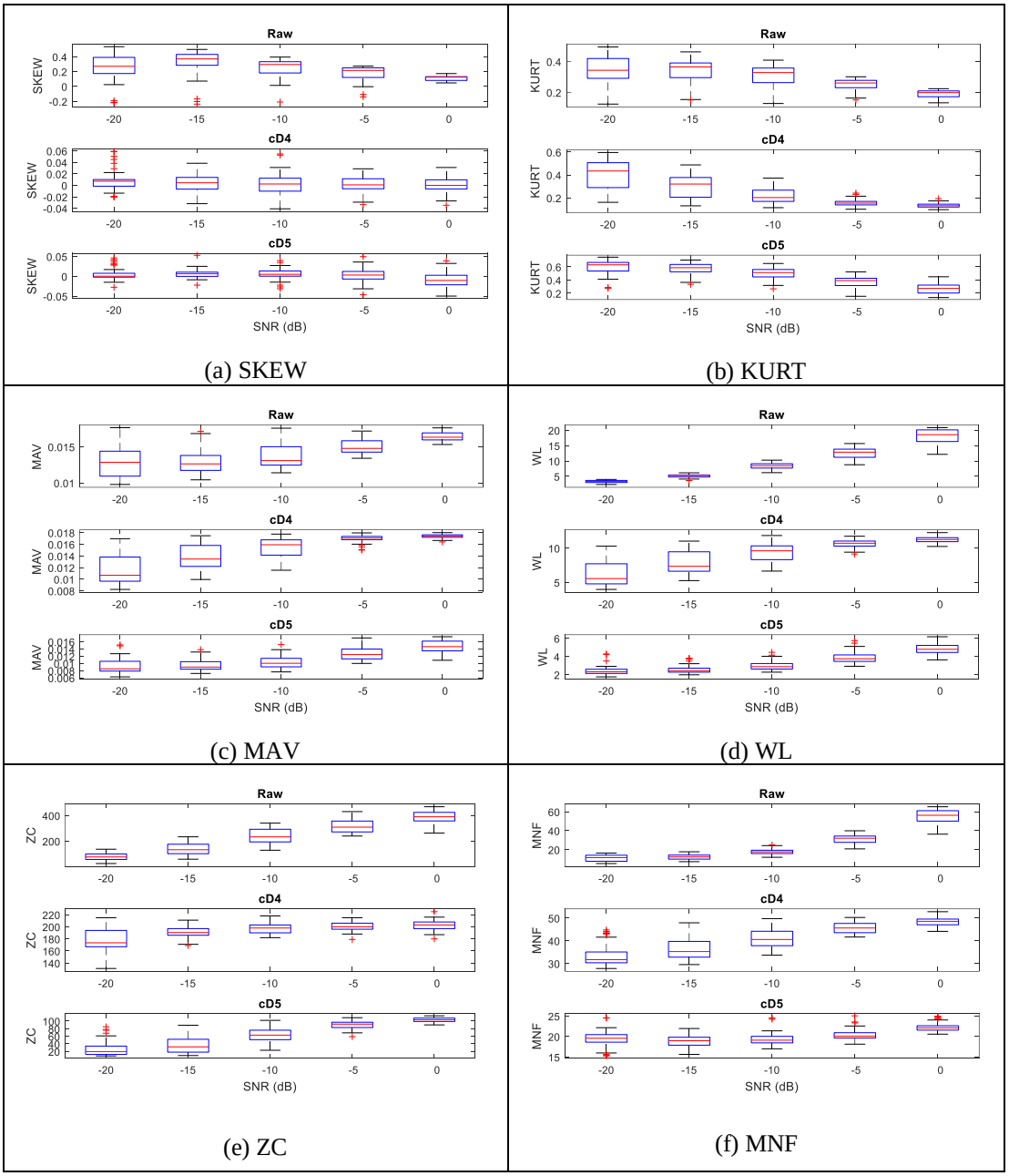

(a) SKEW (b) KURT

(c) MAV (d) WL

(e) ZC (f) MNF

Fig. 4.6. Boxplots of feature values determined using the SMRC data as a function of SNR. (a) SKEW. (b) KURT. (c) MAV. (d) WL. (e) ZC. (f) MNF.

Table 4.5. Mean and standard deviation of CC from different single features obtained with the SMRC data.

Features	Raw	cD4	cD5
SKEW	0.5541 ± 0.0754	-0.0896 ±0.0935	0.2054 ± 0.1834
KURT	0.6400± 0.0409	0.6982 ± 0.0877	0.7678 ± 0.0162
MAV	0.4903 ± 0.1109	0.7152 ± 0.0244	0.7137 ± 0.0219
WL	0.9663 ± 0.0085	0.7738 ± 0.0244	0.8264 ± 0.0282
ZC	0.8321 ± 0.0358	0.5064 ± 0.0602	0.8359 ± 0.0208
MNF	0.9146 ± 0.0296	0.7114 ± 0.0858	0.5247 ± 0.0679

Table 4.6. Mean and standard deviation of CC from different pairs of features obtained with the SMRC data.

Features	Raw	cD4	cD5
SKEW+KURT	0.3765±0.1037	0.5980±0.1137	0.7398±0.0573
SKEW+WL	0.7591±0.2312	0.6599±0.0518	0.8295±0.0374
SKEW+ZC	0.7686±0.0848	0.3412±0.0292	0.7966±0.0833
SKEW+MAV	0.3903±0.1008	0.5491±0.1365	0.6882±0.0475
SKEW+MNF	0.7743±0.0894	0.7103±0.0545	0.5002±0.0312
KURT+WL	0.9475±0.0261	0.7192±0.0353	0.8649±0.0281
KURT+ZC	0.8822±0.0329	0.6907±0.0673	0.8005±0.0278
KURT+MAV	0.5172±0.0533	0.6732±0.0508	0.7083±0.0327
KURT+MNF	0.8844±0.0364	0.7385±0.0414	0.7211±0.0685
WL+ZC	0.8837±0.0470	0.7177±0.0473	0.8382±0.0248
WL+MAV	0.9144±0.0392	0.7235±0.0458	0.8586±0.0184
WL+MNF	0.9566±0.0097	0.6953±0.0821	0.7251±0.0841
ZC+MAV	0.8597±0.0417	0.6994±0.0549	0.7936±0.0229
ZC+MNF	0.9272±0.0229	0.7158±0.0517	0.7610±0.1661
MAV+MNF	0.8517±0.0870	0.7331±0.0392	0.5857±0.1108

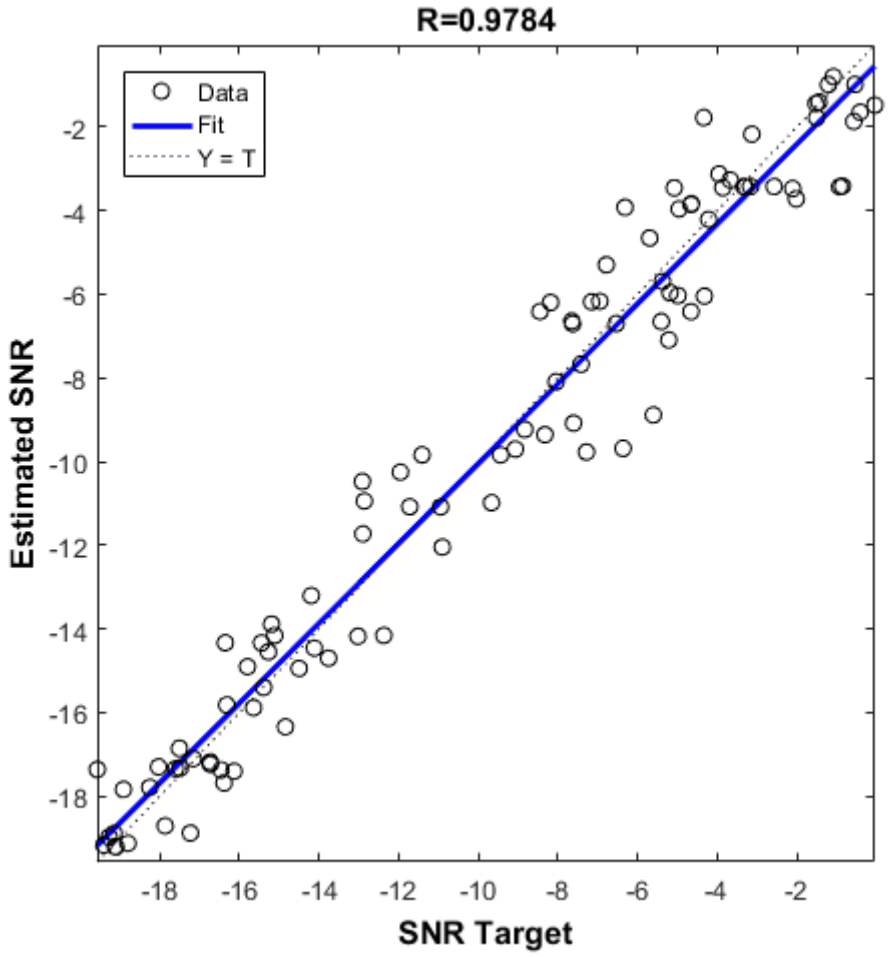

Fig. 4.7. Correlation plot between the SNR target and the estimated SNR from NN when the input is the WL features determined using the SMRC dataset.

4.2.2. Discussion

In this section, we investigated more insights into the results from Section 4.2.1. Fig. 4.8(Left column) shows the raw, cD4, and cD5 EMG data from SMRC, respectively. Fig. 4.8(Right column) shows their corresponding absolute difference of two adjacent amplitudes from the signals in the left column. It is evident that the absolute difference of two adjacent amplitudes from the WL feature determined using the raw EMG and cD5 data are better than those from the cD4 data. As a result, the average CC value from WL using the raw EMG data provides the best result at

0.9663 compared to that from cD4 at 0.7738 and cD5 at 0.8264. Moreover, these results are in agreement with the boxplots shown in Fig. 4.6(d).

We can gain more insight into SKEW and KURT from histograms. Fig. 4.9(Left column) shows histograms from raw, cD4, and cD5 in the top, middle, and bottom rows, respectively. We can see that the histograms from the cD4 and cD5 data are more symmetry than those from the raw EMG data. As a result, the SKEW values are more overlapped. These results agree with the boxplot of SKEW values as a function of 5 SNR levels shown in Fig. 4.6(a). Also, they agree with the average CC values. In other words, the raw EMG data give better average CC (0.5541) compared to that from cD4 (-0.0896) and cD5 (0.2054) data when SKEW is used as a feature. However, the tailedness of histograms can be distinguished among raw, cD4, and cD5 EMG data when SNRs increase. Therefore, the average CC values from KURT using raw, cD4, and cD5 data are comparable and better than those from SKEW at 0.6400, 0.6982, and 0.7678, respectively. These are also supported by the degree of separation of the boxplots shown in Fig. 4.6(a)-(b).

We can understand MNF better with power spectra. Fig. 4.9(Right column) shows the power spectra from the raw, cD4, and cD5 EMG data in the top, middle, and bottom rows, respectively. The power spectra from the raw EMG and cD4 data have a higher degree of separation than those from the cD5 data with SNR increment. In other words, the cD5 data do not give a difference in MNF when SNRs increase because of their similarity in power spectra. Therefore, the average CC value from MNF using the raw EMG data gives the best result (0.9146) compared to those from MNF using the cD4 (0.7114) and cD5 (0.5247) data. Also, we can see that it has an excellent agreement separation from boxplots indicated in Fig. 4.6(f).

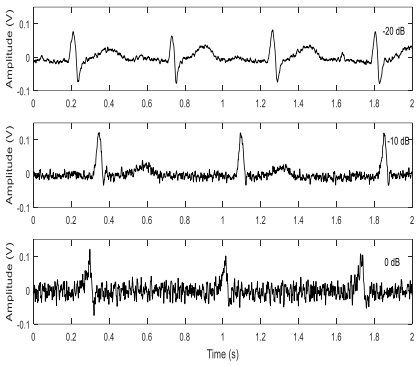

(a) Raw EMG signals.

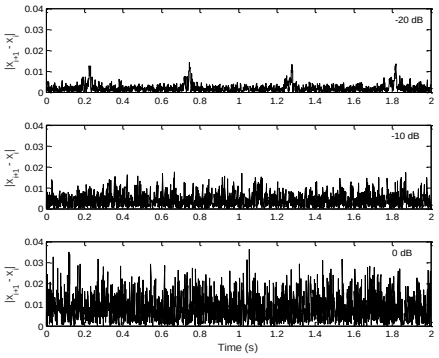

(d) $|x_{i+1}\text{-}x_i|$ of signals from (a).

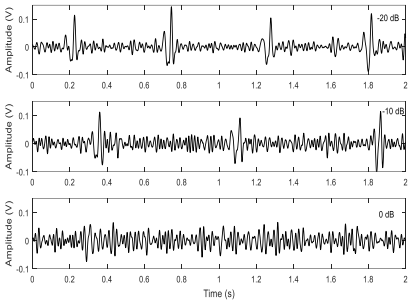

(b) cD4 decomposition level.

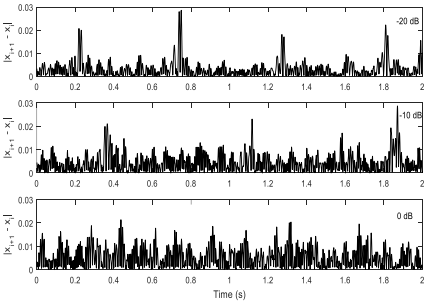

(e) $|x_{i+1}\text{-}x_i|$ of signals from (b).

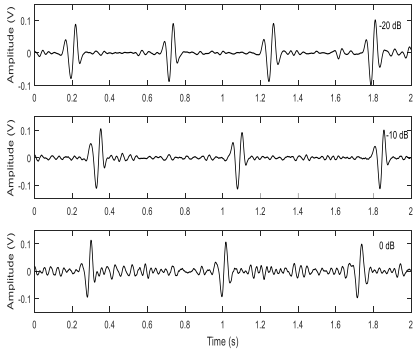

(c) cD5 decomposition level.

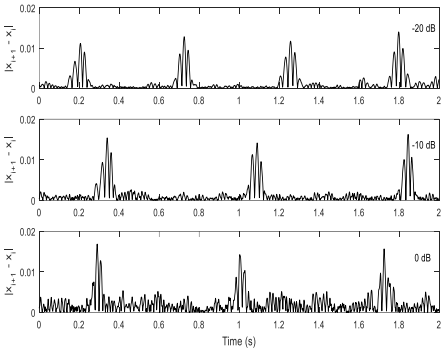

(f) $|x_{i+1}\text{-}x_i|$ of signals from (c).

Fig. 4.8. Example of the SMRC signals and their corresponding absolute of difference of two adjacent amplitudes (|xi+1-xi|) are shown in the left and right columns, respectively. The top, middle, and bottom rows show the results from raw EMG signals, cD4 decomposition level, and cD5 decomposition level, respectively.

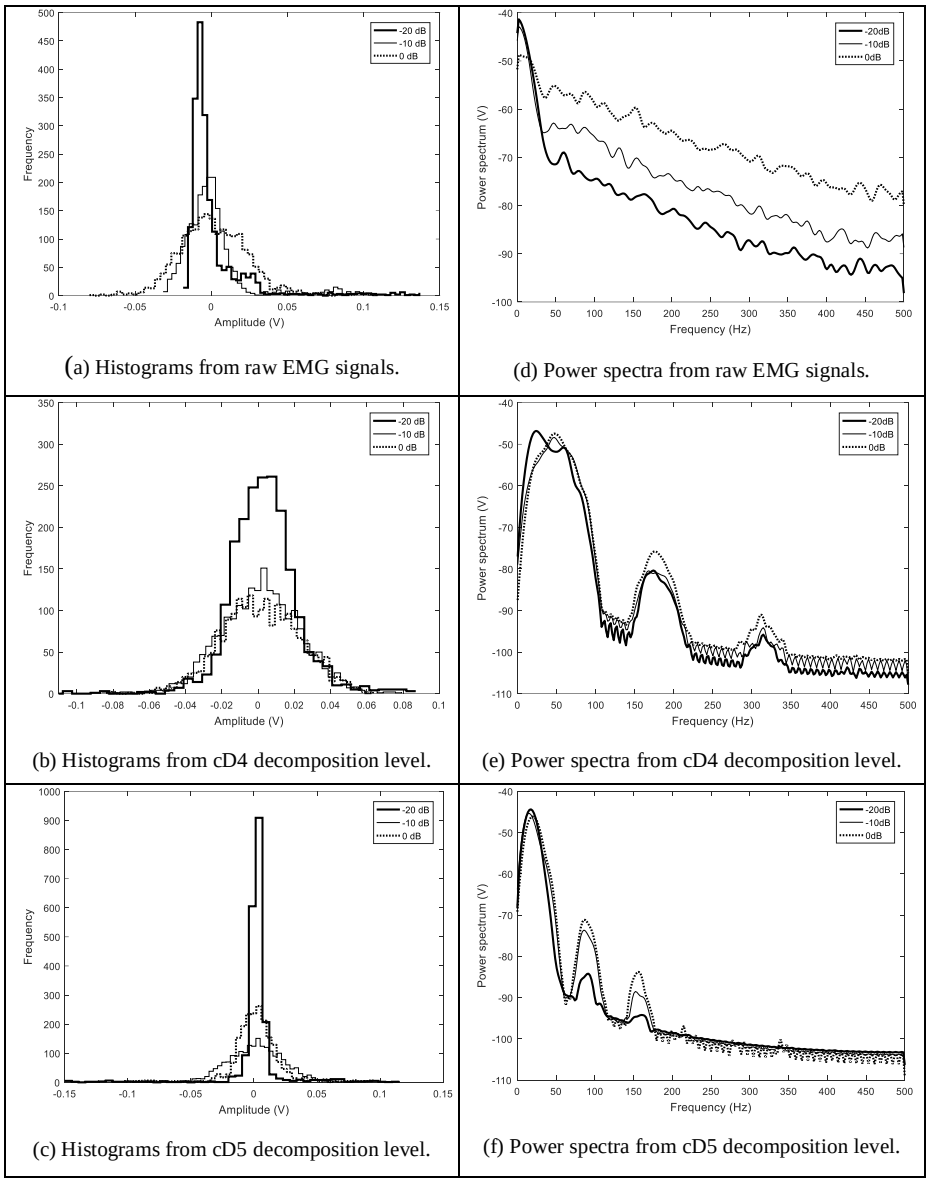

(a) Histograms from raw EMG signals.

(d) Power spectra from raw EMG signals.

(b) Histograms from cD4 decomposition level.

(e) Power spectra from cD4 decomposition level.

(c) Histograms from cD5 decomposition level.

(f) Power spectra from cD5 decomposition level.

Fig. 4.9. Histograms and power spectra from the SMRC data are shown in the left and right columns, respectively. The top, middle, and bottom rows show the results from raw EMG signals, cD4 decomposition level, and cD5 decomposition level, respectively.

4.3. Threshold estimation in EMG signals contaminated with ECG interference

4.3.1. Results

We implemented the threshold value estimation algorithm using the SNR in the EMG signal contaminated with the ECG interference as the input of neural network. The method was described in Section 3.4. Table 4.7 shows five trials of mean and standard deviation for the threshold values (Th1, Th2) and their estimations ($Th1_{est}$, $Th2_{est}$) from 100 SMRC testing data when the training data are from 300 SMSC datasets. As a result, the average values of Th1 (7.77- 8.04) are slightly lower than those of $Th1_{est}$ (9.20 - 9.37). However, the average values of Th2 (5.72-6.19) and $Th2_{est}$ (5.94-6.14) are comparable. Moreover, the average values of MSE_{Th1} and MSE_{Th2} are comparable in all trials.

Table 4.7. Mean and standard deviation of Th1, Th2, $Th1_{est}$, $Th2_{est}$, and MSE from the SMRC data.

Trials	Th1	$Th1_{est}$	MSE_{Th1}	Th2	$Th2_{est}$	MSE_{Th2}
1st	7.77±1.52	9.27±0.73	5.55±9.91	5.91±2.09	6.06±0.81	5.32±8.36
2nd	8.03±1.68	9.20±0.86	5.64±8.28	6.01±1.98	6.14±0.55	4.59±7.01
3rd	7.93±1.41	9.32±0.89	4.42±5.12	5.72±1.97	5.98±0.40	4.30±6.73
4th	7.92±1.59	9.27±0.84	4.83±7.09	6.19±1.99	5.95±0.92	4.92±7.96
5th	8.04±1.54	9.37±0.87	5.23±6.44	5.90±1.90	5.94±0.41	4.04±6.42

After Th1 and Th2 are estimated, they are used in DSWT noise removal algorithm. A comparison of CC for DSWT noise removal algorithm based on estimated threshold ($DSWT_{est}$), DSWT noise removal algorithm based on optimal threshold ($DSWT_{opt}$), HPF noise removal techniques across SMRC dataset is shown in Table 4.8. The results show that CC values from $DSWT_{est}$ and $DSWT_{opt}$ are better than those from HPF for SMRC dataset. It cannot be deniable that the $DSWT_{opt}$ gives the best result from the 1^{st} to 5^{th} trial. These results indicate that it is possible to estimate Th1 and Th2 using simulated data and employ the results to the real data.

Moreover, after Th1 and Th2 are estimated, they are used in DSWT noise removal algorithm. A comparison of CC for DSWT noise removal algorithm based on estimated threshold ($DSWT_{est}$), DSWT noise removal algorithm based on optimal threshold ($DSWT_{opt}$), bandpass filter (BPF) noise removal techniques across SMRC dataset is shown in Table 4.9. The cut-off frequency of BPF 15.625-31.25 Hz was used. The results show that CC values from $DSWT_{est}$ and $DSWT_{opt}$ are better than those from BPF for SMRC dataset. It cannot be deniable that the $DSWT_{opt}$ gives the best result from the 1st to 5th trial. These results indicate that it is possible to estimate Th1 and Th2 using simulated data and employ the results to the real data.

Table 4.8. Comparison of CC for HPF, $DSWT_{opt}$ and $DSWT_{est}$ noise removal techniques from SMRC dataset.

Trials	HPF	$DSWT_{opt}$	$DSWT_{est}$
1st	0.8469 ± 0.1352	0.9482 ± 0.0441	0.9419 ± 0.0510
2nd	0.8495 ± 0.1370	0.9477 ± 0.0434	0.9402 ± 0.0533
3rd	0.8567 ± 0.1284	0.9510 ± 0.0373	0.9461 ± 0.0400
4th	0.8572 ± 0.1368	0.9494 ± 0.0402	0.9445 ± 0.0427
5th	0.8686 ± 0.1123	0.9500 ± 0.0421	0.9444 ± 0.0467

Table 4.9. Comparison of CC for BPF, $DSWT_{opt}$ and $DSWT_{est}$ noise removal techniques from SMRC dataset.

Trials	BPF	$DSWT_{opt}$	$DSWT_{est}$
1st	0.3270 ± 0.1683	0.9455 ± 0.0479	0.9396 ± 0.0504
2nd	0.3088 ± 0.1782	0.9479 ± 0.0461	0.9425 ± 0.0512
3rd	0.3047 ± 0.1926	0.9557 ± 0.0395	0.9498 ± 0.0482
4th	0.3188 ± 0.1675	0.9570 ± 0.0350	0.9517 ± 0.0385
5th	0.3050 ± 0.1627	0.9505 ± 0.0401	0.9447 ± 0.0439

4.4. SNR estimation in EMG signals contaminated with power line interference

4.4.1. Results

4.4.1.1. Feature evaluation

We determined six features from the contaminated EMG signals at five SNR levels generated using the method given in Section 3.5.1. Fig. 4.10 shows the boxplots from six features determined using SMSC data as a function of SNR. Fig. 4.10(a) shows the boxplots of SKEW from raw, cD4, and cD5 data in the top, middle, and bottom panels, respectively. Fig. 4.10(b)-(f) show similar boxplots from other 5 features, namely, KURT, MNF, WL, ZC, and MAV. The KURT feature from the raw, cD4, and cD5 data gives the best separation of boxplot as shown in in the top, middle, and bottom panel of Fig. 4.10(b). However, the SKEW feature from cD4 and cD5 decomposition levels does not give a good separation of boxplot as shown in Fig 4.10(a).

4.4.1.2. SNR estimation

We implemented the SNR estimation algorithm as described in Section 3.5.2 and demonstrated the performance of SNR estimation for single feature and paired features using CC in Table 4.10 and 4.11, respectively. Table 4.10 shows the mean and standard deviation for CC from different single features obtained with the SMSC data when these 6 features are calculated using raw, cD4, and cD5 EMG data. We can clearly see that the KURT feature from the raw EMG data gives the best average CC at 0.9928. The best average CC from cD4 is 0.9830. Furthermore, the average CC values from the MAV feature are close to those from the KURT feature at approximately 0.9866, 0.9701, and 0.7018, respectively. Table 4.11 shows the mean and standard deviation for CC from different pairs of features obtained with the SMRC data. We can clearly see that the combination of (KURT+MAV) and (KURT+MNF) from the raw EMG data give the best average CC at 0.9951. Fig 4.9 shows an example of the correlation plot for the SNR estimation from NN with the KURT feature from the raw EMG data. The

CC value of 0.9936 agrees well with the results from the KURT feature using the raw data (0.9928 ± 0.0035) as shown in Table 4.10.

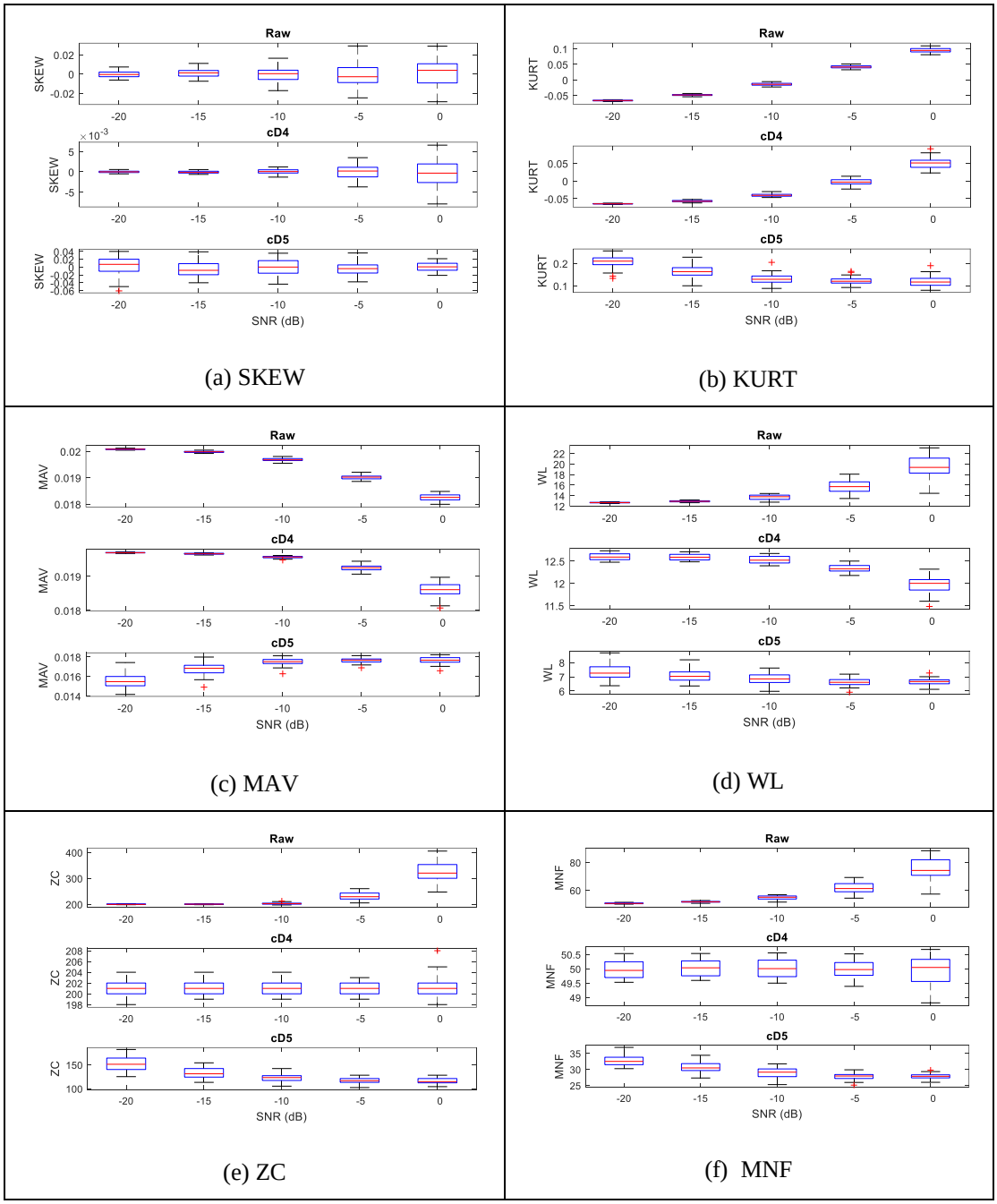

Fig. 4.10. Boxplots of feature values determined using SMSC data as a function of SNR. (a) SKEW. (b) KURT. (c) MAV. (d) WL. (e) ZC. (f) MNF

Table 4.10. Mean and standard deviation of CC from different single features obtained with SMRC data.

Feature	Raw	cD4	cD5
SKEW	0.3662 ± 0.0929	0.6745 ± 0.0654	0.1779 ± 0.1184
KURT	0.9928 ± 0.0035	0.9830 ± 0.0013	0.6464 ± 0.0482
MAV	0.9866 ± 0.0018	0.9701 ± 0.0054	0.7018 ± 0.0449
WL	0.9156 ± 0.0145	0.8033 ± 0.0388	0.4236 ± 0.0890
ZC	0.8869 ± 0.0230	0.0603 ± 0.0441	0.6818 ± 0.0446
MNF	0.9304 ± 0.0157	0.0476 ± 0.0713	0.6700 ± 0.0285

Table 4.11. Mean and standard deviation of CC from different pairs of features obtained with SMRC data.

Feature	Raw	cD4	cD5
SKEW+KURT	0.9935 ± 0.0013	0.9806 ± 0.0059	0.9853 ± 0.0044
SKEW+WL	0.9148 ± 0.0343	0.9735 ± 0.0364	0.9834 ± 0.0108
SKEW+ZC	0.8666 ± 0.0446	0.9895 ± 0.0028	0.9865 ± 0.0057
SKEW+MAV	0.9838 ± 0.0098	0.9872 ± 0.0032	0.9876 ± 0.0032
SKEW+MNF	0.9332 ± 0.0262	0.9892 ± 0.0016	0.9872 ± 0.0047
KURT+WL	0.9940 ± 0.0022	0.9799 ± 0.0169	0.9884 ± 0.0028
KURT+ZC	0.9940 ± 0.0017	0.9875 ± 0.0026	0.9879 ± 0.0042
KURT+MAV	0.9951 ± 0.0013	0.9864 ± 0.0026	0.9869 ± 0.0025
KURT+MNF	0.9951 ± 0.0006	0.9879 ± 0.0030	0.9895 ± 0.0029
WL+ZC	0.9299 ± 0.0314	0.9773 ± 0.0111	0.9888 ± 0.0029
WL+MAV	0.9878 ± 0.0033	0.9893 ± 0.0023	0.9883 ± 0.0023
WL+MNF	0.9563 ± 0.0038	0.9852 ± 0.0060	0.9867 ± 0.0024
ZC+MAV	0.9870 ± 0.0049	0.9837 ± 0.0142	0.9850 ± 0.0045
ZC+MNF	0.9622 ± 0.0068	0.9876 ± 0.0028	0.9876 ± 0.0033
MAV+MNF	0.9903 ± 0.0021	0.9884 ± 0.0021	0.9874 ± 0.0024

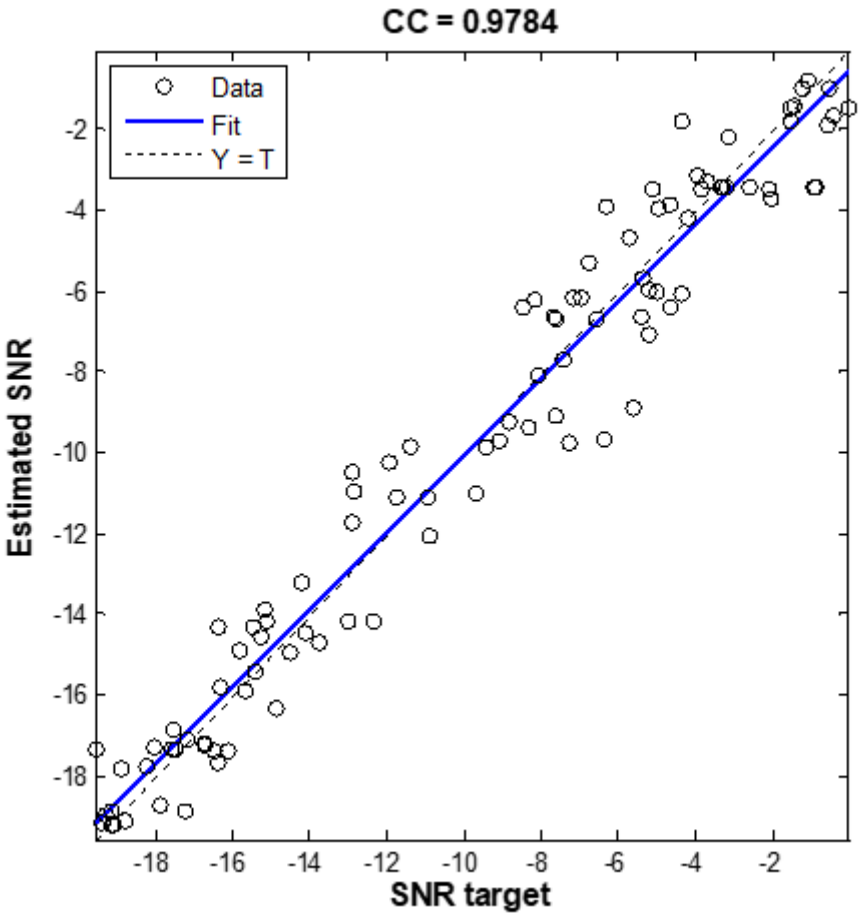

Fig. 4.11. Correlation plot between the SNR target and the estimated SNR from NN when the input is the KURT features determined using the SMRC dataset.

4.4.2. Discussion

In this section, we investigated more insights into the results from Section 4.4.1. Fig. 4.12(Left column) shows the raw, cD4, and cD5 EMG data from SMSC, respectively. Fig. 4.12(Right column) shows their corresponding absolute difference of two adjacent amplitudes from the signals in the left column. It is evident that the absolute difference of two adjacent amplitudes from the WL feature determined using the raw EMG and cD4 data are better than those from the cD5 data. As a result, the average CC value from WL using the raw EMG data provides the best result at

0.9156 compared to that from cD4 at 0.8033 and cD5 at 0.4236. Moreover, these results are in agreement with the boxplots shown in Fig. 4.10 (d).

We can gain more insight into SKEW and KURT from histograms. Fig. 4.13(Left column) shows histograms from raw, cD4, and cD5 in the top, middle, and bottom rows, respectively. We can see that the histograms from the cD4 and cD5 data are more symmetry than those from the raw EMG data. As a result, the SKEW values are more overlapped. These results agree with the boxplot of SKEW values as a function of 5 SNR levels shown in Fig. 4.10(a). Also, they agree with the average CC values. In other words, cD4 data give better average CC (0.6745) compared to that from the raw EMG (0.3662) and cD5 (0.1779) data when SKEW is used as a feature. However, the tailedness of histograms can be distinguished among raw, cD4, and cD5 EMG data when SNRs increase. Therefore, the average CC values from KURT using raw, cD4, and cD5 data are better than those from SKEW at 0.9928, 0.9830, and 0.6464, respectively. These are also supported by the degree of separation of the boxplots shown in Fig. 4.10(a)-(b).

We can understand MNF better with power spectra. Fig. 4.13(Right column) shows the power spectra from the raw, cD4, and cD5 EMG data in the top, middle, and bottom rows, respectively. The power spectra from the raw EMG and cD4 data have a higher degree of separation than those from the cD5 data with SNR increment. In other words, the cD5 data do not give a difference in MNF when SNRs increase because of their similarity in power spectra. Therefore, the average CC value from MNF using the raw EMG data gives the best result (0.9304) compared to those from MNF using the cD4 (0.0476) and cD5 (0.6700) data. Also, we can see that it has an excellent agreement separation from boxplots indicated in Fig. 4.10(f).

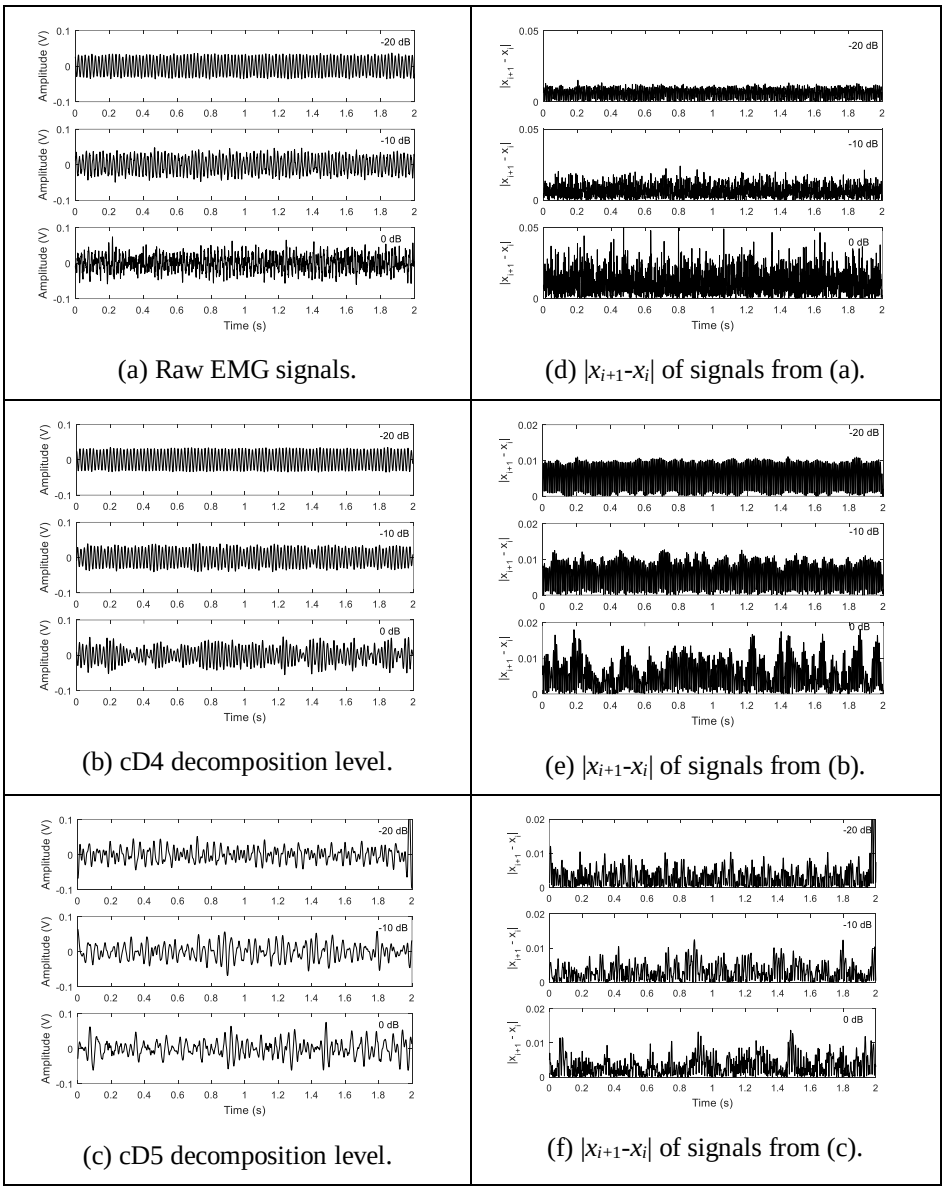

Fig. 4.12. Example of SMSC signal and its corresponding absolute of difference of two adjacent amplitudes ($|x_{i+1} - x_i|$) are shown in the left and right columns, respectively. The top, middle, and bottom rows show the results from raw EMG signals, DSWT at cD4 decomposition level, and DSWT at cD5 decomposition level, respectively.

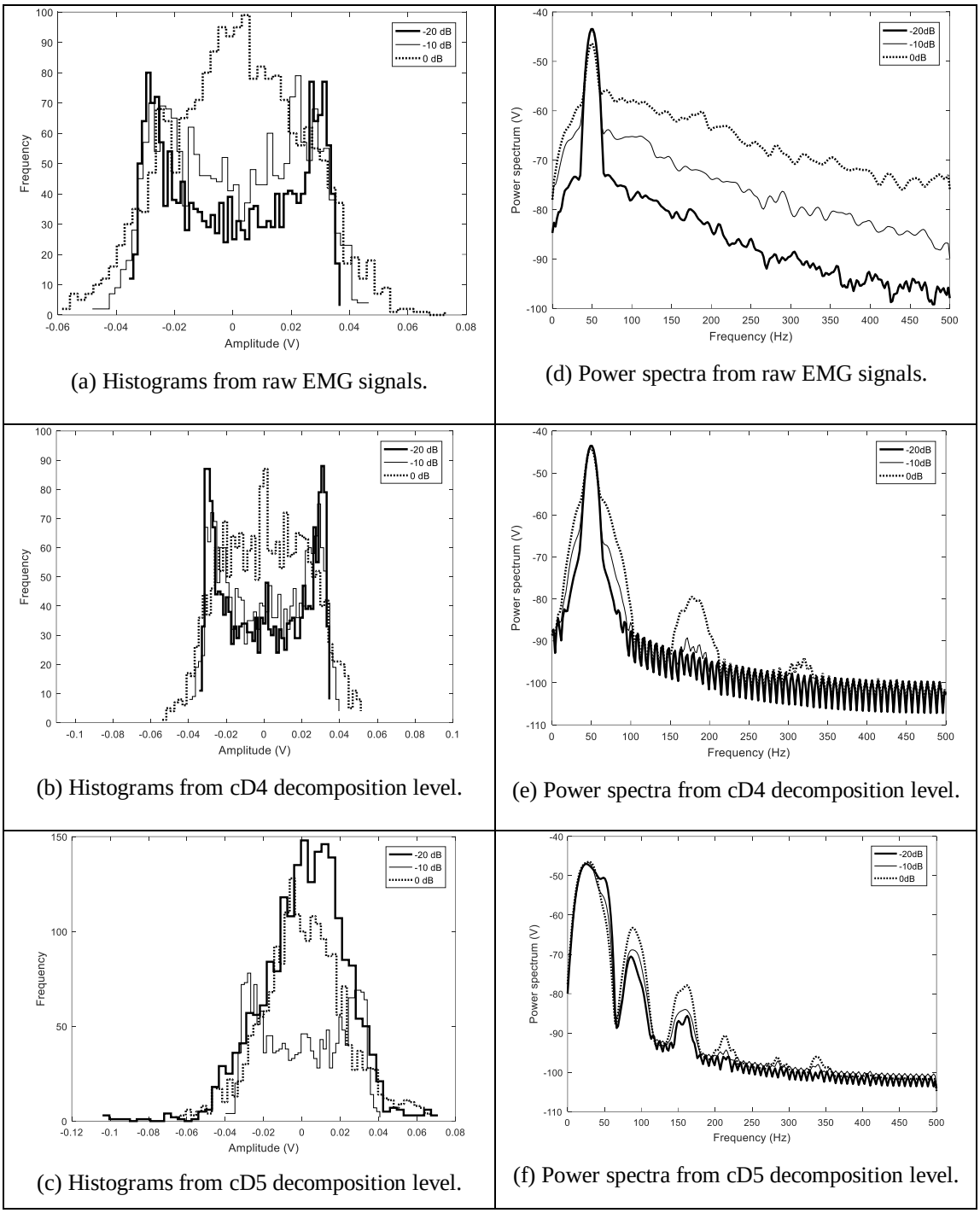

(a) Histograms from raw EMG signals.

(d) Power spectra from raw EMG signals.

(b) Histograms from cD4 decomposition level.

(e) Power spectra from cD4 decomposition level.

(c) Histograms from cD5 decomposition level.

(f) Power spectra from cD5 decomposition level.

Fig. 4.13. Histograms and power spectra from SMSC data are shown in the left and rigth columns, respectively. The top, middle, and bottom rows show the results from raw EMG signals, DSWT at cD4 decomposition level, and DSWT at cD5 decomposition level, respectively.

4.5. SNR estimation in EMG signals contaminated with motion artifact

4.5.1. Results

4.5.1.1. Feature evaluation

We determined six features with the contaminated EMG signals at five SNR levels generated using the method given in Section 3.6.1. Fig. 4.14 shows the boxplots from six features determined using SMSC data as a function of SNR. Fig. 4.14(a) shows the boxplots of SKEW from raw, cD4, and cD5 data in the top, middle, and bottom panels, respectively. Fig. 4.14(b)-(f) show similar boxplots from other 5 features, namely, KURT, MNF, WL, ZC, and MAV. The MNF feature from the cD4 data gives the best separation of boxplot as shown in in the top and middle panel of Fig. 4.14(b). Moreover, the WL and ZC features have a similar pattern of boxplots as shown in Fig. 19(c) and (d). However, the SKEW feature from cD4 and cD5 decomposition levels does not give a good separation of boxplot as shown in Fig 4.14(a).

4.5.1.2. SNR estimation

We implemented the SNR estimation algorithm as described in Section 3.6.2 and demonstrated the performance of SNR estimation for single feature and paired features using CC in Table 4.12 and 4.13, respectively. Table 4.12 shows the mean and standard deviation for CC from different single features obtained with the SMSC data when these 6 features are calculated using raw, cD4, and cD5 EMG data. We can clearly see that the MNF feature from the cD4 data gives the best average CC at 0.9770. The best average CC from the raw EMG data is 0.9699. Furthermore, the average CC values from the WL feature are consistent at approximately 0.9671, 0.9725, and 0.6023, respectively. The average CC values from the ZC feature are comparable that from the WL feature. Table 4.13 shows the mean and standard deviation for CC from different pairs of features obtained with the SMRC data. We can clearly see that the combination of WL and MNF (WL+MNF) from the raw EMG data give the best average CC at 0.9856. Fig 4.15 shows an example of the correlation plot for the SNR estimation from NN with the MNF feature from the raw EMG data. The cc value of 0.9635 agrees well

with the results from the MNF feature using the raw data (0.9699 ± 0.0076) as shown in Table 4.12.

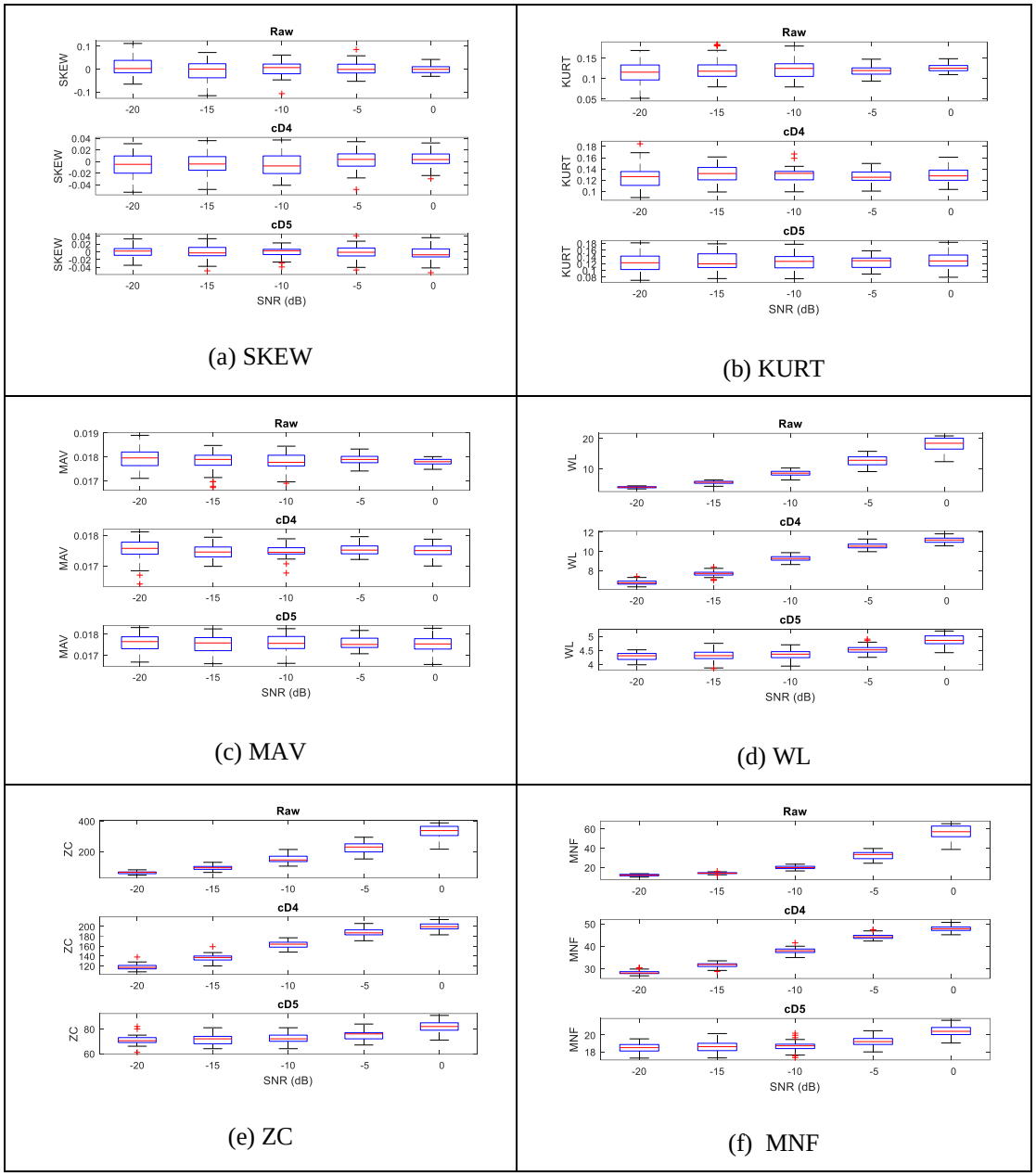

Fig. 4.14. Boxplots of feature values determined using SMSC data as a function of SNR. (a) SKEW. (b) KURT. (c) MAV. (d) WL. (e) ZC. (f) MNF

Table 4.12. Mean and standard deviation of CC from different single features obtained with SMRC data.

Feature	Raw	cD4	cD5
SKEW	0.0853 ± 0.1223	0.0060 ± 0.1736	0.0344 ± 0.0822
KURT	0.1503 ± 0.1301	0.0702 ± 0.1484	0.0104 ± 0.0377
WL	0.9671 ± 0.0055	0.9725 ± 0.0019	0.6023 ± 0.0672
ZC	0.9548 ± 0.0055	0.9522 ± 0.0107	0.5117 ± 0.1105
MAV	0.1935 ± 0.0535	-0.0073 ± 0.2066	0.0298 ± 0.0715
MNF	0.9699 ± 0.0076	0.9770 ± 0.0021	0.5709 ± 0.0816

Table 4.13. Mean and standard deviation of CC from different pairs of features obtained with SMRC data.

Feature	Raw	cD4	cD5
SKEW+KURT	0.3329 ± 0.0886	0.0194 ± 0.0573	0.3096 ± 0.0988
SKEW+WL	0.9624 ± 0.0075	0.2548 ± 0.1905	0.2194 ± 0.1965
SKEW+ZC	0.9495 ± 0.0118	0.1804 ± 0.1710	0.2097 ± 0.2187
SKEW+MAV	0.3121 ± 0.1124	0.3376 ± 0.0944	0.2909 ± 0.0749
SKEW+MNF	0.9682 ± 0.0072	0.2574 ± 0.1266	0.2410 ± 0.1890
KURT+WL	0.9547 ± 0.0142	0.2572 ± 0.1409	0.2901 ± 0.1294
KURT+ZC	0.9476 ± 0.0161	0.2855 ± 0.1340	0.2983 ± 0.1122
KURT+MAV	0.3027 ± 0.0996	0.2537 ± 0.1337	0.2505 ± 0.1488
KURT+MNF	0.9701 ± 0.0062	0.2534 ± 0.1098	0.2706 ± 0.1016
WL+ZC	0.9665 ± 0.0047	0.2726 ± 0.1624	0.3146 ± 0.0724
WL+MAV	0.9633 ± 0.0072	0.2959 ± 0.1248	0.2859 ± 0.0617
WL+MNF	0.9856 ± 0.0027	0.3133 ± 0.0606	0.2949 ± 0.0558
ZC+MAV	0.9469 ± 0.0149	0.2789 ± 0.0813	0.2827 ± 0.0981
ZC+MNF	0.9776 ± 0.0029	0.2583 ± 0.1676	0.3272 ± 0.0766

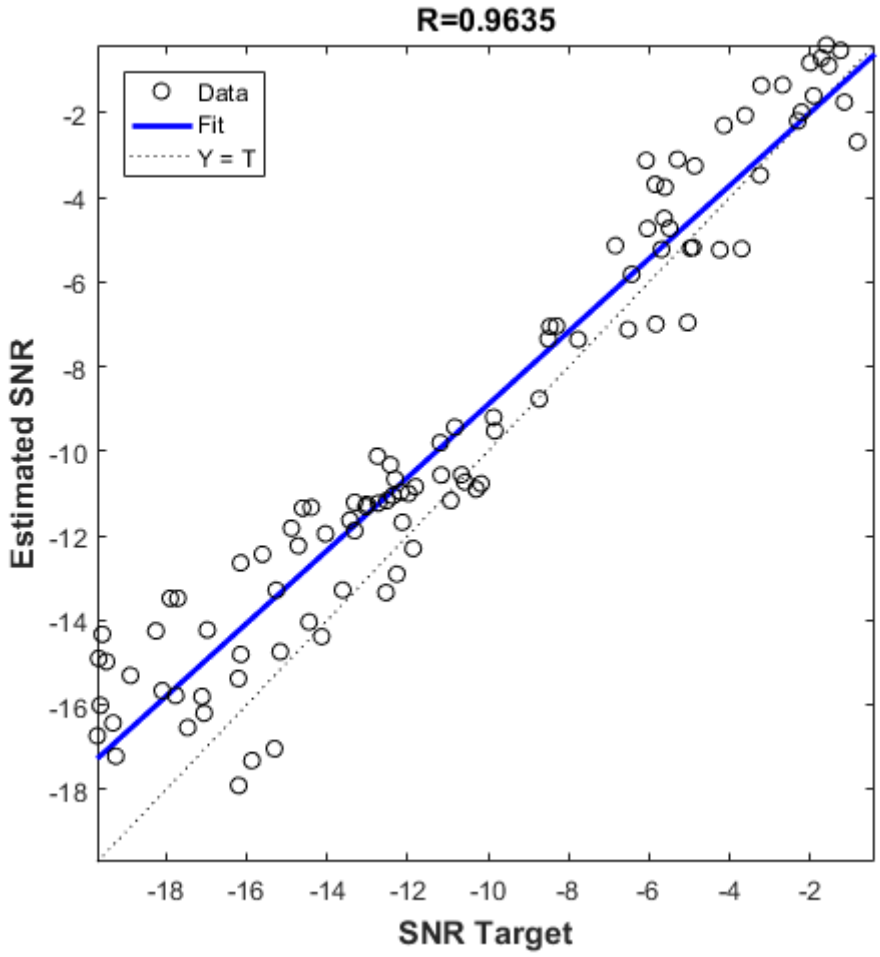

Fig. 4.15. Correlation plot between the SNR target and the estimated SNR from NN when the input is the KURT features determined using the SMRC dataset.

4.5.2. Discussion

In this section, we investigated more insights into the results from Section 4.5.1. Fig. 4.16(Left column) shows the raw, cD4, and cD5 EMG data from SMRC, respectively. Fig. 4.16(Right column) shows their corresponding absolute difference of two adjacent amplitudes from the signals in the left column. It is evident that the absolute difference of two adjacent amplitudes from the MNF feature determined using the raw EMG and cD4 data are better than those from the cD5 data. As a result, the average CC value from WL using the raw EMG data provides the best

result at 0.9699 compared to that from cD4 at 0.9770 and cD5 at 0.5709. Moreover, these results are in agreement with the boxplots shown in Fig. 4.14 (d).

We can gain more insight into SKEW and KURT from histograms. Fig. 4.17(Left column) shows histograms from raw, cD4, and cD5 in the top, middle, and bottom rows, respectively. We can see that the histograms from the cD4 and cD5 data are more symmetry than those from the raw EMG data. As a result, the SKEW values are more overlapped. These results agree with the boxplot of SKEW values as a function of 5 SNR levels shown in Fig. 4.14(a). Also, they agree with the average CC values. In other words, the raw EMG data give better average CC (0.0853) compared to that from cD4 (0.0060) and cD5 (0.0344) data when SKEW is used as a feature. However, the tailedness of histograms can be distinguished among raw, cD4, and cD5 EMG data when SNRs increase. Therefore, the average CC values from KURT using raw and cD4 data are comparable and better than those from SKEW at 0.1503 and 0.0702, respectively. These are also supported by the degree of separation of the boxplots shown in Fig. 4.14(a)-(b).

We can understand MNF better with power spectra. Fig. 4.17(Right column) shows the power spectra from the raw, cD4, and cD5 EMG data in the top, middle, and bottom rows, respectively. The power spectra from the raw EMG and cD4 data have a higher degree of separation than those from the cD5 data with SNR increment. In other words, the cD5 data do not give a difference in MNF when SNRs increase because of their similarity in power spectra. Therefore, the average CC value from MNF using the raw EMG data gives the best result (0.9699) compared to those from MNF using the cD4 (0.9770) and cD5 (0.5709) data. Also, we can see that it has an excellent agreement separation from boxplots indicated in Fig. 4.14(f).

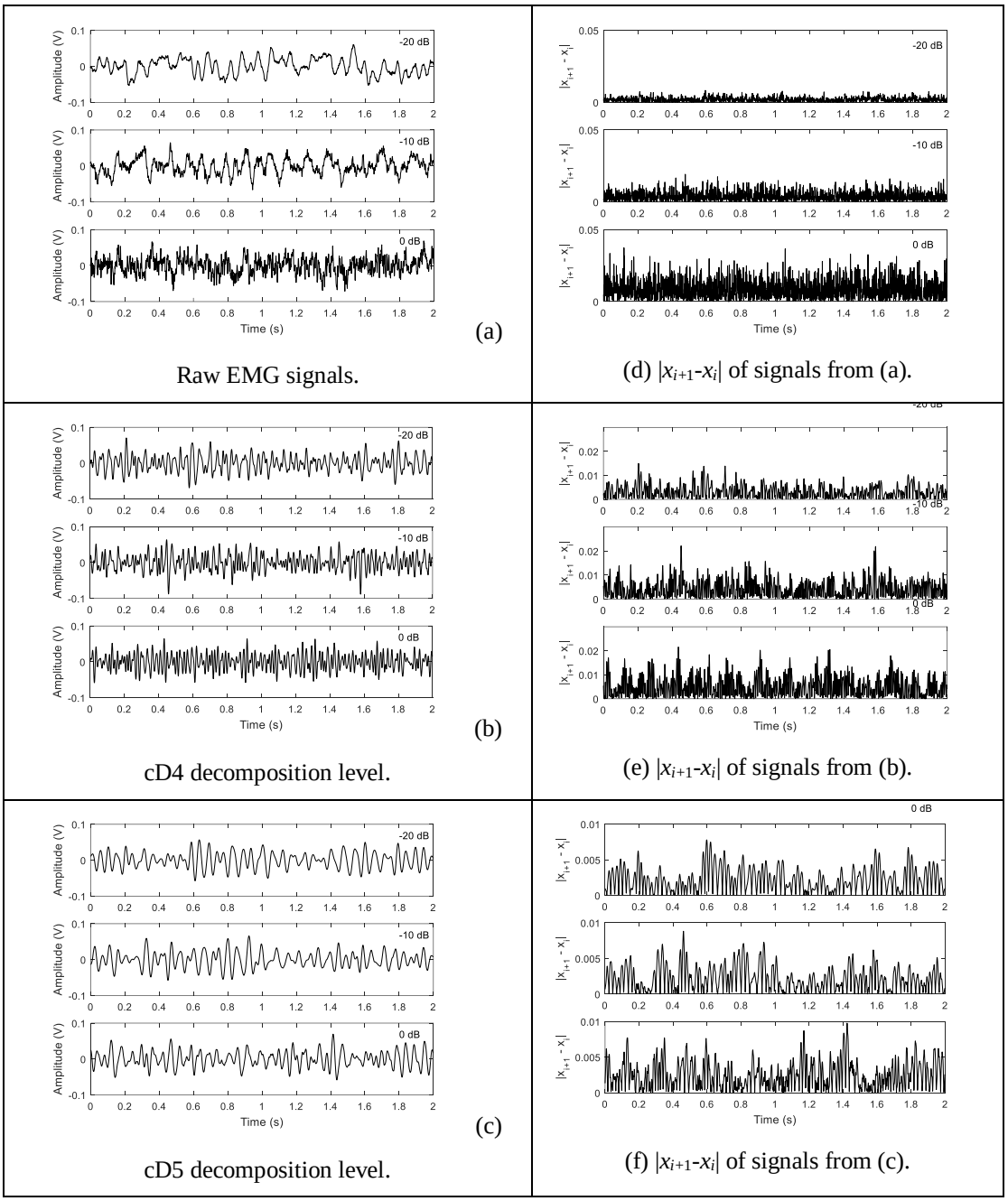

Fig. 4.16. Example of SMSC signal and its corresponding absolute of difference of two adjacent amplitudes (|xi+1-xi|) are shown in the left and right columns, respectively. The top, middle, and bottom rows show the results from raw EMG signals, DSWT at cD4 decomposition level, and DSWT at cD5 decomposition level, respectively.

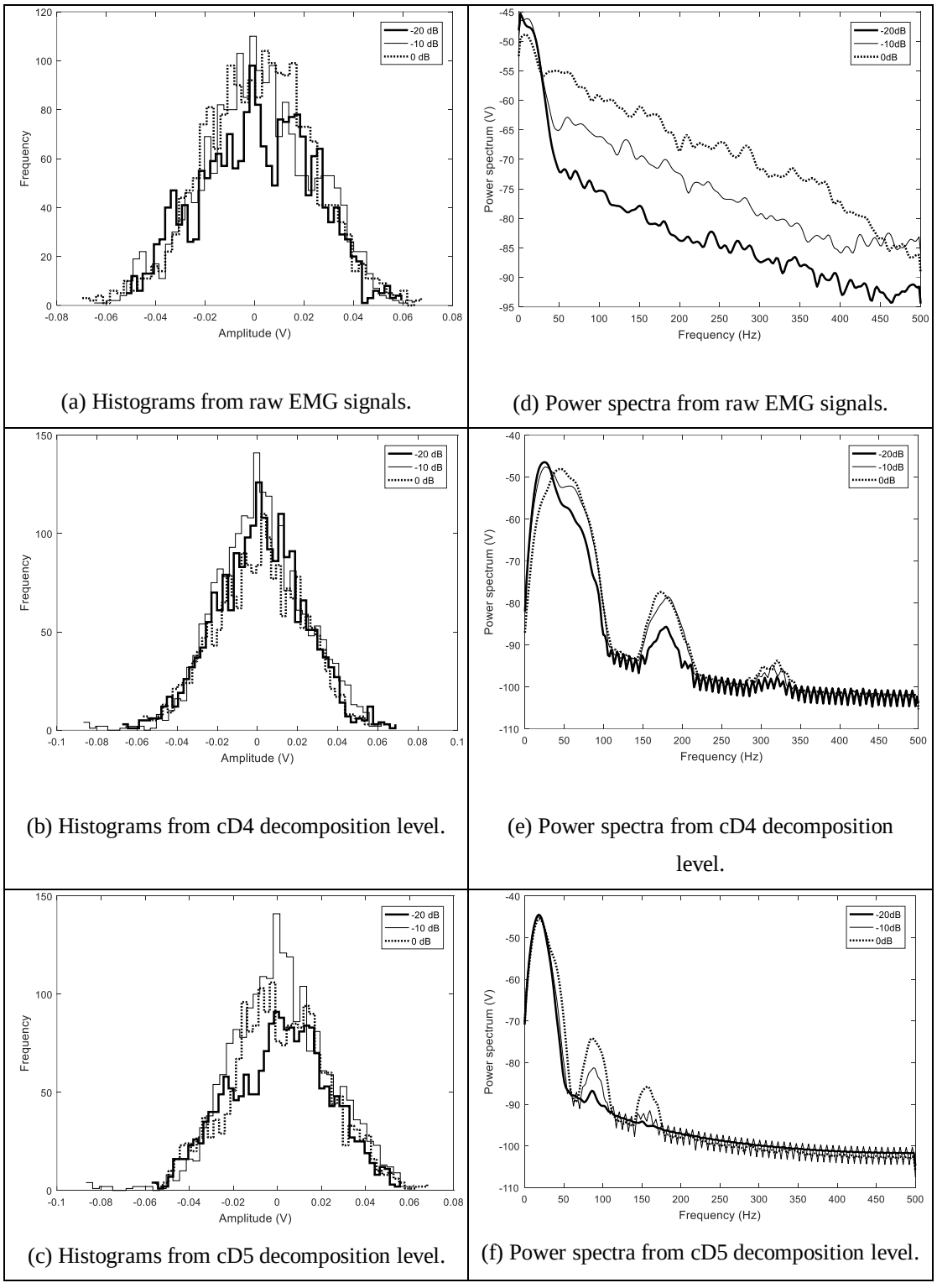

(a) Histograms from raw EMG signals.

(d) Power spectra from raw EMG signals.

(b) Histograms from cD4 decomposition level.

(e) Power spectra from cD4 decomposition level.

(c) Histograms from cD5 decomposition level.

(f) Power spectra from cD5 decomposition level.

Fig. 4.17. Histograms and power spectra from SMSC data are shown in the left and right columns, respectively. The top, middle, and bottom rows show the results from raw EMG signals, DSWT at cD4 decomposition level, and DSWT at cD5 decomposition level, respectively.

CHAPTER 5

CONCLUSIONS AND FUTURE WORK

In this chapter, we present the conclusions of this thesis and future work. The conclusions can be divided into 5 main modules: removal of ECG interference based on DSWT, SNR estimation in EMG signals contaminated with ECG interference, threshold estimation in EMG signals contaminated with ECG interference, SNR estimation in EMG signals contaminated with power line interference, and SNR estimation in EMG signals contaminated with motion artifact are described in Section 5.1.1, Section 5.1.2, Section 5.1.3, Section 5.1.4, and Section 5.1.5, respectively. In addition, the future work is presented in Section 5.2.

5.1. Conclusions

5.1.1. Removal of ECG interference based on DSWT

We presented an application of DSWT to removing ECG interference in EMG signals with consideration of SNR level. The proposed method consists of 3 main steps, namely, DSWT decomposition, thresholding, and DSWT reconstruction. In the first step, the contaminated EMG signal is decomposed using 5-level DSWT with the Symlet wavelet function. In the second step, the coefficients in cD4 and cD5, which are contaminated by the ECG interference, are subjected to nonlinear thresholding. In other words, the detail coefficients, whose absolute values are less than or equal to the threshold level, are set to zero. The threshold level was varied from 0 to 10 with step size 1. Finally, in the third step, the cleaned EMG signal was reconstructed by inverse DSWT of the thresholded coefficients.

The proposed method was evaluated using simulated EMG signals contaminated with ECG interference at 9 SNR levels from -20 to 20 dB with 5 dB increments. There were two types of ECG interference in this study, namely, simulated and real ECG signals. With both types of data, MAE, CC, and RE for DSWT were better than those for HPF. Moreover, DSWT significantly outperforms HPF at the low

SNR from -10 dB to -20 dB. Results show that an EMG signal contaminated with ECG at different SNR levels requires different threshold levels. The optimal threshold for each SNR level in this paper was obtained offline by exhaustive search, which is impractical for real-time applications. The results suggest a possible future research direction in developing a system that can estimate the SNR level in an EMG signal contaminated with ECG interference.

5.1.2. SNR estimation in EMG signals contaminated with ECG interference

We presented the method for estimating SNR in the EMG signal contaminated with the ECG interference consisting of two main parts, namely, feature evaluation and SNR estimation. We evaluated six popular features used in the EMG recognition system consisting of SKEW, KURT, MAV, WL, ZC, and MNF. The results show that WL gave the best performance. Subsequently, WL was used as an input of NN for SNR estimation. While we used the simulated EMG data artificially contaminated with the simulated ECG data in the training stage, the simulated EMG data artificially contaminated with the real ECG data were used in the testing stage. The best average correlation coefficient at 0.9663 can be obtained when WL is used as an input of NN.

5.1.3. Threshold estimation in EMG signals contaminated with ECG interference

We presented the method for estimating the optimum threshold applied with DSWT for removing the ECG interference contaminated in the EMG signal. SNR was used as an input of NN for threshold estimation. While we used the simulated EMG data artificially contaminated with the simulated ECG data in the training stage, the simulated EMG data artificially contaminated with the real ECG data were used in the testing stage. The estimate threshold values, $Th1_{est}$ and $Th2_{est}$, can be obtained from the NN output. The results show that CC values from $DSWT_{est}$ are comparable to those from $DSWT_{opt}$. However, both of them are better than those from HPF. These results

indicate that the estimate Th1 and Th2 using simulated data can be employed to the real data.

5.1.4. SNR estimation in EMG signals contaminated with power line interference

We presented the method for estimating SNR in the EMG signal contaminated with the power line interference consisting of two main parts, namely, feature evaluation and SNR estimation. The results show that KURT gave the best performance. Subsequently, KURT was used as an input of NN for SNR estimation. We used the simulated EMG data artificially contaminated with the simulated power line interference in the training and testing stages. The best average correlation coefficient at 0.9936 can be obtained when KURT is used as an input of NN.

5.1.5. SNR estimation in EMG signals contaminated with motion artifact

We presented the method for estimating SNR in the EMG signal contaminated with the motion artifact consisting of two main parts, namely, feature evaluation and SNR estimation. The results show that MNF gave the best performance. Subsequently, MNF was used as an input of NN for SNR estimation. We used the simulated EMG data artificially contaminated with the simulated motion artifact in the training and testing stages. The best average correlation coefficient at 0.9635 can be obtained when MNF is used as an input of NN.

5.2. Future work

We show that an EMG signal contaminated with ECG at different SNR levels requires different threshold levels. The optimal threshold for each SNR level in this thesis (Section 4.1) was obtained offline by exhaustive search, which is impractical for real-time applications. The results suggest a possible research direction in developing a system that can estimate the SNR level in an EMG signal contaminated with ECG interference.

Therefore, we have developed the new method of SNR estimation in the EMG signal contaminated with the ECG interference using the feature from the EMG signal as the input of NN. Subsequently, we have developed the new method of threshold estimation in the EMG signal contaminated with the ECG interference using SNR as the input of NN. When we cascade these two systems, we can obtain the optimal threshold values from the NN, when the feature from the EMG signal is the input. As a result, the optimal threshold for each SNR level can be obtained online, which is practical for real-time applications.

Possible future research directions are as follows.

- We may reduce computational complexity by estimating the optimal threshold values from the EMG feature directly, if the SNR estimate is not required in the application.
- In this thesis, we apply the proposed technique to the EMG signal contaminated with the ECG interference only. In the future, we may apply the proposed techniques to power line interference and motion artefact.
- We may further improve the proposed technique so that it can be used with combination of multiple types of noise, such as ECG interference combined with power line interference, motion artefact combined with power line interference, and ECG interference combined with motion artifact.

References

[1] E. J. R. Ramirez and H. Hu, "Stages for developing control systems using EMG and EEG signals: A survey," Sch. of Compt. Sci. and E Lect. Eng., Univ. of Essex, UK, Tech, Rep., CES-513, Jun., 2011.

[2] D. Staudenmann, K. Roeleveld, D. F. Stegeman and J. H. V. Dieën, "Methodological aspects of SEMG recordings for force estimation – A tutorial and review," *J. Electromyogr. Kines.,* 20 (2010) 375-387.

[3] R. H. Chowdhury, M. B. I. Reaz, and M. A Bin Mohd Ali, "Surface electromyography signal processing and classification techniques," *Sensors.,* vol. 13, pp. 12431-12466, 2013.

[4] G. Balestra, S. Frassinelli, M. Knaflitz, and F. Molinari, "Time-frequency analysis of surface myoelectric signals during athletic movement," *IEEE Eng. Med. Biol. Mag.,* vol. 20, pp. 106-115, 2001.

[5] F. B. Stulen, "A technique to monitor localized muscular fatigue using frequency domain analysis of the myoelectric signal," Ph.D. thesis, Massachusetts Institute of Technology, Cambridge, 1980.

[6] B. Pandey and R. B. Mishra, "A practical measuring system for intestinal pressure activity and its clinical application," *Expert Sys. Appl.,* vol.36, pp. 9201–9213, 2009.

[7] K. Isamu, M. Masahiro, N. Daisuke, Y. Hiroshi, and K. Nobuki, "An evolvable hardware chip for prosthetic hand controller," *Proc. 7th Int. Conf. Micro Electron.,* 6 August 2002.

[8] F. Christian, W. Andreas, K. Konstantin, and H. Gunter, "Application of EMG signals for controlling exoskeleton robots," *Biomed Tech (Berl).,* vol. 51, no. (5-6), pp. 314-9, December 2006.

[9] A. Barreto, S. Scargle, and M. Adjouadi, "A practical EMG-based human-computer interface for users with motor disabilities," *J. Rehabil. Res. Dev.,* vol. 37, pp. 53 – 64, 2000.

[10] M. A. Oskoei and H. Hu, “Myoelectric control systems—A survey,” *Biomed. Signal Process. Control*., vol. 2, pp. 275–294 , 2007.

[11] A. Phinyomark, P. Phukapattranont, and C. Limsakul, “Feature reduction and selection for EMG signal classification,” *Expert Syst. Appl.,* vol. 39, pp. 7420-7431, Jun. 2012.

[12] J. Rafee, M. A. Rafee, F. Yavari, and M. P. Schoen, “Feature extraction of forearm EMG signals for prosthetics,” *Expert Sys. Appl.,* vol. 38, no.4, pp.4058-4067, 2011.

[13] G. F. Inbar and A. E. Noujaim, “On surface EMG spectral characterization and its application to diagnostic classification,” *IEEE Trans. Biomed. Eng.,* vol. 31, pp. 597-604, 1984.

[14] C. J. De Luca, L. Donald Gilmore, M. Kuznetsov, and S. H. Roy, “Filtering the surface EMG signal: movement artifact and baseline noise contamination,” *J. Biomech.,* vol. 43. pp. 1573-1579, 2010.

[15] L. Frey Law, C. Krishnan, and K. Avin, “Modeling nonlinear errors in surface electromyography due to baseline noise: A new methodology,” *J. Biomech.,* vol. 44, pp. 202-205, 2011.

[16] J. J. Galiana- Merino, D. Ruiz- Fernandez, and J.J. Martinez- Espla, “Power line interference filtering on surface electromyography based on the stationary wavelet packet transform,” *Comput. Meth. Prog. Bio.,* vol.3, pp.338-346, 2013.

[17] J.D.M. Drake and J.P. Callagham, “Elimination of electrocardiogram contamination from electromyogram signals: An evaluation of currently used removal techniques,” *J. Electromyogr. Kines.,* vol. 16, pp. 175-187, 2006.

[18] C. Marque, C. Bisch, R. Dantas, S. Elayoubi, V. Brosse, and C. Pe´rot, “Adaptive filtering for ECG rejection from surface EMG recordings,” *J. Electromyogr. Kines.,* vol. 15, pp. 310-315, 2005.

[19] G. Lu, J.S. Brittain, P. Holland, J. Yianni, A.L. Green, J.F. Stein, T.Z. Aziz and S. Wang, “Removing ECG noise from surface EMG signals using adaptive filtering,” *Neuroendocrinol. Lett.,* vol. 462, pp. 14-19, 2009.

[20] S. Abbaspour, A. Fallah, M. Linden, and H. Gholamhosseini, "A novel approach for removing ECG interferences from surface EMG signals using a combined ANFIS and wavelet," *J. Electromyogr. Kines.,* vol.26, pp. 52-59, 2016.

[21] P. Zhou, "Eliminating cardiac contamination from myoelectric control signals developed by targeted muscle reinnervation," *Physiol Meas.,* vol. 27, pp. 1311-1327, 2007.

[22] C. Kezi Selva Vijila and C.Ebbie Selva Kumar, "Cancellation of ECG in electromyogram using back propagation network," *Proc. IEEE. T. Vis, Comput. Gr. Int. Conf.,* pp. 1-5, 2009.

[23] P. Zhou, M. M. Lowery, R. F. Weir, and T.A. Kuiken, "Elimination of ECG Artifacts from Myoelectric Prosthesis Control Signals Developed by Targeted Muscle Reinnervation," *Proc. IEEE Eng. Med. Biol. 27th A. Conf.,* Shanghai, China, September 1-4, 2005.

[24] S. Abbaspour and A. Fallah, "A combination method for electrocardiogram rejection from surface electromyogram," *J. Biomed. Master. Res. A.,* vol.8, pp. 13-19, 2014.

[25] E. A. Clancy, E. L. Morin, and R. Merletti, "Sampling, noise-reduction and amplitude estimation issues in surface electromyography," *J. Electromyogr. Kines.,* vol.12, pp.1–16, 2002.

[26] R. G. T. Mello, L. F. Oliveira, and J. Nadal, "Digital Butterworth filter for subtracting noise from low magnitude surface electromyogram," *Comput. Meth. Prog. Bio.,* vol. 87, pp. 28–35, 2007.

[27] M. Malboubi, F. Razzazi, and M. Aliyari, "Elimination of power line noise from EMG signals using an efficient adaptive laguerre filter," *Proc., ICSES, Gliwice,* Poland, September, 2010.

[28] M. J. D. Silva, "Characterization of QRS complex in ECG signals applying wavelet transform," *Proc., ICMEAE Int. Conf.,* pp. 86-89, 2005.

[29] R. Istenic, P. A. Kaplanis, C. S. Pattichis, and D. Zazula, "Analysis of Neuromuscular Disorders Using Statistical and Entropy Metrics on Surface EMG," *WSEAS Trans Signal Proces.,* no. 2, vol. 4, pp.1790-5052, February 2008.

[30] S. Conforto, T. D'Alessio, and S. Pignatelli, "Optimal rejection of movement artefacts from myoelectric signals by means of a wavelet filtering procedure," *J. Electromyogr. Kines.,* vol. 9, pp. 47-57, 1999.

[31] M. Garcia, M. Martinez-Iniesta, J. Rodenas, J. J. Rieta, and R. Alcaraz, "A novel wavelet-based filtering strategy to remove powerline interference from electrocardiograms with atrial fibrillation," *Physiol. Meas.,* vol. 39, no. 11, p. 115006, Nov. 2018.

[32] M. Aneja and B. Singh, "Powerline Interference Reduction in ECG Using Combination of MA Method and IIR Notch," *IJRTE.,* vol. 2, Jan. 2009.

[33] S. Thalkar and D. Upasani, "Various Techniques for Removal of Power Line Interference From ECG Signal," *Int J Sci Res.,* vol 4, no. 12, pp. 12-23, December 2013.

[34] C. Levkov, G. Mihov, R. Ivanov, I. Daskalov, I. Christov, and I. Dotsinsky, "Removal of power-line interference from the ECG: a review of the subtraction procedure," *Biomed. Eng. OnLine.,* vol. 4, p. 50, Aug. 2005.

[35] A. Fratini, P. Bifulco, M. Romano, F. Clemente, and M. Cesarelli, "Simulation of surface EMG for the analysis of muscle activity during whole body vibratory stimulation," *Comput. Methods Programs Biomed.,* vol. 113, no. 1, pp. 314–322, Jan. 2014.

[36] J. J. Morley and E. Traum, "The effects of dorso-lumbar motion restriction on EMG activity of selected muscles during running," *J. Bodyw. Mov. Ther.,* vol. 22, no. 1, pp. 166–177, Jan. 2018.

[37] A. Fratini, M. Cesarelli, P. Bifulco, and M. Romano, "Relevance of motion artifact in electromyography recordings during vibration treatment," *J. Electromyogr. Kinesiol.,* vol. 19, no. 4, pp. 710–718, Aug. 2009.

[38] I. Rodríguez-Carreño, A. Malanda-Trigueros, L. Gila-Useros, J. Navallas-Irujo, and J. Rodríguez-Falces, "Filter design for cancellation of baseline-fluctuation in needle EMG recordings," *Comput. Methods Programs Biomed.*, vol. 81, no. 1, pp. 79–93, Jan. 2006.

[39] F. N. Jamaluddin et al., "Estimation of wavelet threshold value for surface EMG baseline removal," *Proc. IEEE EMBS Conference on Biomedical Engineering and Sciences (IECBES).*, 2016, pp. 102–105.

[40] N. W. Willigenburg, A. Daffertshofer, I. Kingma, and J. H. V. Dieën, "Removing ECG contamination from EMG recordings: A comparison of ICA-based and other filtering procedures," *J. Electromyogr. Kines.*, vol. 22, no. 3, pp. 485-493, 2012.

[41] A. Agostinelli, A. Sbrollini, C. Giuliani, S. Fioretti, F. D. Nardo, and L. Burattini, "Segmented beat modulation method for electrocardiogram estimation from noisy recordings," *Med. Eng. Phys.*, vol. 38, no. 6, pp. 560–568, Jun. 2016.

[42] S. Jain, M. K. Ahirwal, A. Kumar, V. Bajaj, and G. K. Singh, "QRS detection using adaptive filters: A comparative study," *ISA Trans.*, vol. 66, pp. 362–375, Jan. 2017.

[43] A. Appathurai, J. J. Carol, S. N. Kumar, and A. J. G. Malar, "A Study on ECG signal Characterization and Practical Implementation of Some ECG Characterization Techniques," *Measurement*, May 2019.

[44] R. Ritzmann, A. Kramer, M. Gruber, A. Gollhofer, and W. Taube, "EMG activity during whole body vibration: motion artifacts or stretch reflexes?," *Eur. J. Appl. Physiol.*, vol. 110, no. 1, pp. 143–151, Sep. 2010.

[45] A. Fratini, A. La Gatta, P. Bifulco, M. Romano, and M. Cesarelli, "Muscle motion and EMG activity in vibration treatment," *Med. Eng. Phys.*, vol. 31, no. 9, pp. 1166–1172, Nov. 2009.

[46] P. S. Hamilton, M. Curley, and R. Aimi, "Effect of adaptive motion-artifact reduction on QRS detection.," *Biomed. Instrum. Technol.*, vol. 34, no. 3, pp. 197–202, 2000.

[47] M. R. Ahsan, M. I. Ibrahimy, and O. O. Khalifa, “Neural Network Classifier for Hand Motion Detection from EMG Signal,” *Proc.5th Kuala Lumpur International Conference on Biomedical Engineering*, 2011, pp. 536–541.

[48] M. R. Ahsan, M. I. Ibrahimy, and O. O. Khalifa, “Hand motion detection from EMG signals by using ANN based classifier for human computer interaction,” *Proc. Simulation and Applied Optimization 2011 Fourth International Conference on Modeling.*, 2011, pp. 1–6.

[49] M. Zivanovic and M. González-Izal, “Simultaneous powerline interference and baseline wander removal from ECG and EMG signals by sinusoidal modeling,” *Med. Eng. Phys.*, vol. 35, no. 10, pp. 1431–1441, Oct. 2013.

[50] L. Frey Law, C. Krishnan, and K. Avin, “Modeling nonlinear errors in surface electromyography due to baseline noise: A new methodology,” *J. Biomech.*, vol. 44, no. 1, pp. 202–205, Jan. 2011.

[51] I. Rodríguez, L. Gila, A. Malanda, C. Campos, and G. Morales, “Baseline removal from EMG recordings,” *Conf. Proc. 23th Annu. Int. Conf. IEEE Eng. Med. Biol. Soc. IEEE Eng. Med. Biol. Soc. Annu. Conf.*, vol. 2, pp. 1034–1037, 2001.

[52] F. Nougaroua, D. Massicottea, and M. Descarreaux, “Efficient procedure to remove ECG from sEMG with limited deteriorations: Extraction, quasi-periodic detection and cancellation,” *Biomed. Signal Process. Control.*, vol. 39, pp. 1-10, 2018.

[53] S. Yazdani, M. R. Azghani , and M. H. Sedaaghi, “A new algorithm for ECG interference removal from single channel EMG recording,” *Australas Phys Eng Sci Med.*, vol. 40, no. 3, pp 575–584, 2017.

[54] J. B. Muriel, F. Romero, F. J. Alonso, K. Gianikellis, “A simple SSA-based de-noising technique to remove ECG interference in EMG signals,” *Biomed. Signal Process. Control.*, vol. 30, pp. 117-126, 2016.

[55] Y. Zheng and X. Hu, “Interference Removal from Electromyography Based on Independent Component Analysis,” *IEEE Trans. Neural Syst. Rehabil. Eng.*, vol. 27, no. 5, pp. 887–894, May 2019.

[56] N. Miljković, N. Popović, O. Djordjević, L. Konstantinović, and T. B. Šekara, "ECG artifact cancellation in surface EMG signals by fractional order calculus application," *Comput. Methods Programs Biomed.*, vol. 140, pp. 259–264, Mar. 2017.

[57] G. T. Allison, "Trunk muscle onset detection technique for EMG signals with ECG artefact," *J. Electromyogr. Kinesiol. Off. J. Int. Soc. Electrophysiol. Kinesiol.*, vol. 13, no. 3, pp. 209–216, Jun. 2003.

[58] J. Mateo, E. M. Sánchez-Morla, and J. L. Santos, "A new method for removal of powerline interference in ECG and EEG recordings," *Comput. Electr. Eng.*, vol. 45, pp. 235–248, Jul. 2015.

[59] N. M. Verulkar, P. H. Zope, and S. R. Suralkar, "Filtering Techniques for Reduction of Power Line Interference in Electrocardiogram Signals," *Int J Eng Res Tech.*, vol. 1, no. 9, pp. 1-7, November 2012.

[60] I. Ahmad, F. Ansari, and U. Dey, "Power line interference noise removal in ECG-A Comparative study," *Int. J. Compt. Sci. Engr (IJCSE).*, vol. 7, no.2, pp. 13-18, Feb 2015.

[61] I. I. Christov and I. K. Daskalov, "Filtering of electromyogram artifacts from the electrocardiogram," *Med. Eng. Phys.*, vol. 21, no. 10, pp. 731–736, Dec. 1999.

[62] S. Yacoub and K. Raoof, "Power line interference rejection from surface electromyography signal using an adaptive algorithm," *IRBM*, vol. 29, no. 4, pp. 231–238, Sep. 2008.

[63] M. Ladrova, R. Martinek, J. Nedoma, and M. Fajkus, "Methods of Power Line Interference Elimination in EMG Signal," *Journal of Biomimetics, Biomaterials and Biomedical Engineering (JBBBE).*, vol. 40, no. pp. 64-70, 2019.

[64] I. Christov, R. Raikova, and S. Angelova, "Separation of electrocardiographic from electromyographic signals using dynamic filtration," *Medical Engineering & Physics.*, vol. 57, pp 1-10, 2018.

[65] J. N. F. Mak, Y. Hu, and K. D. K. Luk, "An automated ECG-artifact removal method for trunk muscle surface EMG recordings," *Med Eng Phys.,* vol. 32, no. 8, pp. 840-848, 2010.

[66] M. Redfern, R. Hughes, and D. Chaffin, "High-pass filtering to remove electrocardiographic interference from torso EMG recordings," *Clin. Biomech.,* vol. 8, no. 1, pp. 44–48, Jan. 1993.

[67] J. D. C. Juniora, J. M. D. Seixas, and A. M. F. L. M. D. Sa, "A template subtraction method for reducing electrocardiographic artifacts in EMG signals of low intensity," *Biomed. Signal Process. Control.,* vol. 47, pp. 380-386, 2019.

[68] R. J. Marker and K. S. Maluf, "Effects of electrocardiography contamination and comparison of ECG removal methods on upper trapezius electromyography recordings," *J. Electromyogr. Kines.,* vol. 24, no. 6, pp. 902-909, 2014.

[69] Y. Slim and K. Raoof, "Removal of ECG interference from surface respiratory electromyography," *IRBM.,* no. 4, vol. 31, pp. 209-220, 2010.

[70] C. Zhan, L. F. Yeung, Z. Yang, "A wavelet-based adaptive filter for removing ECG interference in EMGdi signals," *J. Electromyogr. Kines.,* vol. 20, no. 3, pp. 542-549, 2010.

[71] W. Jenkal, R. Latif, A. Toumanari, A. Dliou, O. El B'charri, and F. M. R. Maoulainine, "An efficient algorithm of ECG signal denoising using the adaptive dual threshold filter and the discrete wavelet transform," *Biocybern. Biomed. Eng.,* vol. 36, no. 3, pp. 499–508, Jan. 2016.

[72] M. Rakshit and S. Das, "An efficient ECG denoising methodology using empirical mode decomposition and adaptive switching mean filter," *Biomed. Signal Process. Control.,* vol. 40, pp. 140–148, Feb. 2018.

[73] J. Piskorowski, "Time-efficient removal of power-line noise from EMG signals using IIR notch filters with non-zero initial conditions," *Biocybern Biomed Eng.,* vol. 33, no. 3, pp. 171-178, 2013.

[74] P. C. Bhaskar, M. D. Uplane, “High Frequency Electromyogram Noise Removal from Electrocardiogram Using FIR Low Pass Filter Based on FPGA,” *Proc. Technol.,* vol.25, pp. 497-504, 2016.

[75] V. Tscharner, B. Eskofier, and P. Federolf, “Removal of the electrocardiogram signal from surface EMG recordings using non-linearly scaled wavelets,” *J. Electromyogr. Kines.*, vol. 21, no.4, pp. 683-688, 2011.

[76] A. Sbrollini et al., “Surface electromyography low-frequency content: Assessment in isometric conditions after electrocardiogram cancellation by the Segmented-Beat Modulation Method,” *Inform. Med. Unlocked.,* vol. 13, pp. 71–80, Jan. 2018.

[77] H. Liang, Z. Lin, and F. Yin, “Removal of ECG contamination from diaphragmatic EMG by nonlinear filtering,” *Nonlinear Anal. Theory Methods Appl.,* vol. 63, no. 5, pp. 745–753, Nov. 2005.

[78] A. Diab, M. Hassan, C. Marque, and B. Karlsson, “Performance analysis of four nonlinearity analysis methods using a model with variable complexity and application to uterine EMG signals,” *Med. Eng. Phys.,* vol. 36, no. 6, pp. 761–767, Jun. 2014.

[79] G. Luo and Z. Yang, “The application of ECG cancellation in diaphragmatic electromyographic by using stationary wavelet transform” *Biomed. Eng. Lett.*, no. 3, vol. 8, pp 259–266, 2018.

[80] M. Niegowski and M. Zivanovic “Wavelet-based unsupervised learning method for electrocardiogram suppression in surface electromyograms,” *Med Eng Phys.,* vol. 38, no. 3, pp. 248-256, 2016.

[81] J. Joy and P. Manimegalai, “Wavelet Based EMG Artifact Removal from ECG Signal,” *J. Eng. Comput. Appl. Sci.,* vol. 2, no. 8, pp. 55–58, Aug. 2013.

[82] K. D. Priya, G. S. Rao, and P. S. V. S. Rao, “Comparative Analysis of Wavelet Thresholding Techniques with Wavelet-wiener Filter on ECG Signal,” *Procedia Comput. Sci.,* vol. 87, pp. 178–183, Jan. 2016.

[83] H.-Y. Lin, S.-Y. Liang, Y.-L. Ho, Y.-H. Lin, and H.-P. Ma, “Discrete-wavelet-transform-based noise removal and feature extraction for ECG signals,” *IRBM*, vol. 35, no. 6, pp. 351–361, Dec. 2014.

[84] A. Nishad, A. Upadhyay, R. B. Pachori, and U. R. Acharya, “Automated classification of hand movements using tunable-Q wavelet transform based filter-bank with surface electromyogram signals,” *Future Gener. Comput. Syst.*, vol. 93, pp. 96–110, Apr. 2019.

[85] M. Ferdjallah and R. E. Barr, “Frequency-domain digital filtering techniques for the removal of powerline noise with application to the electrocardiogram,” *Comput. Biomed. Res.*, vol. 23, no. 5, pp. 473–489, Oct. 1990.

[86] D. T. Mewett, H. Nazeran, and K. J. Reynolds, “Removing power line noise from recorded EMG,” *Conf. Proc. 23th Annu. Int. Conf. IEEE Eng. Med. Biol. Soc. IEEE Eng. Med. Biol. Soc. Annu. Conf.*, vol. 3, pp. 2190–2193, 2001.

[87] S. Yacoub, K. Raouf, and H.Eleuch, “Filtering of Cardiac and Power Line in Surface Respiratory EMG Signal,” *Commun. Pure Appl. Math.*, vol. 4, p. 365, Sep. 2010.

[88] S. Yacoub and K. Raoof, “Noise Removal from Surface Respiratory EMG Signal,” *International Journal of Electronics and Communication Engineering. (IJECE).*, vol 2, no. 2, pp. 266-273, 2008.

[89] M. Golabbakhsh, M. Masoumzadeh, and M. Sabahi, “ECG and Power Line Noise Removal from Respiratory EMG Signal Using Adaptive Filters,” *Majlesi J. Electr. Eng.*, vol. 5, Dec. 2011.

[90] O. Singh and R. K. Sunkaria, “Powerline interference reduction in ECG signals using empirical wavelet transform and adaptive filtering,” *J. Med. Eng. Technol.*, vol. 39, no. 1, pp. 60–68, Jan. 2015.

[91] X. Sui, K. Wan, and Y. Zhang, “Pattern recognition of SEMG based on wavelet packet transform and improved SVM,” *Optik*, vol. 176, pp. 228–235, Jan. 2019.

[92] R. Mali, M. Khadtare, and U. Bombale, “Removal of 50Hz PLI using Discrete Wavelet Transform for Quality Diagnosis of Biomedical ECG Signal,” *Int. J. Comput. Appl.*, vol. 23, Jun. 2011.

[93] T. D. Bui and G. Chen, “Translation-invariant denoising using multiwavelets,” *IEEE Trans. Signal Process.*, 46 (1998) 3414-3420.

[94] T. Oo, P. Phukpattaranont, and P. Klabklay, “Effects of SNR on removing ECG noise from EMG signal using DSWT,” *Proc. 15th Int. Conf. Electr. Eng. Comput. Telecommun. Inf. Technol. ECTI-CON*, pp. 253–256, 2018.

[95] T. Oo, and P. Phukpattaranont, “Accounting for SNR in an Algorithm using Wavelet Transform to Remove ECG Interference from EMG Signals”, *Fluctuation and Noise Letters,* Accepted for publication.

[96] T. Gronfors, T. Sihvonen, V. Lamsa, and N. Paivinen, “Spectral Factors and Medical Parameters of EMG Signals,” *IET 3rd International Conference On Advances in Medical, Signal and Information Processing - MEDSIP*, pp. 1–4, 2006.

[97] S. Thongpanja, A. Phinyomark, F. Quaine, Y. Laurillau, C. Limsakul, and P. Phukpattaranont,” Probability density functions of stationary surface EMG signals in noisy environments*.,” IEEE Trans. Instrum. Meas.,* 65 (2016) 1547-1557.

[98] K. Nazarpour, A. H. Al-Timemy, G. Bugmann, and A. Jackson, “A note on the probability distribution function of the surface electromyogram signal,” *Brain Res. Bull.*, vol. 90, pp. 88–91, Jan. 2013.

[99] G. R. Naik and D. K. Kumar, “Evaluation of higher order statistics parameters for multi channel sEMG using different force levels,” *Conf. Proc. Annu. Int. Conf. IEEE Eng. Med. Biol. Soc. IEEE Eng. Med. Biol. Soc. Annu. Conf.*, vol. 2011, pp. 3869–3872, 2011.

[100] A. Phinyomark, S. Hirunviriya, C. Limsakul, and P. Phukpattaranont, “Evaluation of EMG feature extraction for hand movement recognition based on Euclidean distance and standard deviation,” *Proc. 15th Int. Conf. Electr. Eng. Comput. Telecommun. Inf. Technol. ECTI-CON*, pp. 856–860, 2010.

[101] G. M. Hägg and J. Suurküla, "Zero crossing rate of electromyograms during occupational work and endurance tests as predictors for work related myalgia in the shoulder/neck region," *Eur. J. Appl. Physiol.*, vol. 62, no. 6, pp. 436–444, 1991.

[102] S. Thongpanja, A. Phinyomark, P. Phukpattaranont, and C. Limsakul, "Mean and Median Frequency of EMG Signal to Determine Muscle Force Based on Time-Dependent Power Spectrum," *Elektron. Ir Elektrotechnika*, vol. 19, pp. 51–56, Mar. 2013.

[103] G. D. Fraser, A. D. C. Chan, J. R. Green, and D. T. Macisaac, "Automated biosignal quality analysis for electromyography using a one-class support vector machine," *IEEE Trans. Instrum. Meas.*, vol.63, pp. 2919-2930, 2014.

[104] S. Garimella, S. H. Mallidi, and H. Hermansky, "Regularized auto-associative neural networks for speaker verification," *IEEE Signal Process Lett.*, vol.19, pp.841–844, 2012.

[105] S. E. Hussein, O. A. Hassan, and M. H. Granat, "Assessment of the potential iridology for diagnosing kidney disease using wavelet analysis and neural networks," *Biomed. Signal Process. Control.*, vol.8, pp.534–541, 2013.

[106] K. S. Narendra and S. Mukhopadhyay, "Adaptive control using neural networks and approximate models," *IEEE Trans. Neural Netw.*, vol.8, pp. 475-485, 1997.

[107] M. I. Ibrahimy, R. Ahsan, and O. O. Khalifa, "Design and Optimization of Levenberg-Marquardt based Neural Network Classifier for EMG Signals to Identify Hand Motions," *Meas. Sci. Rev.*, vol. 13, no. 3, pp. 142–151, Jun. 2013.

[108] P. McCool, G. D. Fraser, A. D. C. Chan, L. Petropoulakis, and J. J. Soraghan, "Identification of contaminant type in surface electromyography (EMG)," *IEEE Trans. Neural Syst. Rehabil. Eng.*, vol. 22, pp. 774-783, 2014.

[109] P. E. McSharry, G. D. Clifford, L. Tarassenko, and L. A. Smith, "A dynamical model for generating synthetic electrocardiogram signals," *IEEE Trans. Biomed. Eng.*, vol.50, pp. 289-294, 2003.

[110] M. Yochum and S. Binczak, “A wavelet based method for electrical stimulation artifacts removal in electromyogram,” *Biomed. Signal Process. Control.*, vol. 22, pp. 1–10, Sep. 2015.

[111] B. R. de Oliveira *et al.*, “A wavelet-based method for power-line interference removal in ECG signals,” *Res. Biomed. Eng.*, vol. 34, no. 1, pp. 73–86, Jan. 2018

APPENDIX A

RELATED PAPERS

International Journal Publications

A.1 T. Oo, and P. Phukpattaranont, "Accounting for SNR in an Algorithm using Wavelet Transform to Remove ECG Interference from EMG Signals", *Fluctuation and Noise Letters,* Accepted for publication.

International Conference Publications

A.2 T. Oo, P. Phukpattaranont, and P. Klabklay, "Effects of SNR on removing ECG noise from EMG signal using DSWT," *Proc. 15th Int. Conf. Electr. Eng. Comput. Telecommun. Inf. Technol. ECTI-CON*, pp. 253–256, 2018.

Appendix A.1

T. Oo, and P. Phukpattaranont, "Accounting for SNR in an Algorithm using Wavelet Transform to Remove ECG Interference from EMG Signals", *Fluctuation and Noise Letters*, Accepted for publication.

May 13, 2019 11:08:58am WSPC/167-FNL 2050001 ISSN: 0219-4775 2nd Reading

Fluctuation and Noise Letters
Vol. 19, No. 1 (2019) 2050001 (17 pages)

DOI: 10.1142/S0219477520500017

World Scientific
www.worldscientific.com

Accounting for SNR in an Algorithm Using Wavelet Transform to Remove ECG Interference from EMG Signals

Thandar Oo and Pornchai Phukpattaranont*

Department of Electrical Engineering
Faculty of Engineering, Prince of Songkla University
Hat Yai, Songkhla 90112, Thailand
**pornchai.p@psu.ac.th*

Received 5 December 2018
Accepted 2 April 2019
Published

Communicated by Tomislav Stankovski

When the electromyography (EMG) signal is acquired from muscles in the torso, the electrocardiography (ECG) signal coming from heart activity can interfere. As a result, the EMG signal can be contaminated during data collection. In this paper, a technique based on discrete stationary wavelet transform (DSWT) is proposed to remove ECG interference from the EMG signal while taking into account the signal-to-noise ratio (SNR). The contaminated EMG signal is decomposed using 5-level DSWT with the Symlet wavelet function. The coefficients for levels 4 and 5, which are contaminated by ECG, are set to zero when their absolute values are less than or equal to a threshold determined for each SNR level. A clean EMG signal can then be obtained by inverse DSWT mapping of the new thresholded coefficients. We evaluated the performance of the proposed algorithm using simulated EMG contaminated with both simulated and real ECG signals, at 9 SNR levels from −20 to 20 dB with 5 dB increments. The performance based on mean absolute error, correlation coefficient and relative error shows that the DSWT method is better than a high-pass filter.

Keywords: EMG signal; ECG signal; wavelet transform; SNR.

1. Introduction

Electromyography (EMG) records electric currents produced in muscle contractions acquired using electrodes. The electrode converts an ion current to an electron current so that it can be amplified and recorded by an electronic circuit. The EMG signal is generated from motor units, which are nerve–muscle functional units of the neuromuscular system. The potential difference can be measured by either

*Corresponding author.

May 13, 2019 11:09:01am WSPC/167-FNL 2050001 ISSN: 0219-4775 2nd Reading

non-invasive electrodes for surface EMG signals or by invasive electrodes for needle EMG sampling intramuscular EMG signals [1].

There are a variety of applications for EMG signals. The EMG signal can be used not only as an electrodiagnostic medical technique but also as a neurophysiological technique for evaluating and recording the electrical activity produced by skeletal muscles [2]. Moreover, the EMG signal recorded from a muscle contraction has a variety of uses in clinical applications [3], evolvable hardware chip development [4], modern human–computer interaction [5], and electrical wheelchair control [6].

An essential element for enabling the above-described applications is an EMG recognition system. The EMG recognition system consists of three cascaded modules, namely; data pre-processing, feature extraction and classification [7]. The primary purpose of data pre-processing is to remove noise in the EMG signal, which is contaminated by the environment as it passes through various tissues [8]. We focus on removing the electrocardiography (ECG) interference from a contaminated EMG signal in this work. ECG reflects the electrical activity of the heart, and is not only used for measuring and recording that electrical activity but also to assess the rhythm and invariability of a heartbeat. The ECG interference in some applications can contaminate the EMG signal because of the proximity of the trunk muscles and the heart. An example is the measurement of EMG signal from the pectoralis muscle, which can be used as a control signal for shoulder disarticulation prosthesis [9].

From a literature review, there are five techniques for removing ECG interference from a contaminated EMG signal: (1) linear filter [9, 10, 12, 13]; (2) template subtraction [9–11, 14]; (3) adaptive filters including linear ones [9, 11, 14, 16, 17] and non-linear techniques [9, 14–18]; (4) wavelet transform [9, 14]; and (5) combined techniques such as template subtraction combined with a high pass filter [10], artificial neural network (ANN) combined with wavelet transform [15], and adaptive neuro-fuzzy inference system (ANFIS) combined with wavelet transform [11].

Among all the techniques used for removing the ECG interference from the EMG signal, only the linear filter and the wavelet transform do not require a separate additional ECG reference channel. Advantages of these two approaches are their convenient use and the reducing cost of an electrode. Among the linear filter techniques, high pass filtering is one of the most popular methods used for eliminating ECG interference from EMG signals. Most energy of ECG interference is in the range from 0 to 30 Hz. Therefore, a high-pass filter (HPF) with 30 Hz cutoff frequency is used. There are two designs of HPF used for ECG interference removal, namely Butterworth filter [9, 10, 12, 13] and digital finite impulse response filter [11]. In previous studies, the discrete wavelet transform (DWT) with thresholding was proposed to remove ECG interference from EMG signals [9–11]. However, the threshold levels were fixed and determined without consideration of signal-to-noise ratio (SNR). To extend the studies [9–11], we explore the effects of SNR on the appropriate threshold level in an algorithm removing ECG component from EMG signals by using wavelet transform.

May 13, 2019 11:09:01am WSPC/167-FNL 2050001 ISSN: 0219-4775 2nd Reading

The discrete stationary wavelet transform (DSWT) is of interest because of its two crucial properties, time invariance and Gibb phenomena suppression, which benefit a noise removal algorithm as described in Ref. 19. The noise removal algorithm employing these two properties performed very well in eliminating the power line interference from EMG signals in Ref. 20. We use DSWT in this paper because these two properties can be deployed. Moreover, it opens an opportunity for simultaneously removing both ECG interference and power line interference using only one wavelet transform. As a result, we can reduce the computational complexity of the noise removal algorithm. We proposed the DSWT algorithm with a thresholding procedure for removing ECG from EMG signals. The effects of SNR on the threshold level were evaluated with the EMG signal having 9 alternative SNR levels.

The rest of this paper is organized as follows. Section 2 gives briefly relevant details on the DSWT. Section 3 explains the methods for data generation, the proposed ECG removal technique based on DSWT, and the performance metrics used for evaluation. Results are given in Sec. 4. The discussion is provided in Sec. 5. Finally, conclusions are drawn in Sec. 6.

2. DSWT

DWT may be replaced with DSWT in some applications where time-invariance is required. DSWT can be implemented by removing the down-samplers and up-samplers in DWT, and by modifying the filters by upsampling the coefficients from the previous decomposition level. However, DSWT is a redundant transform, which contains the same number of samples between the input and the output at each decomposition level.

Let $x[n]$ be a signal to be decomposed using L-level DSWT. Two outputs from the first level decomposition consist of the approximation coefficients, cA1, from the convolution between the low-pass filter $h_1[n]$ and the input signal $x[n]$ and the detail coefficients, cD1, from the convolution between the high-pass filter $g_1[n]$ and the input signal $x[n]$. Note that the lengths of $x[n]$, cA1 and cD1 are the same. In the next level decomposition, the approximation coefficients, cA1, will be used as input. The filters $h_1[n]$ and $g_1[n]$ are modified by upsampling to $h_2[n]$ and $g_2[n]$. The outputs from second level decomposition can be obtained by convolving cA1 with $h_2[n]$ and $g_2[n]$ resulting in the approximation coefficients cA2 and the detail coefficients cD2, respectively. We can keep repeating these operations until the decomposition level L is reached. Figures 1(a) and 1(b) shows an example of 5-level DSWT decomposition and the upsampling operation for the filters at each decomposition level, respectively. Figure 2 shows an example of 5-level DSWT reconstruction, where $h_j'[n]$ and $g_j'[n]$ are reconstruction low-pass and high-pass filters at level j, respectively.

May 13, 2019 11:09:01am WSPC/167-FNL 2050001 ISSN: 0219-4775 2nd Reading

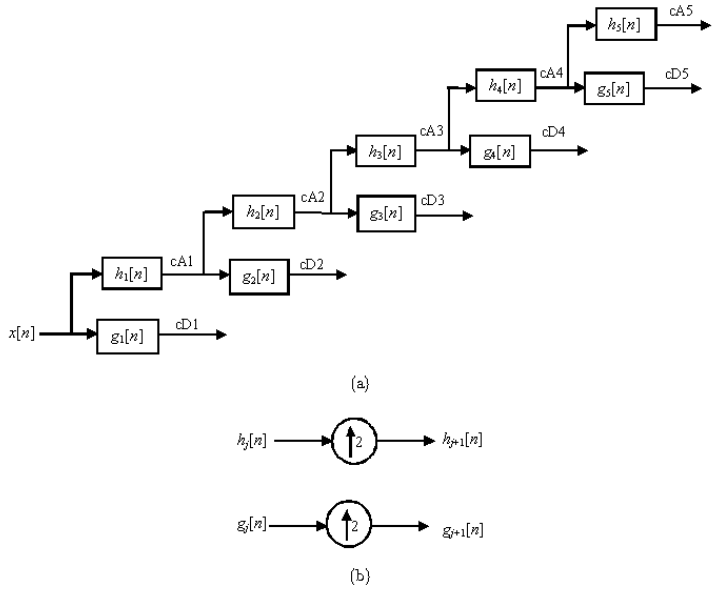

Fig. 1. (a) Example of 5-level DSWT decomposition. (b) Upsampling operation for the filters in each decomposition level.

3. Materials and Methods

3.1. *Data generation*

3.1.1. *Simulated EMG*

A simulated EMG is generated by filtering a white Gaussian noise with a band-pass filter, whose transfer function is given by [21]

$$H(f) - \frac{jf_U^2 f}{(f_L + jf)(f_U + jf)^2} \tag{1}$$

where f_L is the lower frequency parameter, which is random from 30–60 Hz and f_U is the upper-frequency parameter, which is random from 30–100 Hz plus f_L. The length of each signal is 2000 samples, which is equivalent to 2 s at a sampling rate of 1000 Hz. Figure 3 shows the waveform of the simulated EMG generated with $f_L - 45$ Hz and $f_U - 110$ Hz in the time domain (Top panel) and corresponding power spectra in the frequency domain (Bottom panel). We can see that the power spectrum from the simulated EMG signal (solid line) agrees well with that from the bandpass filter $H(f)$ (dotted line).

May 13, 2019 11:09:09am WSPC/167-FNL 2050001 ISSN: 0219-4775 2nd Reading

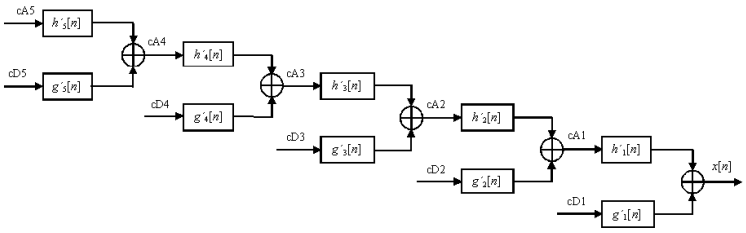

Fig. 2. Example of 5-level DSWT reconstruction.

3.1.2. *Simulated ECG*

We generate a simulated ECG signal using a dynamical model based on three coupled ordinary differential equations, which can be expressed as [22]

$$\dot{x} = \alpha x - \omega y, \tag{2}$$

$$\dot{y} = \alpha y + \omega x, \tag{3}$$

$$z = -\sum_{i\in\{P,Q,R,S,T\}} a_i \Delta\theta_i \exp\left(-\frac{\Delta\theta_i^2}{2b_i^2}\right) - (z - z_0), \tag{4}$$

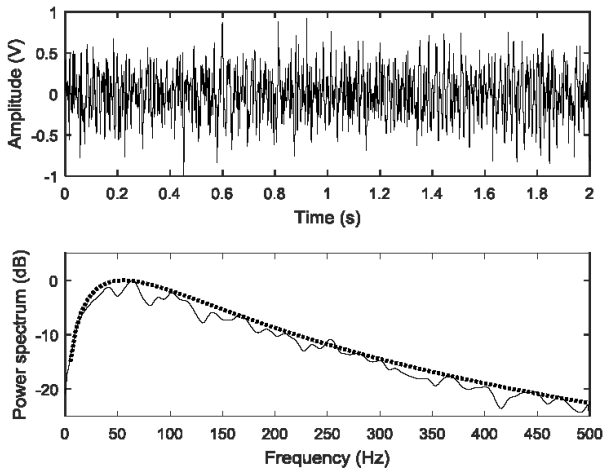

Fig. 3. Simulated EMG in the time domain (Top panel) and its power spectrum in the frequency domain (Bottom panel). Solid line: Power spectrum from the simulated EMG signal. Dotted line: Frequency response of the bandpass filter $H(f)$.

May 13, 2019 11:09:25am WSPC/167-FNL 2050001 ISSN: 0219-4775 2nd Reading

Table 1. Specific parameters used for generating the simulated ECG.

Parameter	Description	P	Q	R	S	T
θ_i (degrees)	Angles of extrema	-70	-15	0	15	100
a_i	z-position of extrema	1.2	-5.0	30.0	-7.5	0.75
b_i	Gaussian width of peaks	0.25	0.1	0.1	0.1	0.4

where $\alpha = 1 - \sqrt{x^2 + y^2}$, $\Delta\theta_i = (\theta - \theta_i) \bmod 2\pi$, $\theta = \text{atan2}(y, x)$ (the four quadrant arctangent of the real parts of the elements of x and y, with $-\pi \leq \text{atan2}(y, x) \leq \pi$) and ω is the angular velocity of the trajectory as it moves around the limit cycle. The parameters θ_i, a_i and b_i for the PQRST points are suggested by visualization of ECG from a healthy subject. In this paper, the values used for all three parameters in the simulation are given in Table 1. The simulated ECG signal was generated with a sampling frequency of 256 Hz. Mean heart rate was randomly selected from 60–100 beats per min. Figure 4 shows an example of simulated ECG signals from 2 mean heart rates in the time domain (Top panel) and their power spectra in the frequency domain (Bottom panel).

3.1.3. *Real ECG*

The real ECG signal was obtained from the MIT-BIH arrhythmia database. We acquired a normal ECG beat from 40 records with 20 s for each record. Subsequently,

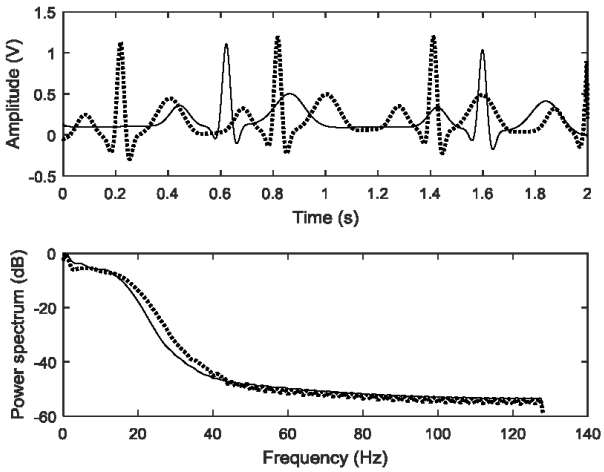

Fig. 4. Examples of simulated ECG signals in the time domain (Top panel) and their power spectra in the frequency domain (Bottom panel) when the mean heart rates are 60 (solid line) and 100 (dotted line) beats per min.

May 13, 2019 11:09:33am WSPC/167-FNL 2050001 ISSN: 0219-4775 2nd Reading

each record was resampled from 360 to 1000 Hz to match with the sampling rate of the EMG signal. Finally, each 20-s data were segmented into 2 s data.

3.1.4. *EMG contamination*

We generated 9 types of EMG signals contaminated with the ECG interference, namely with SNR levels from -20 to 20 dB at 5 dB increments. The SNR was calculated using the equation given by

$$\mathrm{SNR} = 10\log_{10}\left(\frac{P_x}{P_n}\right), \tag{5}$$

where P_x was an average power of the EMG signal and P_n was an average power of the ECG interference. Two datasets were generated. While the first dataset consisted of the simulated EMG signal contaminated with the simulated ECG interference, the second dataset comprised the simulated EMG signal contaminated with the real ECG interference. Details of generating each dataset are as follows:

- Simulated EMG contaminated with simulated ECG (SMSC): Fifty simulated ECG signals and 50 simulated EMG signals were randomly chosen and mixed with amplitude scaling to produce the EMG signals contaminated with ECG at each desired level of SNR.
- Simulated EMG contaminated with real ECG (SMRC): The procedure was similar to the first dataset, except that the simulated ECG signal was replaced with the real ECG signal. As a result, fifty simulated EMG signals contaminated with real ECG interference were obtained at each SNR level.

3.2. *Methods*

We describe a noise removal model in this section. Figure 5 shows a general block diagram of noise removal in the contaminated EMG signal, where x_u is an uncontaminated EMG signal, n_0 is an ECG interference, x_c is a contaminated EMG signal and x_{cl} is a contaminated EMG signal that is cleaned by noise removal algorithm. After noise removal, the performance of the technique can be measured using criteria based on the mean absolute error (MAE), correlation coefficient (CC) and relative error (RE). The MAE can be expressed as [20]

$$\mathrm{MAE} = \frac{1}{N}\sum |x_u - x_{\mathrm{cl}}|. \tag{6}$$

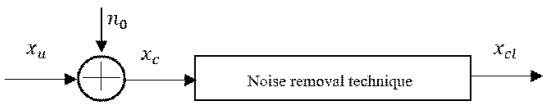

Fig. 5. General block diagram of noise removal in the contaminated EMG signal.

May 13, 2019 11:09:35am WSPC/167-FNL 2050001 ISSN: 0219-4775 2nd Reading

The closer the MAE is to 0, the better is the noise removal. The CC is given by [10, 11, 20],

$$\mathrm{CC} = \frac{\sum_{i-1}^{N}(x_u(i) - \bar{x}_u)(x_{\mathrm{cl}}(i) - \bar{x}_{\mathrm{cl}})}{\sqrt{\sum_{i-1}^{N}(x_u(i) - \bar{x}_u)^2}\sqrt{\sum_{i-1}^{N}(x_{\mathrm{cl}}(i) - \bar{x}_{\mathrm{cl}})^2}}, \tag{7}$$

where $\bar{x}_u$ is the mean value of uncontaminated EMG signal and $\bar{x}_{\mathrm{cl}}$ is the mean value of cleaned EMG signal. The closer the CC is to 1, the better is the noise removal. The RE can be expressed as [11, 15]

$$\mathrm{RE} = \frac{\sum\{P_{x_u}(f) - P_{x_{\mathrm{cl}}}(f)\}^2}{\sum P_{x_u}(f)^2}, \tag{8}$$

where $P_{x_u}(f)$ is the power spectrum of uncontaminated EMG signal and $P_{x_{\mathrm{cl}}}(f)$ the power spectrum of cleaned EMG signal. The closer the RE is to 0, the better is the noise removal.

3.2.1. *ECG interference removal algorithm based on DSWT*

The proposed method for removing the ECG interference from the EMG signal based on DSWT consists of three main stages, namely, DSWT decomposition, thresholding and DSWT reconstruction. Details on each stage are as follows:

Stage (1) Decompose the contaminated EMG signal using 5-level DSWT with the Symlet wavelet function. The Symlet wavelet function was chosen in this paper from the guideline on its successful removal of ECG interference from EMG signal in previous publications [9, 15]. Table 2 shows the frequency bands for the wavelet coefficients in the decomposition. We can see that the cutoff frequency of HPF used for removing ECG interference, which is 30 Hz [9, 10, 12, 13], agrees well with the combined frequency range of cA5 and cD5.

Stage (2) Process the coefficients at cD4 and cD5, which are contaminated by the ECG interference, with a non-linear thresholding procedure. In other words, the coefficients for cD4 and cD5, whose absolute values are less than or equal to the threshold value, are set to zero. The threshold values are varied from 0 to 10 with increments of 1. As a result, $11 \times 11 = 121$

Table 2. Frequency bands in the 5-level DSWT decomposition.

Level (k)	cAk (Hz)	cDk (Hz)
1	0–250	250–500
2	0–125	125–250
3	0–62.5	62.5–125
4	0–31.25	31.25–62.5
5	0–15.625	15.625–31.25

May 13, 2019 11:09:36am WSPC/167-FNL 2050001 ISSN: 0219-4775 2nd Reading

combinations of threshold levels for cD4 and cD5 are tested. The thresholds that give the best performance based on MAE are selected as optimal. Note that the coefficients in cA5 are set to zero because there are no EMG components in this frequency band.

Stage (3) Obtain the cleaned EMG signal by applying inverse DSWT to the new coefficients after thresholding from Stage (2).

3.2.2. *Performance measurements*

The performance of the DSWT method was compared with the linear filter technique based on Butterworth HPF [10]. The Butterworth filter was designed using a fourth-order HPF with cutoff frequency 30 Hz and was implemented in both forward and reverse directions to avoid phase distortions. The performance of the DSWT method was evaluated and compared based on MAE, CC and RE using mean and standard deviation from 50 signal implementations at each SNR.

4. Results

We implemented the ECG interference removal algorithm based on DSWT as described in Secs. 3.2.1 and demonstrated its performance using MAE, CC and RE in Tables 3, 4 and 5, respectively. Table 3 shows a comparison of MAE for DSWT and HPF noise removal techniques using SMSC and SMRC datasets. Results indicate that DSWT outperforms HPF. Across the SMSC cases, MAE from DSWT decreased approximately from 0.15 to 0.08 when SNR increased from -20 to 20 dB. However, MAE for HPF was quite comparable at every SNR, at approximately 0.20. Across SMRC cases, a similar trend as with SMSC for SNR from 0 to 20 dB was obtained. However, with SNR from -20 to -5 dB, MAE across SMRC was higher than across SMSC when compared by SNR.

A comparison of CC for DSWT and HPF noise removal techniques across SMSC and SMRC datasets is shown in Table 4. The results show that CC for DSWT was

Table 3. Comparison of MAE for DSWT and HPF noise removal techniques.

SNR (dB)	SMSC		SMRC	
	DSWT	HPF	DSWT	HPF
-20	0.1598 ± 0.0301	0.2296 ± 0.0359	0.4146 ± 0.1034	0.7396 ± 0.2293
-15	0.1468 ± 0.0305	0.2071 ± 0.0465	0.2968 ± 0.0717	0.4181 ± 0.1266
-10	0.1286 ± 0.0252	0.2122 ± 0.0520	0.1930 ± 0.0401	0.2894 ± 0.0567
-5	0.1180 ± 0.0289	0.2021 ± 0.0393	0.1600 ± 0.0306	0.2477 ± 0.0493
0	0.1168 ± 0.0295	0.2097 ± 0.0441	0.1311 ± 0.0288	0.2167 ± 0.0430
5	0.1070 ± 0.0226	0.2057 ± 0.0501	0.1070 ± 0.0248	0.2129 ± 0.0488
10	0.0986 ± 0.0223	0.2189 ± 0.0460	0.0987 ± 0.0212	0.2021 ± 0.0421
15	0.0871 ± 0.0195	0.2060 ± 0.0409	0.0942 ± 0.0225	0.2137 ± 0.0440
20	0.0829 ± 0.0187	0.2129 ± 0.0464	0.0832 ± 0.0180	0.2065 ± 0.2078

May 13, 2019 11:09:37am WSPC/167-FNL 2050001 ISSN: 0219-4775 2nd Reading

Table 4. Comparison of CC for DSWT and HPF noise removal techniques.

SNR (dB)	SMSC		SMRC	
	DSWT	HPF	DSWT	HPF
−20	0.9564 ± 0.0156	0.9529 ± 0.0143	0.8373 ± 0.0808	0.5813 ± 0.1577
−15	0.9717 ± 0.0105	0.9634 ± 0.0169	0.9161 ± 0.0356	0.7948 ± 0.1021
−10	0.9815 ± 0.0066	0.9615 ± 0.0197	0.9611 ± 0.0171	0.9019 ± 0.0512
−5	0.9856 ± 0.0067	0.9663 ± 0.0125	0.9738 ± 0.0097	0.9418 ± 0.0268
0	0.9863 ± 0.0075	0.9634 ± 0.0162	0.9813 ± 0.0084	0.9582 ± 0.0175
5	0.9889 ± 0.0047	0.9645 ± 0.0186	0.9876 ± 0.0069	0.9609 ± 0.0184
10	0.9915 ± 0.0038	0.9601 ± 0.0180	0.9903 ± 0.0043	0.9655 ± 0.0151
15	0.9937 ± 0.0028	0.9652 ± 0.0137	0.9919 ± 0.0038	0.9624 ± 0.0154
20	0.9944 ± 0.0028	0.9618 ± 0.0171	0.9943 ± 0.0023	0.9644 ± 0.0155

better than for HPF. When the SNR increased from −20 to 20 dB, the CC for DSWT increased from 0.96 to 0.99 across SMSC cases. However, CC for HPF was entirely consistent at approximately 0.96, independent of the SNR. With SMRC data, at SNR from 0 to 20 dB, a similar trend as with SMSC was seen. However, for SNR from −20 to −5 dB, CC across SMRC was lower than across SMSC when compared at similar SNR.

A comparison of RE for DSWT and HPF noise removal techniques is shown in Table 5. Across SMSC, RE for DSWT was better than for HPF. Across SMRC, we can see that DSWT (0.2) provided a significantly better average RE than HPF (45.4) at SNR −20 dB. Also, a similar pattern is seen for SNR −15 and −10 dB.

The SNR of the contaminated EMG signal affected the optimal threshold level. Table 6 shows the optimal threshold levels based on MAE in DSWT noise removal. Significant differences in the threshold levels between the two datasets are observed at SNR −20 and −15 dB for both cD4 and cD5. The threshold levels with SMRC are smaller than those with SMSC, which may be caused by an attempt to remove other types of artifacts, such as power line interference, contaminating the EMG signals.

Table 5. Comparison of RE for DSWT and HPF noise removal techniques.

SNR (dB)	SMSC		SMRC	
	DSWT	HPF	DSWT	HPF
−20	0.0153 ± 0.0199	0.0514 ± 0.0420	0.2045 ± 0.2263	45.38 ± 67.2631
−15	0.0142 ± 0.0152	0.0607 ± 0.0546	0.1054 ± 0.2155	2.0230 ± 3.7012
−10	0.0120 ± 0.0136	0.0774 ± 0.0634	0.0164 ± 0.0170	0.2648 ± 0.4327
−5	0.0124 ± 0.0210	0.0647 ± 0.0399	0.0586 ± 0.0624	0.0724 ± 0.0866
0	0.0258 ± 0.0340	0.0798 ± 0.0550	0.0346 ± 0.0389	0.0666 ± 0.0560
5	0.0380 ± 0.0435	0.0791 ± 0.0617	0.0102 ± 0.0129	0.0723 ± 0.0616
10	0.0074 ± 0.0094	0.0892 ± 0.0582	0.0047 ± 0.0069	0.0651 ± 0.0496
15	0.0137 ± 0.0172	0.0727 ± 0.0464	0.0051 ± 0.0057	0.0825 ± 0.0494
20	0.0066 ± 0.0117	0.0770 ± 0.0521	0.0046 ± 0.0048	0.0748 ± 0.0547

May 13, 2019 11:09:38am WSPC/167-FNL 2050001 ISSN: 0219-4775 2nd Reading

Table 6. Comparison of optimal threshold levels based on MAE.

SNR (dB)	SMSC		SMRC	
	cD4	cD5	cD4	cD5
−20	7.98 ± 1.86	5.76 ± 1.29	4.70 ± 2.44	3.74 ± 2.51
−15	9.42 ± 0.84	5.30 ± 1.09	6.02 ± 1.60	4.70 ± 2.53
−10	8.00 ± 0.90	4.92 ± 1.29	7.36 ± 1.75	5.02 ± 1.86
−5	7.42 ± 0.99	4.90 ± 1.11	7.26 ± 1.12	5.78 ± 1.63
0	7.42 ± 0.97	4.76 ± 0.92	7.26 ± 1.10	5.14 ± 1.26
5	7.12 ± 1.02	5.04 ± 1.34	7.12 ± 0.92	4.70 ± 1.04
10	7.16 ± 1.09	5.34 ± 1.26	7.22 ± 0.79	4.90 ± 1.31
15	7.00 ± 0.99	5.62 ± 1.24	7.48 ± 1.18	5.30 ± 1.30
20	7.16 ± 1.15	5.38 ± 1.14	7.40 ± 1.23	5.22 ± 1.07

5. Discussion

In this section, we explored more insights into the results from Sec. 4. Figure 6 shows an example of signals from DSWT thresholding. Figure 6(a) shows the EMG signal contaminated with the simulated ECG at SNR of −20 dB. Figure 6(b) depicts the

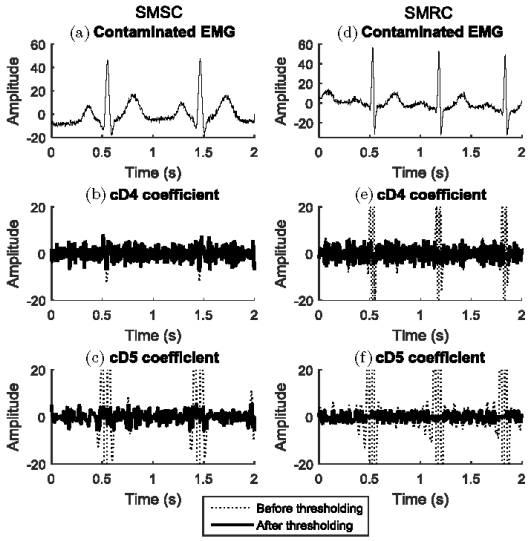

Fig. 6. While the left column shows an example of results with SMSC, the right column shows an example of results with SMRC data. The top, middle and bottom rows show EMG signal contaminated with ECG at SNR −20 dB, signals from DSWT at cD4 decomposition level and signals from DSWT at cD5 decomposition level, respectively. Dotted line: Detail coefficients before thresholding. Thick line: Detail coefficients after thresholding.

May 13, 2019 11:09:48am WSPC/167-FNL 2050001 ISSN: 0219-4775 2nd Reading

signals from DSWT at cD4 decomposition level before thresholding with a dotted line and after thresholding with a solid line. The optimal threshold is 8. Therefore, the coefficients from cD4 decomposition level before thresholding, whose absolute values are greater than 8, are truncated to 0. Figure 6(c) shows similar processing for coefficients in cD5 decomposition level with the optimal threshold 6. Figures 6(d)–6(f) show the results from the EMG signal contaminated with real ECG at SNR of −20 dB. The optimal thresholds for the coefficients in cD4 and cD5 decomposition levels are 6 and 3, respectively. We can see the ECG signal component in cD4 of SMRC, but it is invisible in SMSC. These results indicate that the real ECG signal has the frequency range 31.25–62.5 Hz, which cannot be removed using the Butterworth HPF with cutoff frequency 30 Hz as proposed in Ref. 10.

After thresholding, the cleaned EMG signal was reconstructed. Figure 7(a) shows the cleaned EMG signal from DSWT obtained by inverse DSWT of thresholded coefficients, from Figs. 6(b)–6(c), compared with the cleaned EMG signal from HPF (Fig. 7(b)) and the uncontaminated EMG signal (Fig. 7(c)). We can see that both DSWT and HPF give similar waveforms compared to the uncontaminated EMG signal. Figure 8(a) shows the absolute errors of cleaned EMG signal from DSWT and

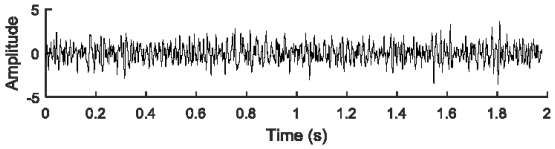

(a) Cleaned EMG signal from DSWT (SMSC)

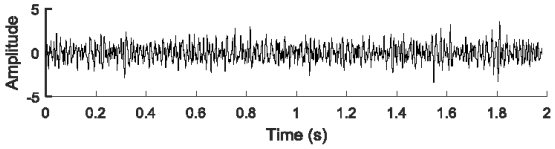

(b) Cleaned EMG signal from HPF (SMSC)

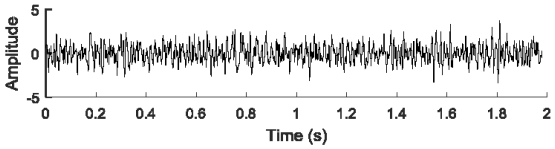

(c) Uncontaminated EMG signal (SMSC)

Fig. 7. Example of cleaned signals and the uncontaminated EMG signal from SMSC. (a) Cleaned EMG signal obtained by inverse DSWT of thresholded decomposition, from Figs. 7(b) and 7(c). (b) Cleaned EMG signal from HPF. (c) Uncontaminated EMG signal.

May 13, 2019 11:09:51am WSPC/167-FNL 2050001 ISSN: 0219-4775 2nd Reading

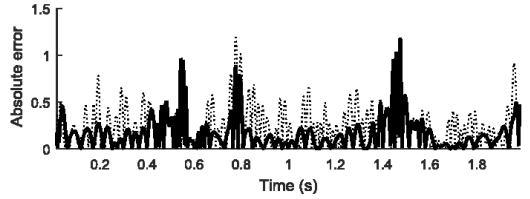

(a)

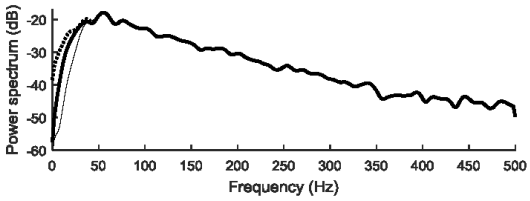

(b)

Fig. 8. Comparison of cleaned EMG signals and uncontaminated EMG signal in SMSC data. (a) Absolute errors of cleaned EMG signal from DSWT and uncontaminated EMG signal (solid line) compared to those of cleaned EMG signal from HPF and uncontaminated EMG signal (dotted line). (b) The power spectrum of cleaned EMG signal from DSWT (thick line) compared to that of uncontaminated EMG signal (dotted line) and cleaned EMG signal from HPF (thin line).

uncontaminated EMG signal (solid line) compared to those of the cleaned EMG signal from HPF and uncontaminated EMG signal (dotted line). We can see that the results from DSWT are better than from HPF, which matches the MAE for DSWT (0.1771) being better than that for HPF (0.2563). Figure 8(b) shows the power spectrum for DSWT (thick line) compared with those for HPF (thin line) and uncontaminated EMG (dotted line). The power spectrum for DSWT is closer to that from uncontaminated EMG compared to that from HPF. These results are in agreement with RE. In other words, RE for DSWT is 0.0131 compared to 0.0460 for HPF.

Similar results were obtained from SMRC data. Figure 9 shows cleaned signals and their corresponding uncontaminated EMG signal in SMRC data. In Fig. 9(b), we can see that HPF cannot completely remove ECG interference at a time around 0.4–0.6, 1.2 and 1.8–2 s. These may be caused by other types of noise, such as power line interference in the EMG signals. However, the cleaned EMG signal from DSWT shown in Fig. 9(a) not only provides a significantly better result than HPF but also has an excellent agreement with the uncontaminated EMG signal shown in Fig. 9(c).

The absolute errors of cleaned EMG signal from DSWT and uncontaminated EMG signal (solid line) compared to those of cleaned EMG signal from HPF and uncontaminated EMG signal (dotted line) are shown in Fig. 10(a). We can see that

May 13, 2019 11:09:55am WSPC/167-FNL 2050001 ISSN: 0219-4775 2nd Reading

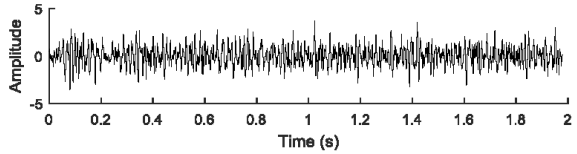

(a) Cleaned EMG signal from DSWT (SMRC)

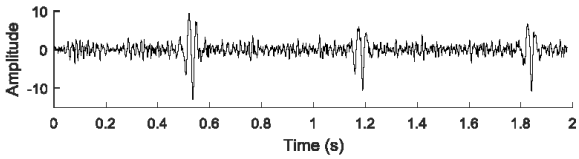

(b) Cleaned EMG signal from HPF (SMRC)

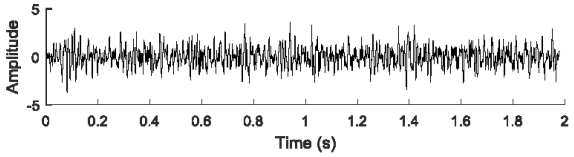

(c) Uncontaminated EMG signal (SMRC)

Fig. 9. Example of cleaned signals and the uncontaminated EMG signal from SMRC. (a) Cleaned EMG signal from DSWT-based algorithm, as in Figs. 7(e) and 7(f). (b) Cleaned EMG signal from HPF. (c) Uncontaminated EMG signal.

DSWT gives better results than HPF does. As a result, MAE and CC for DSWT are noticeably better than those for HPF. In other words, while MAE and CC for DSWT are 0.4490 and 0.8353, MAE and CC for HPF are 0.8298 and 0.4831. Figure 10(b) shows the power spectra for DSWT (thick line), HPF (thin line) and uncontaminated EMG (dotted line). We can see that the power spectrum for DSWT is comparable with that for uncontaminated EMG. However, the power spectrum for HPF is significantly different from that of uncontaminated EMG. These results agree with RE for DSWT (0.1947) compared with that for HPF (43.6027).

When there are variations in the EMG recording, the power spectra of the EMG signal change. For example, the dominant frequency of the EMG recording decreases as a result of muscle fatigue, which can be measured using the median frequency [23]. The performances that we reported were based on the average and standard deviation of MAE, CC and RE from the simulated EMG signals generated by the bandpass filter with variation in bandwidths. Therefore, the proposed approach would be applicable from the perspective of variations in the EMG recording.

May 13, 2019 11:09:59am WSPC/167-FNL 2050001 ISSN: 0219-4775 2nd Reading

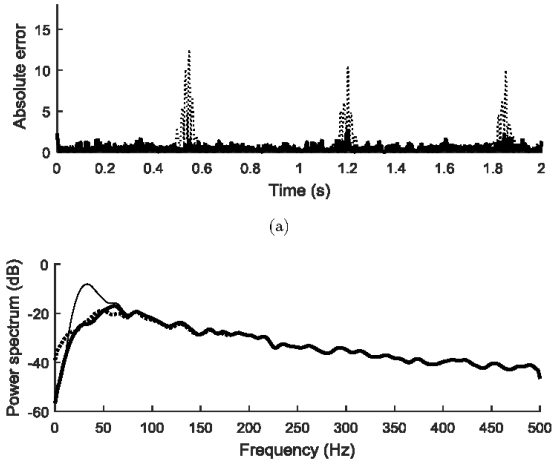

Fig. 10. Comparison of cleaned EMG signals and uncontaminated EMG signal from SMRC. (a) Absolute errors of cleaned EMG signal from DSWT and uncontaminated EMG signal (solid line) compared to those of cleaned EMG signal from HPF and uncontaminated EMG signal (dotted line). (b) The power spectrum of cleaned EMG signal from DSWT (thick line) compared to that of uncontaminated EMG signal (dotted line) and cleaned EMG signal from HPF (thin line).

6. Conclusions

We present an application of DSWT to removing ECG interference in EMG signals with consideration of SNR level. The proposed method consists of three main steps, namely, DSWT decomposition, thresholding and DSWT reconstruction. In the first step, the contaminated EMG signal is decomposed using 5-level DSWT with the Symlet wavelet function. In the second step, the coefficients in cD4 and cD5, which are contaminated by the ECG interference, are subjected to non-linear thresholding. In other words, the detail coefficients, whose absolute values are less than or equal to the threshold level, are set to zero. The threshold level is varied from 0 to 10 with step size 1. Finally, in the third step, the cleaned EMG signal is reconstructed by inverse DSWT of the thresholded coefficients.

The proposed method was evaluated using the simulated EMG signal contaminated with the ECG interference at 9 SNR levels from -20 to 20 dB with 5 dB increments. There were two types of ECG interference in this study, namely, simulated and real ECG signals. With both types of data, MAE, CC and RE for DSWT were better than those for HPF. Moreover, DSWT significantly outperformed HPF at the low SNR from -10 to -20 dB. Results show that the EMG signal

May 13, 2019 11:10:03am WSPC/167-FNL 2050001 ISSN: 0219-4775 2nd Reading

contaminated with ECG at different SNR levels requires different threshold levels. The optimal threshold for each SNR level in this paper was obtained offline by exhaustive search, which is impractical for real-time applications. The results suggest a possible future research direction in developing a system that can estimate the SNR level in an EMG signal contaminated with ECG interference.

Acknowledgments

This work was jointly funded by the Graduate School, Prince of Songkla University through Thailand's Education Hub for ASEAN Countries (TEH-AC) scholarship and the Thailand Research Fund and Faculty of Engineering, Prince of Songkla University through Contract No. RSA5980049. Also, the authors would like to thank the Research and Development Office (RDO), Prince of Songkla University and Associate Professor Dr. Seppo Karrila, Faculty of Science and Technology, Prince of Songkla University for commenting on the paper.

References

[1] D. Staudenmann, K. Roeleveld, D. F. Stegeman and J. H. V. Dieën, Methodological aspects of SEMG recordings for force estimation — A Tutorial and Review, *J. Electromyogr. Kines.* **20** (2010) 375 387.

[2] G. Balestra, S. Frassinelli, M. Knaflitz and F. Molinari, Time-frequency analysis of surface myoelectric signals during athletic movement, *IEEE Eng. Med. Biol. Mag.* **20** (2001) 106 115.

[3] B. Pandey and R. B. Mishra, A practical measuring system for intestinal pressure activity and its clinical application, *Expert Sys. Appl.* **36** (2009) 9201 9213.

[4] I. Kajituni, M. Murakawa, D. Nishikawa, H. Yokoi, N. Kajihara, M. Iwutu, D. Keymeulen, H. Sakanashi and T. Higuchi, An evolvable hardware chip for prosthetic hand controller, *Proc. 7th Int. Conf. Microelectrons*, Granada, Spain, 6 August 2002, pp. 179 186.

[5] A. Barreto, S. Scargle and M. Adjouadi, A practical EMG-based human-computer interface for users with motor disabilities, *J. Rehabil. Res. Dev.* **37** (2000) 53 64.

[6] M. A. Oskoei and H. Hu, Myoelectric control systems — A survey, *Biomed. Signal Process. Control* **2** (2007) 275 294.

[7] A. Phinyomark, P. Phukapattranont and C. Limsakul, Feature reduction and selection for EMG signal classification, *Expert Syst. Appl.* **39** (2012) 7420 7431.

[8] G. F. Inbar and A. E. Noujaim, On surface EMG spectral characterization and its application to diagnostic classification, *IEEE Trans. Biomed. Eng.* **31** (1984) 597 604.

[9] P. Zhou, Eliminating cardiac contamination from myoelectric control signals developed by targeted muscle reinnervation, *Physiol Meas.* **27** (2007) 1311 1327.

[10] J. D. M. Drake and J. P. Callagham, Elimination of electrocardiogram contamination from electromyogram signals: An evaluation of currently used removal techniques, *J. Electromyogr. Kines.* **16** (2006) 175 187.

[11] S. Abbaspour, A. Fallah, M. Linden and H. Gholamhosseini, A novel approach for removing ECG interferences from surface EMG signals using a combined ANFIS and wavelet, *J. Electromyogr. Kines.* **26** (2016) 52 59.

[12] R. Istenic, P. A. Kaplanis, C. S. Pattichis and D. Zazula, Analysis of neuromuscular disorders using statistical and entropy metrics on surface EMG, *WSEAS Trans Signal Proces.* **4** (2008) 1790 5052.

May 13, 2019 11:10:03am WSPC/167-FNL 2050001 ISSN: 0219-4775 2nd Reading

[13] S. Conforto, T. D'Alessio and S. Pignatelli, Optimal rejection of movement artifacts from myoelectric signals by means of a wavelet filtering procedure, *J. Electromyogr. Kines.* **9** (1999) 47 57.

[14] P. Zhou, M. M. Lowery, R. F. Weir and T. A. Kuiken, Elimination of ECG artifacts from myoelectric prosthesis control signals developed by targeted muscle reinnervation, *Proc. IEEE Eng. Med. Biol. 27th Conf.* Shanghai, China, 1 4 September (2005), pp. 5276 5279.

[15] S. Abbaspour and A. Fallah, A combination method for electrocardiogram rejection from surface electromyogram, *J. Biomed. Master. Res. A.* **8** (2014) 13 19.

[16] C. Marque, C. Bisch, R. Dantas, S. Elayoubi, V. Brosse and C. Pérot, Adaptive filtering for ECG rejection from surface EMG recordings, *J. Electromyogr. Kines.* **15** (2005) 310 315.

[17] G. Lu, J. S. Brittain, P. Holland, J. Yianni, A. L. Green, J. F. Stein, T. Z. Aziz and S. Wang, Removing ECG noise from surface EMG signals using adaptive filtering, *Neuroendocrinol. Lett.* **462** (2009) 14 19.

[18] C. Kezi Selva Vijila and C. Ebbie Selva Kumar, Cancellation of ECG in electromyogram using back propagation network, *Proc. 2009 Int. Conf. on Advances in Recent Technologies in Communication and Computing*, Kottayam, Kerala, India, 2009, pp. 630 634.

[19] T. D. Bui and G. Chen, Translation-invariant denoising using multiwavelets, *IEEE Trans. Signal Process.* **46** (1998) 3414 3420.

[20] J. J. Galiana-Merino, D. Ruiz-Fernandez and J. J. Martinez-Espla, Power line interference filtering on surface electromyography based on the stationary wavelet packet transform, *Comput. Meth. Prog. Bio.* **3** (2013) 338 346.

[21] P. McCool, G. D. Fraser, A. D. C. Chan, L. P. Petropoulakis and J. J. Soraghan, Identification of contaminant type in surface electromyography (EMG) signals, *IEEE Trans. Neural Syst. Rehabil. Eng.* **22** (2014) 774 783.

[22] P. E. McSharry, G. D. Clifford, L. Tarassenko and L. A. Smith, A dynamical model for generating synthetic electrocardiogram signals, *IEEE Trans. Biomed. Eng.* **50** (2003) 289 294.

[23] F. B. Stulen, A technique to monitor localized muscular fatigue using frequency domain analysis of the myoelectric signal, Ph.D. thesis, Massachusetts Institute of Technology, Cambridge (1980).

Appendix A.2

T. Oo, P. Phukpattaranont, and P. Klabklay, “Effects of SNR on removing ECG noise from EMG signal using DSWT,” *Proc. 15th Int. Conf. Electr. Eng. Comput. Telecommun. Inf. Technol. ECTI-CON*, pp. 253–256, 2018.

2018 15th International Conference on Electrical Engineering/Electronics, Computer, Telecommunications and Information Technology

Effects of SNR on removing ECG noise from EMG signal using DSWT

Thandar Oo and Dr. Pornchai Phukpattaranont*
Department of Electrical Engineering,
Faculty of Engineering, Prince of Songkla University,
Hat Yai, Songkhla,Thailand
thandaroo25.tdo@ gmail.com*, pornchai.p@psu.ac.th

Prapakorn Klabklay, MD
Department of Orthopaedic Surgery and Physical Medicine
Faculty of Medicine, Prince of Songkla University,
Hat Yai, Songkhla,Thailand
kprapako@medicine.psu.ac.th

Abstract—The electromyography (EMG) signal records the electrical potential difference across the skeletal muscle in every part of the body whereas the electrocardiography (ECG) signal measures the electrical potential difference across only the heart. For example, when the EMG signal is collected from muscles in the torso, the ECG signal coming up from the heart activity can interfere with the EMG signal. In this way, the EMG signal can be contaminated with the ECG interference during data collection. In this paper, we propose the improved optimal thresholding method based on discrete stationary wavelet transform (DSWT) in various 5-level SNR used for removing the ECG interference from the contaminated EMG signal. No prior studies have evaluated the performance evaluation of mean absolute error (MAE) and correlation coefficient (CC) for this proposed method to estimate the optimal threshold value in SNR 5 levels. The results show that the ECG interference is removed from the contaminated EMG signal by using the optimal wavelet thresholding method based on DSWT at various 5 levels of SNR. A proposed removal technique is better than the traditional thresholding method.

Keywords— electromyography (EMG), ECG interference, discrete stationary wavelet transform (DSWT)

I. INTRODUCTION

The EMG signal is generated from motor units, which are the nerve-muscle functional unit of the neuromuscular system [1]. The potential difference can be measured by either non-invasive electrodes from surface EMG signals or invasive electrodes from needle EMG or intramuscular EMG signals [2]. In this paper, we focus on the EMG signal acquired using surface electrodes only. The electrodes convert an ion current to an electron current so that it can be amplified and acquired by an electronics circuit.

The amplitude of the EMG signal can be ranged either from 0 to 10 mV (peak-to-peak) or 0 to 1.5 mV (rms). Moreover, the frequency range of EMG signal is limited to 0 Hz to 500 Hz for the usable energy of the signal. However, the dominant energy of the EMG signal is in between 50 Hz and 150 Hz range. The EMG signal recorded from a muscle contraction has a variety of usefulness including clinical applications [3], robotic applications [4], engineering applications [5], modern human computer interaction [6], electrical wheelchair control [7], and industrial applications [8].

One of important processes used in above described applications is a development of EMG recognition system. The EMG recognition system consists of three cascaded modules, namely, data pre-processing, feature extraction, and classification [7]. The main process in data pre-processing is to remove noise in the EMG signal, which is contaminated from environment while passing on different tissues [8]. We will focus on removing the electrocardiography (ECG) interference from the contaminated EMG signal in this work. The EMG signal records the electrical potential difference across the skeletal muscle in every part of the body whereas the ECG signal measures the electrical potential difference across only the heart. However, when the EMG signal is collected from muscles in the torso, it may be interfered by the ECG signal coming up from the heart activity.

In previous studies, the discrete wavelet transform (DWT) with thresholding value was proposed to remove the ECG interference from the EMG signal [11], [12], [13]. However, the performance was evaluated with the EMG signal contaminated with the ECG interference at signal to noise ratio (SNR) 0 dB only. To extend the studies in [11], [12], [13], we study the ECG interference removal algorithm from the contaminated EMG signal using the discrete stationary wavelet transform (DSWT) with the optimal thresholding method at various SNR levels.

II. MATERIALS AND METHODS

A. Simulation Data

All EMG data were collected by a commercial EMG measurement system (MP150, BIOPAC system). For amplifying the EMG signals, they were used with a gain of 1000 across the bandwidth from 10 to 500 Hz. The EMG data were recorded at a sampling frequency rate of 1000 Hz. The EMG signal with SNR > 18 dB was considered as the uncontaminated EMG signal. The ECG interference was obtained from MIT-BIH arrhythmia database. There are 5 levels of the EMG signal contaminated with the ECG interference, namely, -20 dB, -10 dB, 0 dB, 10 dB, and 20 dB. Twenty normal ECG recordings were chosen and randomly multiplied by an amplitude scaling to produce the EMG signal contaminated with the ECG interference at each SNR level.

978-1-5386-3555-1/18/$31.00 ©2018 IEEE

B. *Proposed algorithm*

The proposed algorithm for removing the ECG interference from the EMG signal consists of 3 main stages namely DSWT decomposition, thresholding, and DSWT reconstruction. Details on each stage are as follows.

- *Stage (1)*: Decompose the contaminated EMG signal using three-level DSWT with the Meyer wavelet function.
- *Stage (2)*: Process the approximation coefficients at level 1, 2, and 3, which are contaminated by the ECG interference, with a nonlinear thresholding procedure.
- *Stage (3)*: Obtain the clean EMG signal from the new coefficients by using inverse DSWT.

The first stage is to decompose the EMG signal contaminated by the ECG interference using DSWT. DSWT is a shift-invariant transformation. The EMG signal was decomposed using the Meyer wavelet function into various subbands as shown in Fig. 1. Then, in the second stage, the subband signals are separated into two types including approximation coefficients and detail coefficients. The approximation coefficients (cA_1, cA_2 and cA_3), which are contaminated by the ECG interference, are processed with a nonlinear thresholding procedure. In other words, the approximation coefficients, which have their absolute values greater than or equal to the threshold value, are set to zero. To obtain the optimal threshold value for removing ECG interference from contaminated EMG signal, the thresholding level from 0 to 10 with a step size of 1 were tested. The threshold value that gives the best performance based on either mean absolute error (MAE) or correlation coefficient (CC) are selected as the optimal threshold. The MAE can be expressed as [9]

$$\mathrm{MAE} = \frac{1}{N}\sum(x_u - x_{cl}) \tag{1}$$

where x_u is uncontaminated EMG signal and x_{cl} is a contaminated EMG signal that is cleaned by a noise removal process. The closer value of MAE to 0 indicates the better result of noise removal. The CC is given by [10], [11], [13]

$$\mathrm{CC} = \frac{\sum_{i=1}^{N}(x_u(i)-\overline{x_u})(x_{cl}(i)-\overline{x_{cl}})}{\sqrt{\sum_{i=1}^{N}(x_u(i)-\overline{x_u}(i))^2}\sqrt{\sum_{i=1}^{N}(x_{cl}(i)-\overline{x_{cl}}(i))^2}} \tag{2}$$

The closer value of CC to 1 indicates the better result of noise removal.

In the third stage, the clean EMG signal is obtained from the new coefficients by using inverse DSWT signal for reconstruction.

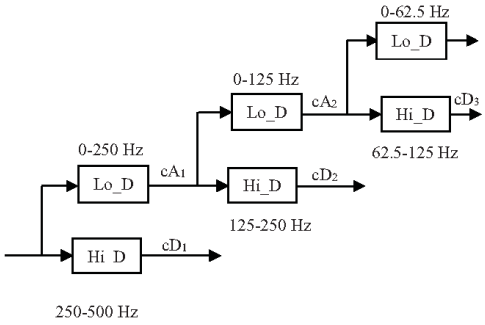

Fig. 1. Signal subbands resulting from three-level decomposition using DSWT.

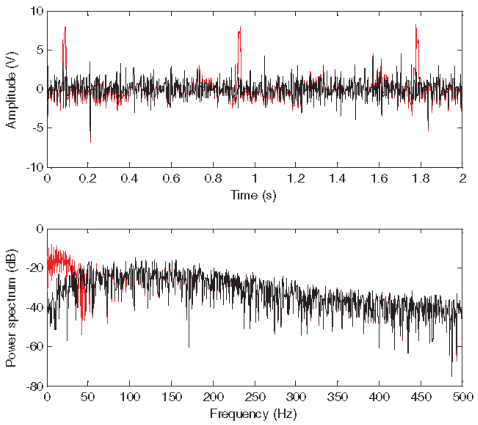

Fig. 2. The comparison between the EMG signal contaminated with the ECG interference at SNR 0 dB (Red) and the uncontaminated EMG signal (Black) in time domain (top panel) and frequency domain (bottom panel).

III. Results and Discussion

A. *DSWT Decomposition*

Fig. 2 shows an example of the EMG signal contaminated with the ECG interference at SNR 0 dB (Red) and the uncontaminated EMG signal (Black) in time domain (top panel) and frequency domain (bottom panel). We can clearly see the ECG interference contaminated in the EMG signal in the time domain. Moreover, the frequency components of the ECG interference are clearly visible in the frequency domain.

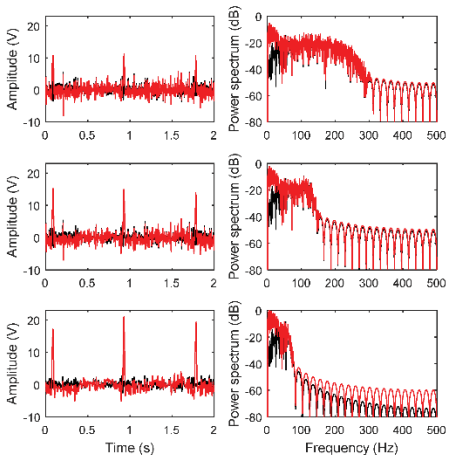

Fig. 3. Approximation coefficients obtained by applying three-level DSWT decomposition to the EMG signal contaminated with ECG interference at SNR 0 dB (Red) and the uncontaminated EMG signal (Black) in the time domain (Left column) and in the frequency domain (Right column). The approximation coefficients at level 1, 2, and 3 are shown the top, middle, and bottom rows, respectively.

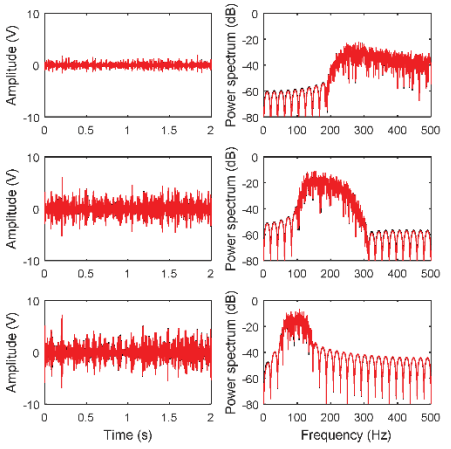

Fig. 4. Detail coefficients obtained by applying three-level DSWT decomposition to the EMG signal contaminated with ECG interference at SNR 0 dB (Red) and the uncontaminated EMG signal (Black) in the time domain (Left column) and in the frequency domain (Right column). The detail coefficients at level 1, 2, and 3 are shown the top, middle, and bottom rows, respectively.

Fig. 3 and 4 show the approximation and detail coefficients obtained by applying three-level DSWT decomposition to the EMG signal contaminated with ECG interference at SNR 0 dB (Red) and the uncontaminated EMG signal (Black) in the time domain (Left column) and in the frequency domain (Right column). The ECG interference is clearly seen in the approximation coefficients both in the time domain and frequency domain.

B. Optimal Wavelet Thresholding

Fig. 5 shows the approximation coefficients at level 1, 2, and 3 before thresholding (Red) and after thresholding with the threshold value 2.65 (Black) in the top, middle, and bottom panels, respectively. The threshold value 2.65 was selected from the average of 20 optimal threshold values that gave the best CC. The approximation coefficient that has its absolute value greater than 2.65 is set to zero.

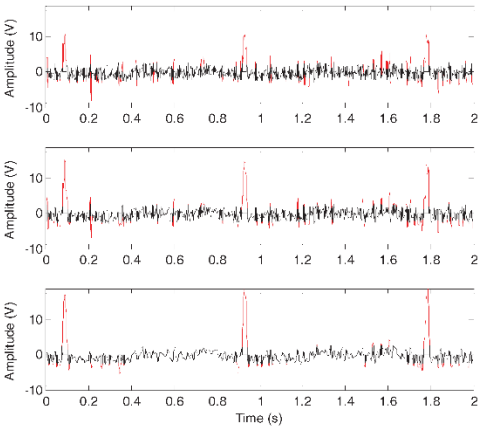

Fig. 5. Approximation coefficients at level 1, 2, and 3 before thresholding (Red) and after thresholding with the threshold value 2.65 (Black) are shown in the top, middle, and bottom panels, respectively.

C. DSWT Reconstruction

After the approximation coefficients were processed with the thresholding technique, they were combined with the detail coefficients and were processed with reconstruction algorithm through inverse DSWT. Fig. 6 shows a comparison between the uncontaminated EMG signal (Black) and the reconstructed clean EMG signal (Red) and in time domain (top panel) and frequency domain (bottom panel). We can clearly see very good agreement between the uncontaminated EMG signal and the reconstructed clean EMG signal. The CC value determined from both signals shown in Fig. 6 is 0.9380.

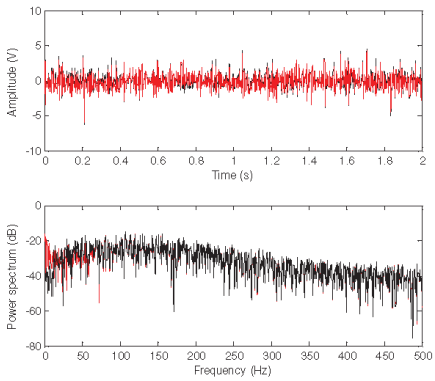

Fig. 6. Comparison between the uncontaminated EMG signal (Black) and the reconstructed clean EMG signal (Red) and in time domain (top panel) and frequency domain (bottom panel).

D. Performance Evaluation

Table I shows the performance comparisons for ECG interference removal using the thresholding technique based on DSWT from 5 levels of SNR, namely, -20 dB, -10 dB, 0 dB, 10 dB, and 20 dB, with MAE and CC. The best results can be seen in SNR 20 dB indicating by the closer value of MAE to 0 and the closer value of CC to 1 because the ECG interference is very low in this case. When the SNR values decrease from 20 dB to -20 dB, the average optimal threshold values decrease from 4.00 to 0.25 in MAE case and from 3.58 to 0.30 in CC case. At SNR -20 dB, we can obtain the average MAE 0.39 and the average CC 0.86 using the proposed technique. These results indicate that to achieve the best performance on ECG interference removal, the optimal threshold value must be adaptive based on the SNR value.

TABLE I. PERFORMANCE COMPARISONS FOR ECG INTERFERENCE REMOVAL USING THE THRESHOLDING TECNIQUE BASED ON DSWT FROM 5 LEVELS OF SNR.

SNR(dB)	Th_MAE*	MAE	Th_CC**	CC
-20	0.25 ± 0.44	0.39 ± 0.07	0.30 ± 0.47	0.86 ± 0.05
-10	0.30 ± 0.47	0.32 ± 0.06	0.35 ± 0.49	0.91 ± 0.04
0	2.00 ± 1.12	0.26 ± 0.04	2.65 ± 1.39	0.95 ± 0.01
10	3.45 ± 1.05	0.12 ± 0.01	3.25 ± 0.64	0.98 ± 0.00
20	4.00 ± 0.97	0.05 ± 0.00	3.58 ± 1.12	0.99 ± 0.00

*Th_MAE shows the average and standard deviation of 20 optimal threshold values that gave the best MAE.
**Th_CC shows the average and standard deviation of 20 optimal threshold values that gave the best CC.

IV. CONCLUSIONS

In summary, this study proposed the technique for removing the ECG interference from the contaminated EMG signal using the optimal wavelet thresholding method based on DSWT. The threshold values of 0 to 10 with a step size were tested to obtain the optimal threshold. The performance of noise removal was evaluated using MAE and CC. Results show that the EMG signals contaminated with the ECG interference at different SNR require different optimal threshold values. These suggest a possible future research direction on developing the system that can estimate the SNR values from the EMG signal contaminated with the ECG interference.

ACKNOWLEDGMENT

This work was funded by Graduate School, Prince of Songkla University through Thailand's Education Hub for ASEAN Countries (TEH-AC) scholarship.

REFERENCES

[1] E. J. R. Ramirez and H. Hu, "Stages for developing control systems using EMG and EEG signals: A survey," Sch. of Compt. Sci. and E Lect. Eng., Univ. of Essex, UK, Tech, Rep., CES-513, Jun., 2011.

[2] R. H. Chowdhury, M. B. I. Reaz, and M. A Bin Mohd Ali, "Surface electromyography signal processing and classification techniques," *Sensors*, vol. 13, pp. 12431-12466, 2013.

[3] B. Pandey and R. B. Mishra, "A practical measuring system for intestinal pressure activity and its clinical application," *Expert Sys. Appl.*, vol. 36, no. 5, pp. 9201 9213, 2009.

[4] F. Christian, W. Andreas, K. Konstantin, and H. Gunter, "Application of EMG signals for controlling exoskeleton robots," Biomed Tech (Berl)., vol. 51, no. (5-6), pp. 314-9, December 2006.

[5] R. Merletti and P. A. Pakker. *Electromyography, physiology, engineering and noninvasive applications*. Hoboken, NJ: John Wiley & Sons, 2004.

[6] A. Barreto, S. Scargle, and M. Adjouadi, "A practical EMG-based human-computer interface for users with motor disabilities," *J. Rehabil. Res. Dev.*, vol. 37, no. 1, pp.53 64, Jan.-Feb., 2000

[7] M. A. Oskoei and H. Hu, "Myoelectric control systems A survey," *Biomed. Signal Process. Control*, vol. 2, no. 4, pp. 275 294, Oct. 2007.

[8] A. Phinyomark, P. Phukapattranont, and C. Limsakul, "Feature reduction and selection for EMG signal classification," *Expert Syst. Appl.*, vol.39, pp. 7420-7431, Jun. 2012.

[9] J. J. G. Merino, D. R. Fernandez, and J. J. M. Espla, "Power line interference filtering on surface electromyography based on the stationary wavelet packet transform," *Comput. Meth. Prog. Bio.*, vol.3, pp.338-346, 2013.

[10] J. D. M. Drake and J. P. Callagham, "Elimination of electrocardiogram contamination from electromyogram signals: An evaluation of currently used removal techniques," *J. Electromyogr. Kines.*, vol. 16, pp. 175-187, 2006.

[11] S. Abbaspour, A. Fallah, M. Linden, and H. Gholamhosseini, "A novel approach for removing ECG interferences from surface EMG signals using a combined ANFIS and wavelet," *J. Electromyogr. Kines.*, vol.26, pp. 52-59, 2016.

[12] P. Zhou, "Eliminating cardiac contamination from myoelectric control signals developed by targeted muscle reinnervation," *Physiol Meas.*, vol. 27, pp. 1311-1327, 2007.

[13] S. Abbaspour and A. Fallah, "A combination method for electrocardiogram rejection from surface electromyogram," *J . Biomed. Master. Res. A.*, vol.8, pp. 13-19, 2014.

VITAE

Name Miss Thandar Oo

Student ID 5910130044

Educational Attainment

Degree	Name of Institution	Year of Graduation
Bachelor of Engineering (Electrical Engineering)	Technological University (Myitkyina, Myanmar)	2012
Master of Engineering (Electrical Engineering)	Mandalay Technological University	2015

Scholarship Awards during Enrolment

1. Ph.D. Program from Thailand's Education Hub for ASEAN Countries (TEH-AC) scholarship, Prince of Songkla University, Thailand.

List of Publication and Proceeding

International Journals

T. Oo, and P. Phukpattaranont, "Accounting for SNR in an Algorithm using Wavelet Transform to Remove ECG Interference from EMG Signals", Fluctuation and Noise Letters, Accepted for publication.

Conference Proceedings

T. Oo, P. Phukpattaranont, and P. Klabklay, "Effects of SNR on removing ECG noise from EMG signal using DSWT," *Proc. 15th Int. Conf. Electr. Eng. Comput. Telecommun. Inf. Technol. ECTI-CON*, pp. 253–256, 2018.